Recurrent excitation and inhibition in the Renshaw cell-motoneuron circuit of the lumbar spinal cord

Niall J. Moore

Thesis submitted for the degree of
Doctor of Philosophy

Department of Neuroscience, Physiology and Pharmacology
UCL
2014

Declaration

I, Niall John Moore confirm that the work presented in this thesis is my own. Where information has been derived from other sources, I confirm that this has been indicated in the thesis.

Niall J. Moore	Date

Abstract

Motor output from spinal motoneurons is influenced by interneuron networks in the ventral horn of the spinal cord. This thesis presents electrophysiological investigations of two separate but complementary aspects of the neuronal networks that influence this motor output. The first investigation focuses on inhibition of lumbar motoneurons. The second characterises the excitatory synapse formed by motoneuron axon collaterals onto Renshaw cells, which are interneurons that mediate recurrent inhibition onto motoneurons.

Previous studies on neonatal rats have shown that inhibition of motoneurons is mediated a mixed GABAergic and glycinergic response. Whole-cell voltage-clamp recordings of spinal motoneurons obtained from juvenile ($P8-14$) mice demonstrated that motoneuron inhibition is mostly mediated by glycine. GABA currents were not co-detected with glycine during this age range in the mouse. Further experiments, in which the relative content of pre-synaptic GABA and glycine was manipulated, showed that GABA is not co-released with glycine by premotor interneurons.

Quantal analysis of paired recordings of pre-synaptic motoneurons and post-synaptic Renshaw cells showed that this excitatory synapse exhibits a large number of release sites and a high probability of release. This is suggestive of highly reliable synaptic transmission between the two cell types. Comparison of the number of release sites estimated from paired recordings with those estimated from responses evoked by ventral root stimulation revealed that on average six motoneurons project onto every Renshaw cell. We conclude that:

- In mature animals motoneuron inhibition is mainly glycinergic.
- The Renshaw cell to motoneuron synapse has a high efficiency of transmission.
- The degree of convergence of motoneurons to Renshaw cells is very high.

The last two conclusions suggest that firing in motoneurons pools reliably induces firing in the population of connected Renshaw cells.

Acknowledgements

First and foremost, I would to thank my supervisor Dr. Marco Beato for giving me the opportunity to complete this work and for his expert tuition and guidance throughout my four years working with him. It has been a pleasure working in his lab and I shall always be very grateful for the great care and attention he has given me. I doubt there are many places in the world where I could have learned so much and enjoyed myself as much as I did at the same time.

I would also like to thank Dr. Gary Bhumbra for his continuous help over the years and his patience with my dearth of knowledge. The seemingly endless range of topics that Gary can give expert advice on has been beneficial to both my research and myself.

My family has been a tremendous support throughout my studies. In particular, I would like to thank my Uncle John who has been a great help throughout my PhD. I also want to thank Kirstie, Denis and Ally, who welcomed me into their home when I first moved to London and were fantastic neighbours and friends throughout my studies. The love and support of my Mum, Dad and sister Chloë has always been a great comfort to me throughout my life and this was especially true during my PhD.

Finally, I want to thank my partner Neena for her patience and understanding. She is the best.

Contents

List of Figures

Chapter 1

Introduction

The study of the spinal cord and the neural control of muscles provided much of the groundwork for our understanding of nervous system. Key discoveries such as chemical neurotransmission (Eccles et al. 1954, Eccles and Jaeger 1958) and quantal release (Fatt and Katz 1952, Kuno 1964) in fact originate from investigations of the neuromuscular junction and spinal cord. Compared with many of the higher functions of the central nervous system (CNS) motor output is easily measured and manipulated. Motor output however is controlled by a complex integrative network of neurons. This makes the spinal cord an attractive system in which to study the neurophysiology of both single cells and neuronal networks. At the single cell level there are a number of well defined cell types whose further characterisation is providing more insights into neuron function. The complex neural networks responsible for the control of motoneuron firing are an ideal model for studying how neurons work together to produce a common output.

In this thesis I will investigate two aspects of motoneuron control: first I will describe the inhibitory control of motoneurons and then I will provide a detailed description of synapses forming the recurrent inhibitory circuit. In this introductory chapter I will therefore first discuss the neuronal networks that govern motor output and thus the control of muscles. I will then discuss synaptic transmission and techniques that have been developed in order to describe its properties.

1.1 Spinal circuits and motor control

Control of the motor system by the CNS can be broadly broken down into three components. First, there is descending control from supraspinal centres that initiates voluntary movement and provides modulatory input to spinal networks (Heckman et al. 2003, Hultborn and Kiehn 1992, Grillner et al. 2005). Second, neuronal circuits confined to the spinal cord that provide rhythmic and patterned motor output (Kiehn 2006). Finally, the reflex and sensory feedback circuits that provide information from proprioceptive and tactile receptors and can modulate motoneuron activity accordingly (Hultborn 2006).

1.1.1 Supraspinal projections

Descending motor pathways from supraspinal centres can be separated into three groups of projections, those that project via the corticospinal tract (CST), those that project via ventromedial tracts and those that project via dorsomedial tracts. Classically the CST has been considered to be the 'principal' descending pathway for motor control as fibres that project via this pathway originate in the primary motor cortex (M1). The primary motor cortex, located in the precentral gyrus (Brodman's area 4), was identified as such because the threshold for evoking movement via electrical stimulation of the brain was lower here than elsewhere in the cortex (Leyton and Sherrington 1917, Penfield and Boldrey 1937, Woolsey et al. 1952). The CST descends via the internal capsule to the medullary pyramid in the brain stem. Below the medullary pyramid the majority of projections decussate and cross the midline before continuing down the lateral funiculus finally projecting onto spinal motoneurons (see the blue pathway in Figure 1.1). The axons that do not decussate project via the anterior funiculus, some of which cross the midline once they reach the level of the spinal cord, innervating motoneurons and interneurons. There is also a subset of fibres that project from the primary motor cortex and do not project into the spinal cord but instead follow the corticobulbar pathway. These neurons follow the same path as the CST until the level of the brainstem where they synapse with upper motoneurons of the cranial nerves, thus providing input for control

of muscles of the face, head and neck (see the black pathway in Figure 1.1).

The projections that descend via ventromedial and dorsomedial tracts all originate at the brainstem level. The ventromedial brainstem pathways include the interstitiospinal and tectospinal tracts that arise from the midbrain, the lateral and medial vestibulospinal tracts (Sugiuchi et al. 2004), and the reticulospinal and bulbospinal projections that arise from the pontine and medullary reticular formation (Matsuyama et al. 1997; 1999; see the green pathway 1.1). These pathways all descend via the ventral and ventrolateral funiculi of the spinal cord and innervate neurons in Rexed Lamina VII and VIII. The regions of the spinal cord these pathways innervate give rise to long propriospinal neurons that project bilaterally and link widely seperated parts of the spinal cord including the cervical and lumbar englargements. Lesion studies have suggested that these groups of pathways could be responsible for bilateral postural control of the head, neck and trunk as well proximal limb movements (Lawrence and Kuypers 1968)

The brainstem pathways that descend dorsomedially include the rubrospinal tract which arises from the magnocellular red nucleus (Kennedy 1990, Muir and Whishaw 2000, Küchler et al. 2002) and the the pontospinal tract which arises from the ventrolateral pontine tegmentum (see the red pathway in Figure 1.1). These pathways terminate in the dorsal and lateral regions of the the intermediate zone (Rexed lamina VII and X). These nerves innervate propriospinal interneurons and have local, mainly unilateral projections that are thought to provide additional capacity for flexion based movements at distal joints such as elbow and wrist (Lemon 2008).

While the principal role of descending projections is to provide conscious input for voluntary control, the wide range of neurons these pathways innervate suggests a more complex role for descending projections. The CST in particular has been shown to perform a number of functions (Lemon and Griffiths 2005) which include: descending control of afferent inputs, including nocicipetive inputs (Cheema et al. 1984, Wall and Lidierth 1997), selection, gating and gain control of spinal reflexes (Pierrot-Deseilligny and Burke 2005) and direct excitation and inhibition of motoneurons (Maier et al. 1998, Porter and Lemon 1993). While it is therefore possibly not accurate to consider these

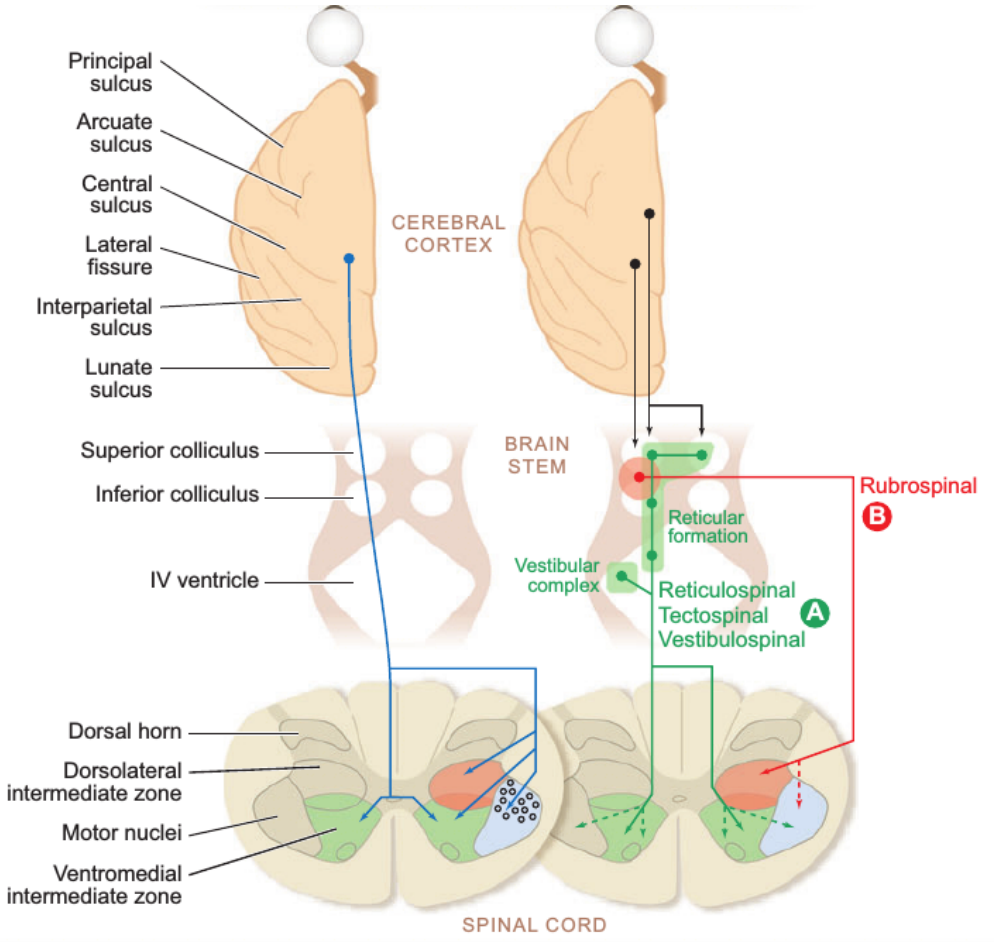

Figure 1.1: Schematic illustration of descending motor control pathways. Corticospinal tract projections are shown in blue on the left hand anatomical scheme. CST projections arise in the cortex and descend to the brainstem after which the majority cross the midline and project via the lateral funicle, while a minority of neurons do not cross the midline and instead descend via the anterior funiculus, with some fibres crossing the midline at the spinal cord level. The black pathway on the right hand anatomical scheme shows the corticobulbar pathway. These neurons also project from the cortex but instead of descending to the spinal cord synapse with the motoneurons of the cranial nerves that innervate muscles of the head, neck face. The ventromedial pathways descending from the brainstem to the spinal cord are shown in green on the right hand scheme. Nerves arising the from the vestibular complex and reticular formation project into the spinal cord via the ventromedial pathway. The red pathway on the right hand scheme illustrates the path of the dorsomedial tracts that include the rubrospinal tract which innervate nerves in the dorsolateral intermediate zone (which is illustrated at the spinal cord level on the left hand scheme). Adapted from Lemon (2008).

pathways as purely motor pathways they are still the source of upstream inputs into neural pathways that determine motor output.

1.1.2 Locomotor circuits

The generation of locomotor behaviour is fundamentally important for movement in both animals and humans and involves complex coordination of many muscles. The majority of the complex rhythmic coordinated muscle activity is produced by localized neuronal networks know as central pattern generators (CPGs). Studies of the lamprey and *Xenopus* tadpole have provided a detailed network structure of the CPGs that control swimming (Grillner 2003, McLean et al. 2000, Roberts et al. 1998) but much less is known about CPGs in mammals (Clarac et al. 2004, Hultborn et al. 1998, Kiehn and Butt 2003, McCrea 1998). Early studies showed that lumbar and cervical spinal cord contained neuronal networks that were sufficient to produce locomotor like activity in the hindlimb and forelimb respectively (see Grillner 2003). However describing the precise location of these CPG networks proved a challenging task. The majority of work investigating mammalian CPGs has focused on the networks that control movement of the hindlimbs (see Kiehn 2006).

Experiments studying the extent to which lumbar CPG networks extend in the rostrocaudal axis have been performed in the cat (Grillner and Zangger 1979), neonatal rat (Bracci et al. 1996, Cowley and Schmidt 1997, Gabbay et al. 2002, Kjaerulff and Kiehn 1996, Kremer and Lev-Tov 1997, Kudo and Yamada 1987) and neonatal mouse (Bonnot and Morin 1998, Bonnot et al. 2002, Christie and Whelan 2005) by recording either spontaneous or drug-induced rhythmic activities before and after sectioning of the spinal cord. These studies found that the capacity of generating rhythmic output is distributed throughout the lumbar enlargement but that isolated rostral segments (L1-3 in rodents and L3-5 in cats) have a greater rhytmogenic capacity than isolated caudal segments (L4-L6 in rodents and L6-S1 in cats).

Studies of the neonatal rat spinal cord in which a bath partition allowed for selective exposure of the upper and lower lumbar levels showed that when upper lumbar levels were exposed to 5-HT and *N*-methyl-D-aspartic (NMDA),

locomotor-like activity could be recorded in both upper and lower sections of the cord (albeit weaker in lower segments Bertrand and Cazalets 2002, Cazalets et al. 1995). However exposing the lower lumbar levels to 5-HT and NMDA induced only tonic activity in the upper segments (Cazalets et al. 1995). This suggests that spinal interneurons directly involved in producing rhythmic activity are contained entirely within the low thoracic and upper lumber sections (i.e. T13-L2). Experiments in intact adult rats arrived at similar conclusion when it was demonstrated that chemical ablation of the grey matter in T13-L2 by kainate injection greatly impaired locomotor capability but injection of kainate more caudally had much less effect on locomotion (Magnuson et al. 2005). However, motoneurons that project from T13-l2 innervate muscles that control movement of hip. Ablation of these rostral segments therefore would affect the ability of the animal to move the limb as a whole. The greater impact on locomotor movements after chemical ablation of the T13-L2, when compared with ablation of more caudal segments, therefore could be due to a general effect on the animals ability to move and not due to a greater loss of CPG networks. In his review on locomotor circuits Kiehn (2006) suggests that the rhythmogenic capacity of different lumbar levels is dependent on the neurotransmitters used to induce rhythmic activity. In the rodent 5-HT alone can produce rhytmic activity when applied to lower thoracic-upper lumbar levels but has no effect when applied to lower lumbar levels (Cowley and Schmidt 1997). However low concentrations of 5-HT when applied with NMDA and acetylcholine (in combination with an acetylcholine esterase inhibitor, Cowley and Schmidt 1997, Kjaerulff and Kiehn 1996) or noradrenaline (Gabbay et al. 2002) could induce rhythmic activity when applied to isolated parts of both rostral and caudal lumbar segments. While there may be a rostrocaudal gradient of rhythmogenic capability it certainly appears that all level of the lumbar spinal cord are capable of rhythm generation depending on the stimulus.

While there has been some dispute over the rostrocaudal distribution of CPGs, in the transverse plane there is much more agreement. Spinal neurons associated with locomotor behaviour have been shown to be located in the ventral side of the spinal cord (laminae VII, VIII and X) by both activity labelling (Cina and Hochman 2000, Dai et al. 2005, Kjaerulff et al. 1994) and electro-

physiological studies (Tresch and Kiehn 1999). This is supported by micro-lesion studies that showed that spontaneous rhythmic bursts were still present in preparations where the dorsal horn was ablated (Kjaerulff and Kiehn 1996, Bracci et al. 1996) and even in an isolated ventral horn preparation (Bracci et al. 1996). These studies therefore suggest that the neural network responsible for the generation of locomotor output is contained entirely within the ventral side of spinal cord.

CPGs however do not act in isolation and receive inputs from commissural interneurons (CINs) that cross the midline via the ventral commissure and produce the left-right coordination necessary for many locomotor movements. CINs can be subdivided into two groups: intersegmental CINs (that project between segments) and intrasegmental CINs (that do not project beyond segments). Intersegmental can be further subdivided into ascending, descending and bifurcating CINs (Bannatyne et al. 2003, Eide et al. 1999, Hoover and Durkovic 1992, Matsuyama et al. 2004, Nakayama et al. 2002, Nissen et al. 2005, Stokke et al. 2002). Descending CINs help bind synergies across the cord by exciting lower contralateral antagonist muscle groups and inhibiting lower contralateral agonist muscle groups (Butt et al. 2002a;b, Butt and Kiehn 2003). Spinal interneurons derived from V0 progenitor cells have been shown to exclusively form ascending commissural connections (Goulding and Pfaff 2005) and genetic ablation of the V0 results in a change in left-right coordination (Lanuza et al. 2004) which suggest ascending CINs may play a role in left-right coordination. Intrasegmental connections are also likely to play a role in left-right coordination. In fact, ablation of ascending CINs did not completely block left-right coordination suggesting other connections are also involved. Knock-out mice that have an abnormal increase in intrasegmental connections have been shown to develop a hopping gait (Kullander et al. 2003). This suggests that intrasegmental CINs may be involved in producing synergistic movements between left and right muscle groups to allow for movements such as hopping or jumping in which both sides move simultaneously.

1.1.3 Reflex pathways

Reflex pathways in the spinal cord are among some of the first neuronal networks to be studied and were the subject of pioneering work by Sir Charles Sherrington and Sir John Eccles during the early years of modern neuroscience (see Sherrington 1906, Hultborn 2006; for review). The spinal reflex pathways provide proprioceptive feedback to the spinal cord during movement. While reflexes tend to be considered as pathways that take place without input from other areas of the CNS it should be noted that during movement they are unlikely to act in isolation and should therefore be considered as part of the integrative system of motor control.

Reflex pathways are arguably the simplest form of neuronal network and are considered to be stereotyped and constant i.e. the same stimulus will always results in the same response. The reflex 'arc' that describes the structural basis of the generalised reflex consists of five elements: i) an 'afferent receptor' that records changes in the limbs and translates them into action potentials. ii) An afferent nerve that conveys that information back into the CNS. iii) A 'reflex centre' in which signals from receptors can be modified by inputs from other parts of the CNS. iv) An efferent motoneuron is modulated by the information conveyed via the reflex pathway. v) The 'effector muscle' that is the target of the reflex pathway. The only pathway described in this section that does not conform to this generalised structure is the recurrent inhibitory pathway mediated by the Renshaw cell. The Renshaw cell is an inhibitory interneuron that receives inputs directly from motoneurons via collateral projections and in turn inhibits motoneurons in synergistic motor pools. There is therefore no information being retrieved from an afferent receptor in this pathway, simply an efferent copy of motoneuron output. However, since it occurs automatically during motoneuron activation, and receives input from a reflex pathway, it is appropriate to describe it here along with the reflex pathways.

Reflex pathways from muscle spindles

Muscle spindles mediate the 'stretch' reflex and are arranged in parallel with extrafusal muscle fibres, attached to connective tissue at both ends of the muscle.

Group Ia and II afferents (grouped due to their size and thus speed of conduction, group I fibres being larger and faster than group II) innervate muscle spindles and become active at different points during muscle contraction. Group Ia fibres (which are mainly associated with the nuclear bag interfusal fibres) become more active during contraction thus conveying information about the change in length and rate of change in length of muscles. The activity of group II fibres however is directly proportional to the innvervated muscles instantaneous length, increasing during lengthening and decreasing during shortening.

Ia fibres project via the dorsal root into the spinal cord and synapse directly with homonymous α-motoneurons as well as Ia reciprocal inhibitory interneurons (Jankowska 1992). Ia reciprocal inhibitory interneurons synapse onto and inhibit antagonist motoneurons, this prevents the direct action of Ia afferents onto motoneurons resulting in simultaneous activation of both agonist and antagonist muscle groups. As well as receiving excitatory inputs from Ia fibres, Ia reciprocal inhibitory interneurons receive inhibitory inputs from Renshaw cells (see figure 1.2, Hultborn et al. 1971a;b;c).

Group II fibres are also known to provide monosynaptic excitation of homonymous α-motoneurons albeit more weakly than group Ia fibres as well producing a varying impact on various motoneuron pools depending on the start of the CNS (Windhorst 2007). In fact, a recent review has suggested that due to the similar patterns of innervation, the functional subdivision of group II fibres and group Ib (see below) should be re-assessed and the subpopulation they innervate should be considered as “group I/II interneurons” (Jankowska and Edgley 2010).

In terms of their impact on movement in general, muscle spindles and the stretch reflex are thought to be involved in the maintenance of posture and stability during movement. Studies involving neurotrophin-3-deficient mice support this conclusion as these mice do not have muscles spindles or primary afferent fibres and are unable to support their own weight as well as exhibiting unnatural postures (Ernfors et al. 1994, Walro and Kucera 1999). It should be noted that muscle spindles are also themselves innervated by γ-motoneurons and thus their activity and output can be modulated by the CNS.

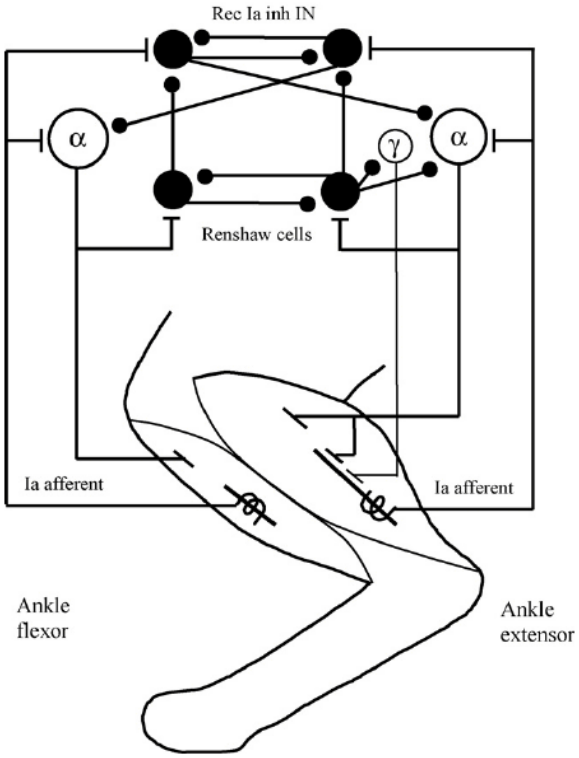

Figure 1.2: Illustration of the reflex pathway of group Ia fibres and of Renshaw cell mediated recurrent inhibition. Straight lines with T junction ends represent excitatory synapses whereas those that end with black circles represent inhibtory connections. On the right hand side of this diagram Ia fibres from the flexor muscles can be seen to project to both flexor α-motoneurons and Ia reciprocal inhibitory interneurons. The α-motoneurons project onto Renshaw cells which form inhibitory synapses onto Ia reciprocal inhibitory interneurons, other Renshaw cells and synergistic motoneurons.(Note flexor Renshaw cells are not shown projecting onto synergistic motoneurons for the sake of maintaining simplicity in the diagram.) Ia reciprocal inhibitory interneurons project onto antagonist α-motoneurons where they form inhibitory synapses. Adapted from (Windhorst 2007).

Reflex pathways from Golgi tendon organ

Golgi tendon organs also provide proprioceptive feedback from muscles to the spinal cord. They are located close to the musculotendinous junction and provide information about the 'force' of muscle contraction. Golgi tendon organs are comprised of collagen fibres intertwined with a Ib afferent nerve fibre. During stretching of the muscle the golgi tendon organ is squeezed and this elicits a depolarization of the Ib fibre, which if strong enough will induce an action potential. Ib afferent fibres thus signal changes in muscle tension and the force of contraction within a muscle. Indeed studies in the cat (Prochazka and Gorassini 1998) and humans (al Falahe et al. 1990) show good correlation between Ib afferent activity and muscle force.

Group Ib afferents have di- and oligosynaptic inhibitory connections to synergistic motoneurons ('autogenic inhibition') and excitatory connections to antagonist motoneuron pools (Schomburg 1990). Ib interneurons receive a wide range of convergent inputs from Ia afferents, Ib afferents from different muscles and from other sensory afferents including cutaenous and joint receptors (Schomburg 1990). As well as autogenic actions Ib reflex pathways have been associated with the attunement of force across different muscles depending on the requirements of the desired movement (Schomburg 1990). This proposed action of Ib afferent pathways is supported by the high degree of multisensorial convergence onto Ib interneurons as they this allows incorporation of a large amount of complex information concerning skin, contact, limb movement and the length/tension of muscles.

1.1.4 Recurrent inhibition

In early electrophysiological recordings of spinal cord activity Renshaw (1941) demonstrated that 'antidromic motor volleys' that produced excitation in a subset of motoneurons also resulted in the inhibition of neighbouring motoneurons. Later Renshaw (1946) showed that the same antidromic motor volleys resulted in prolonged spike activity in a subset ventral interneurons. These ventral interneurons are now known as Renshaw cells (being named after their discov-

erer by Sir John Eccles, Eccles et al. 1954) and mediate recurrent inhibition of α-motoneurons. Renshaw cells receive excitatory input from motoneurons and project back onto homonymous motoneurons as well as innervating heteronymous Renshaw cell (Ryall et al. 1971, Ryall and Piercey 1971) and homonyous Ia reciprocal inhibitory interneurons (see figure 1.2 Hultborn et al. 1971a;b;c).

Early studies identified a 'Renshaw cell area' in lamina VII using both single cell (Thomas and Wilson 1965) and population recordings (Willis 1971). Anatomical studies along with combined recording and immunolabelling work has led to a validated criteria for morphological identification (Alvarez et al. 1997, Carr et al. 1998). In particular calbindin immunoreactivity combined with anatomical location and cell size has proven to be useful in identifying Renshaw cells (Geiman et al. 2000, Mentis et al. 2006). However expression of calbindin on non-Renshaw cells means that this criterion should be used with caution (Zhang et al. 1990) and ideally should be combined with the presence of VAChT positive boutons opposite the cell membrane.

Despite the first description of recurrent inhibition in the spinal cord occurring well over half a century ago (Renshaw 1941) and the ease with which cells can be identified by both electrophysiological and anatomical techniques, there is still no consensus on a functional role for recurrent inhibition. While the isolated circuit appears to have a simple function in limiting motoneuron firing during repetitive stimulation (Eccles et al. 1954), as our understanding of the complex circuitry that governs motoneuron output has increased it has become clear that recurrent inhibition probably fulfils a more nuanced function (Windhorst 1996, Hultborn 2006, Windhorst 2007). The possible roles of recurrent inhibition suggested by more current work shall be discussed in more detail in later chapters.

1.2 Synaptic transmission at the motoneuron-Renshaw cell recurrent inhibitory circuit

The recurrent inhibitory circuit formed between motoneurons and Renshaw cells is comprised of both excitatory and inhibitory synapses. The excitatory

response of Renshaw cells to motoneuron inputs has been shown to consist of a mixed nicotinic and glutamatergic response (Lamotte d'Incamps and Ascher 2008). Although the identity of neurotransmitters released at this synapse is still not entirely clear (Richards et al. 2014). At the Renshaw cell to motoneuron inhibitory synapse co-release of the neurotransmitters GABA and glycine has been observed in the adult cat (Fyffe 1991) and neonatal rat (Schneider and Fyffe 1992). However, new evidence now suggests that in older animals motoneuron inhibition is purely glycineric (Chapter 3 Bhumbra et al. 2012). As this recurrent inhibitory circuit is the subject of the work in this thesis it is prudent to review briefly the neurotransmitters that are released at these synapse and the action of their respective receptors.

1.2.1 Motoneuron to Renshaw cell excitatory synapse

Recordings from Renshaw cells were first published by Renshaw (1946) and showed that a single ventral root stimulation resulted in a high-frequency response that lasted tens of milliseconds. Eccles et al. (1954) showed that an antagonist of nicotinic receptors (nAChRs), di-hydro-β-erythoidine (DHβE), blocked most of the Renshaw cell response to ventral root stimulation and concluded that the motoneuron to Renshaw cell synapse was cholinergic. Their initial explanation for the long duration of Renshaw cell activation after ventral root stimulation was that acetylcholine (ACh) degradation by acetylcholinesterase (AChE) was slow enough that ACh remained in the synaptic cleft for so long that it results in a prolonged response. However Eccles and Jaeger (1958) soon showed that even without AChE, diffusion of ACh from the synaptc cleft would be quicker than the decay of the response. Eccles et al. (1961b) then suggested that extra-synaptic receptors and ACh spillover could account for the long duration of the Renshaw cell response. Studies by Mentis et al. (2005) and Nishimaru et al. (2005) later showed that AMPARs and NMDARs are present along with nAChRs at the motoneuron to Renshaw cell synapse in newborn mice(P0-P4). This led to a new hypothesis that the long duration of the Renshaw cell response was due to the glutamatergic component of the excitatory response. Not only does glutamate dissociate slowly from NMDARs but activa-

tion of these receptors requires a 'priming' depolarization to remove the Mg^{2+} block, which could result in a delay in activation of NMDA receptors and therefore result in a prolonged depolarization. This would also explain the blockade of Renshaw cell response to ventral root stimulation by DHβE as this would block the priming action of ACh thus mask the NMDA mediated glutamatergic component.

A study by Lamotte d'Incamps and Ascher (2008) showed that four excitatory post-synaptic receptors are co-activated at the motoneuron-Renshaw cell synapse. Lamotte d'Incamps and Ascher (2008) demonstrated that AMPARs, NMDARs and two nicotinc receptors (which they suggest are α_7 homomers and $\alpha_4\beta_2$ heteromers) are present at the motoneuron-Renshaw cell synapse. The presence of these four different receptors allows both neurotransmitters to mediate EPSCs with a wide range of kinetics. Homomeric (putative $\alpha 7$) ACh receptors mediate a fast excitatory response with a rise time (τ_r) of ~ 0.5 ms and a decay time constant (τ_d) of ~ 3.6 ms whereas heteromeric (putative $\alpha_4\beta_2$) ACh receptors produce a much longer excitatory current with a τ_r of ~ 1.8 ms and τ_d of ~ 20.2 ms (Lamotte d'Incamps and Ascher 2008). The glutamate receptors also provide both fast and slow responses, with AMPA receptors mediating a fast excitatory current ($\tau_r =\sim 0.9$ ms, $\tau_d =\sim 6$ ms) and NMDA receptors mediating a much slower response ($\tau_r =\sim 4.7$ ms, $\tau_d =\sim 54.6$ ms, Lamotte d'Incamps and Ascher 2008). While the presence of several other receptors appears to support the NMDA receptors 'priming' hypothesis described above, in a later paper Lamotte d'Incamps et al. (2012) note that the difficulty of this explanation is that the after hyperpolarising potential (AHP) of the initial action potential would reintroduce the Mg^{2+} block of the NMDA current thus suppressing further depolarization. Their proposed mechanism by which this is overcome is that observed gap junctions between Renshaw cells could "neutralize the resetting of the Mg block thus allowing repetitive firing"(Lamotte d'Incamps et al. 2012).

Anatomical studies showed that vesicular ACh transporters (VAChT) and vesicular glutamate transporters (VGLUTs) are not present at the same synapses (Mentis et al. 2005, Nishimaru et al. 2005, Walmsley and Tracey 1981, Herzog et al. 2004, Liu et al. 2009). A recent study by Richards et al.

(2014) has suggested that aspartate, not glutamate could be the co-transmitter with ACh at Motoneuron to Renshaw cell synapses. Aspartate has a similar affinity for NMDARs as glutamate (Curras and Dingledine 1992) and its uptake into cells is independent of VGLUTs (Fremeau et al. 2002, Bellocchio et al. 2000, Herzog et al. 2001, Morland et al. 2013, Varoqui et al. 2002). Richards et al. (2014) showed that aspartate is not only present at cholinergic synapses on Renshaw cells but is present in higher concentrations than glutamate. While this does not preclude co-release of glutamate as well, it does suggest that aspartate could be the primary co-transmitter along with ACh.

1.2.2 Renshaw cell to motoneuron inhibitory synapse

In the same paper where the motoneuron to Renshaw cell excitatory synapse was first described to be cholinergic, the authors also showed that application of strychnine reduced recurrent inhibition (Eccles et al. 1954). At the time however it was still not known how strychnine blocked hyperpolarising events nor was it known that glycine was an inhibitory neurotransmitter. It was just over ten years later that it was first suggested that glycine may act as a neurotransmitter when it was noted that glycine concentrations are far higher in the spinal cord than anywhere else in the brain, with concentrations being particularly high in the ventral horns (Aprison and Werman 1965). The inhibitory effect of glycine was first demonstrated in the cat spinal cord, giving the first direct evidence of glycine's inhibitory action and the first evidence of glycinergic inhibition of motoneurons (Curtis et al. 1968; 1971a;b, Werman et al. 1967). It was therefore initially assumed that Renshaw cell inhibition of motoneurons was purely glycinergic. However, a study in the cat spinal cord showed a strychnine resistant component of recurrent inhibition that could be blocked by application of bicuculline. This suggested that GABA was a co-transmitter with glycine at the Renshaw cell to motoneuron synapse (Cullheim and Kellerth 1981). This conclusion was supported by later work in the neonatal rat spinal cord that showed that bicuculline reduced recurrent IPSPs and blocked strychnine resistant currents (Schneider and Fyffe 1992). In the same study, blockade of GABA uptake by application of nipecotic acid and a guvacine was shown to enhance recur-

rent synaptic potentials (Schneider and Fyffe 1992). While this work did not directly show that GABA and glycine were co-released, later work has shown that co-release of GABA with glycine occurs at motoneuron inhibitory synapses in the neonatal rat (Jonas et al. 1998, Jean-Xavier et al. 2007). Recent studies however have suggested that in the adult rodent spinal cord GABA is not co-released with glycine and that in the mature spinal cord motoneuron inhibition is likely to be purely glycinergic (see Chapter 3 Bhumbra et al. 2012). It has been shown that during development of the spinal cord there is a postnatal shift from GABAergic to glycinergic inhibition (Gao et al. 2001, Ma et al. 1993, Tran et al. 2003, Ma et al. 1992). It is therefore possible that in rodents the GABA mediated inhibitory component of recurrent inhibition decreases with age and is no longer present in the mature spinal cord (see Chapter 3 for further discussion).

1.3 Synaptic transmission

In the early days of modern neuroscience there was great debate over how nerve cells communicate with each other. This was known as “the war of the soup and the sparks” (see Valenstein 2006) because of a disagreement between researchers claiming that neurotransmission was electrical and those claiming it was chemical. While early studies demonstrated the existence of chemical neurotransmitters (Elliott 1905, Loewi 1957) there was still controversy over whether chemical release could occur at a speed that could account for the fast ’synaptic delay’ observed by Charles Sherrington that only lasted a fraction of a milisecond (Sherrington 1906). Studies at the neuromuscular junction eventually proved that neurotransmission was mediated by calcium dependent transmitter release (Fatt and Katz 1951) and that it could occur at a speed fast enough to agree with the observed ’synaptic delay’. This was subsequently shown to be true at central synapses as well (Kuno 1964).

We now know that the majority of synaptic transmission is mediated by chemical neurotransmitters and that only a small proportion operate via gap junctions that form direct electrical connections between cells (Bennett and Zukin 2004). In order to understand the structure and function of neural net-

works it is therefore important to be able to define the properties of identified synapses. The most important property of a synapse is of course the post-synaptic effect of the released neurotransmitters as this dictates the type of message being relayed. We can broadly define the effect of neurotransmitter binding as either excitatory (binding to post-synaptic receptors results in cell depolarization and aid generation of action potentials) or inhibitory (binding to post-synaptic receptors results in cell hyperpolarization and/or inhibits the generation of action potentials). The effect of a neurotransmitter is determined not only by the type of post-synaptic receptors present but also by the intrinsic properties of the cell. For example, due to changing intracellular chloride concentrations in the developing spinal cord, GABA transmission is depolarising and thus excitatory in the embryonic cord but in the mature cord it is hyperpolarising and thus inhibitory (see Sibilla and Ballerini 2009; and later chapters for further discussion).

However, the strength of a synaptic connection is not determined by the type of neurotransmitter released but is instead dependent on the synaptic architecture of the connections between the two cells. Connected neurons are known to make multiple connections between each other. The number of connections and where these connections are will influence the effect that neurotransmitter release has on the post-synaptic cell. It is therefore important to provide a quantitative description of synaptic connections.

Recordings of spontaneous end-plate potentials (EPPs) at the neuromuscular junction (NMJ) gave the first evidence that neurotransmitter release is a stochastic process (Fatt and Katz 1952). The observation that the variance of spontaneous EPPs was very low and that of evoked EPPs was high led to the idea that neurotransmitters are released in discrete all-or-none units (i.e. 'quanta') and that the synaptic response is composed of multiple quantal events (Del Castillo and Katz 1954). The concept of quantal release was supported by electron microscopy studies of synapses that showed vesicles are present at the pre-synaptic density (De Robertis and Bennett 1955, Palay and Palade 1955), giving a structural basis for the mechanism of neurotransmitter release. We now know that neurotransmitters are packaged into presynaptic vesicles and that during calcium influx vesicles fuse with the cell releasing neurotrans-

mitters into the synaptic cleft (Jessell and Kandel 1993).

The three basic parameters that are used to describe the operation of a synapse are: the quantal size q (which is defined as the post-synaptic response to a single 'quantal event' i.e. vesicle), the number of release sites n and the probability of release p (this is normally given as the average probability of release across all release sites as it is known that p can vary between sites Rosenmund et al. 1993, Murthy et al. 1997). However defining these synaptic properties experimentally has proven challenging and various methods of 'quantal analysis' that estimate these parameters have been developed. These methods have mainly involved analysis of electrophysiological recordings, occasionally combined with anatomical techniques. Modern imaging techniques have even allowed the estimation of quantal parameters at the level of single release sites. For example, labelling the cell membrane with FM dyes (Branco et al. 2008, Murthy et al. 1997, Zakharenko et al. 2001) and tagging vesicle proteins with pHlourins (Granseth et al. 2006, Gandhi and Stevens 2003) allows quantification of vesicle exocytosis and thus measurement of p.

1.4 Quantal Analysis

Initially statistical models were applied to electrophysiological data in order to validate the 'quantal hypothesis'. Modern quantal analysis techniques are used to estimate quantal parameters and describe of the properties of a given synapse. In early studies of the NMJ the distribution of quantal events was modelled using Poisson statistics (Del Castillo and Katz 1954) however a binomial model was soon found to be more appropriate when modelling synaptic transmission at central synapses (Kuno 1964). Poisson statistics were only applicable to the NMJ due to the large number of release sites and (experimentally controlled) low probability of release (Del Castillo and Katz 1954, Kuno 1964). Binomial or multinomial are more applicable for quantal analysis for central synapse because neither high n nor low p are likely to be true for connections in the CNS.

While the binomial model is an appropriate statistical tool to model neu-

rotransmitter release its application to experimental data is not a simple task. Attempts to use maximum likelihood estimation to derive quantal parameters from amplitude distributions resulted in large errors and this technique was found to be intractable for analysis of most synapses (Robinson 1976a). The number of release sites has been successfully estimated in studies that have combined quantal analysis methods with light and electron microscopy (Korn et al. 1982, Gulyás et al. 1993, Buhl et al. 1997). Most studies estimating quantal parameters rely on amplitude distributions, using the position of peaks as a measurement of q and then determining p from the amplitude distributions (Jack et al. 1981, Redman 1990). While compound binomial distributions have been applied to account for non-uniform release probabilities (Jack et al. 1981, Walmsley et al. 1988), interpretation of quantal peaks is complicated when quantal size and probability of release is not uniform (Stricker et al. 1996, Walmsley et al. 1988). Another complicating factor at central synapses is that, unlike at the NMJ, the quanta at central synapses are very small resulting from as few as 10-20 channel openings (Silver et al. 1996). This means that the signal to noise ratio at most synapses is very poor making quantal events difficult to distinguish from background noise and quantal peaks hard to separate from the distribution.

In order to overcome these limitations several techniques based on analysis of the moments of amplitude distributions were developed. The most widely used of these methods is multiple probability fluctuation analysis (MPFA) which uses the mean and variance of evoked responses recorded at several different release probabilities to estimate quantal parameters (Silver et al. 1998, Silver 2003). I will now briefly describe the theory behind MPFA and the issues surrounding its use for the analysis of experimental data.

1.4.1 Multiple probability fluctuation analysis (MPFA)

If synaptic transmission is modelled as a binomial process the mean amplitude of synaptic response is the product of the three quantal parameters i.e. $\bar{I} = npq$. The variance of responses can therefore be expressed with respect to the quantal parameters,

$$\sigma^2 = nq^2p(1-p) \tag{1.1}$$

The relationship between mean current and variance can be expressed as a parabolic function,

$$\sigma_I^2 = q\bar{I} - \frac{\bar{I}^2}{n} \tag{1.2}$$

MPFA is based on using the above parabolic function to estimate the quantal parameters. By plotting the mean and the variance of synaptic responses recorded at different probabilities of release and fitting a parabolic curve, the above equation can be used to derive estimates for q and n (see Figure 1.3). The quantal size can be calculated from the initial slope of the parabola (see Figure 1.3D and equation 1.2). The number of release sites can be obtained from the quotient of the maximal response over the quantal size, which can both be derived from the parabolic fit (see Figure 1.3D). Probability of release can then be estimated from the mean current of any data set that was recorded during a period of constant p using equation 1.1.

The simplicity of this method however does mean that it is subject to a number of disadvantages as it makes a number of assumptions. MPFA, in its simplest implementation, assumes that transmitter release is synchronous and independent across sites, and that the quantal size and probability of release are uniform at all release sites. These assumptions are unlikely to be true at real synapses. There is an inherent variability at the level of single sites due to the stochastic nature of release. Individual quanta are not released synchronously but instead are released over a finite time course (Barrett and Stevens 1972, Diamond and Jahr 1995, Isaacson and Walmsley 1995). The 'smearing' effect that arises from this variance between different quantal events produces a mean wave form from a single release site that has a lower peak amplitude than individual events (see Figure 1.4A). When PSCs have a rapid decay time constant asynchronous release can also produce an additional variance, because quanta released at different latencies will have different amplitude at the time point where peak amplitude is measured, even if the quantal size is the same. This variance associated with latency of release is a component of the

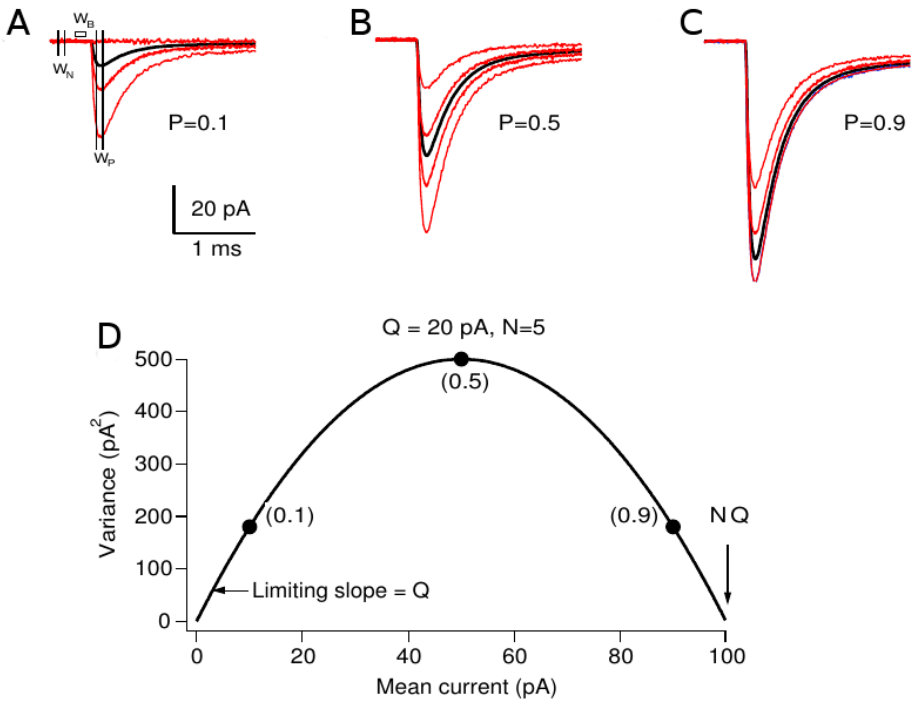

Figure 1.3: An illustration of multiple probability fluctuation analysis. Traces in A,B and C show simulated synaptic currents at a synapse that consists of five release sites and has a quantal size of 20 pA at probabilities of release of 0.1, 0.5 and 0.9 respectively. The open bar shown above trace A designated W_B shows an appropriate area to baseline the traces for the purpose of measuring peak amplitude. The vertical line designated W_N and W_P indicate appropriate windows for measuring the mean and variance of baseline noise and the mean peak of the PSC respectively. The graph in panel D shows the theoretical relationship between mean and variance of the peak PSC amplitude. The solid black line shows a parabolic fit of the simulated data displayed in panels A–C. Also indicated on the graph are the intial slope of the parabola that is used to estimate q and the x-intercept that is used to the estimate the product of n and q. Figure adapted from Silver (2003).

'intrasite variance' (see Figure 1.4A). The other component of intrasite variance is the variability of quantal size between events at individual release sites (Bekkers et al. 1990, Forti et al. 1997, Liu et al. 1999, Silver et al. 1996). There is also variability between the quantal size at different release sites (Bekkers et al. 1990, Borst et al. 1994). The variance of quantal size between release sites (Murthy et al. 1997, Hessler et al. 1993, Walmsley et al. 1988, Jack et al. 1981, Rosenmund et al. 1993) is a further source of variance and is normally referred to as intersite variability (see Figure 1.4B). While corrections for these added variances can be incorporated into MPFA (Silver 2003) they require separate estimation and cannot necessarily be derived from the data set recorded for the purposes of analysis. For example the total variance associated with both intra- and intersite variability can be determined by measuring the peak amplitude of evoked responses aligned by the stimulus in a low probability of release (i.e. with a failure rate of $\sim 80 - 90\%$), in the assumption that only currents mediated by single quanta are observed. However, in experiments with a high level of baseline noise and a small quantal size it may be difficult to distinguish single events, which may lead to an incorrect estimation of variance. The variance associated with different quantal release latencies can then be determined by measuring the peak amplitude of responses aligned by their rise time and deducting this from the total variance (in order to allow for incorporation of quantal variances into MPFA).

MPFA not only requires that recordings are made at many different release probabilities (in order to produce a good parabolic fit) but also requires a larger number of observations be made at each release probability in order to produce reliable estimate of n, p and q. Due to the difficulty of producing long recordings suitable for MPFA between the cell types that are the focus of this thesis, a quantal analysis method based on Bayesian statistics has been used. This is a recently published method (Bhumbra and Beato 2013) that will be explained in detail in the general methods chapter.

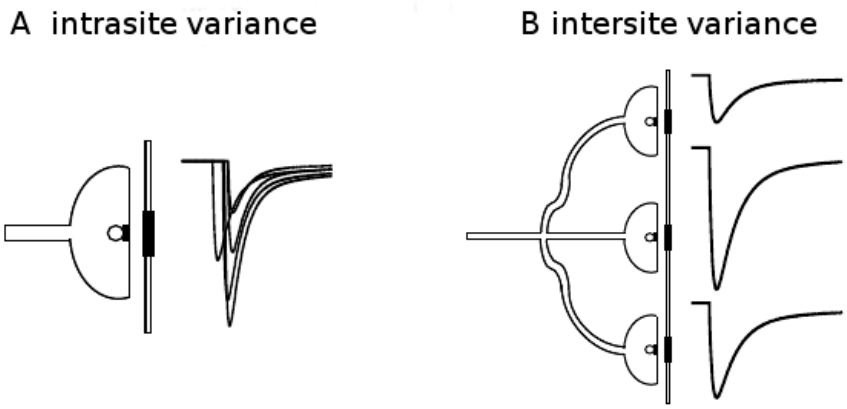

Figure 1.4: An illustration of intrasite and intersite quantal variance. Panel A describes the variance that arise from differences in release at a single synapse. The traces beside the synapse illustrate the variation in the precise timing of the response that can occur during release. Panel B describes the variance associated with differences due to release sites occuring on different parts of a neuron. The traces beside each synapses vary in size depending on their distance from cell soma and/or the recording electrode. Adapted from Silver (2003).

1.5 Aims

The aims of this thesis can be divided into two separate but complementary investigations of different aspects of spinal cord circuitry. The first investigation focuses on the co-release of GABA with glycine onto the spinal motoneurons in the juvenile mouse. The second study investigates the quantal properties of the motoneuron to Renshaw cell excitatory synapse.

As has been briefly discussed above, co-release of GABA with glycine onto mototneurons has been demonstrated in the young rodent spinal cord (Jonas et al. 1998, Jean-Xavier et al. 2007, Schneider and Fyffe 1992) and in the adult cat (Cullheim and Kellerth 1981). However there is also a known developmental shift postnatally in the rodent spinal cord from GABAergic to glycinergic inhibitory transmission (Gao et al. 2001). We therefore conducted a study of inhibitory contacts on lumbar motoneuron in order to determine if GABA is co-released with glycine onto motoneurons in the juvenile mouse spinal cord. This involved first conducting experiments to determine if GABA is co-detected

with glycine at motoneuron inhibitory synapses and subsequently assessing whether GABA is co-released with glycine but not co-detected, and if this has any effect on inhibitory transmission onto motoneurons.

Even though the motoneuron to Renshaw cell excitatory synapse was first described 60 years ago (Eccles et al. 1954) there are still some very basic questions about that synapse that remain unanswered. The second results chapter in this thesis focuses on estimating the quantal parameters at the motoneuron to Renshaw cell excitatory synapses, as well as determining the degree of convergence of motoneurons onto Renshaw cells. Analysing data from paired motoneuron to Renshaw cell recordings produced estimates of the number of contacts between motoneurons and Renshaw cells. Comparing this with quantal estimates obtained from analysis of Renshaw cell excitatory currents induced by ventral root stimulation allowed us to determine the degree of the convergence of motoneurons onto Renshaw cells.

Chapter 2

Materials and methods

Spinal preparations were dissected from mice in which the enhanced green fluorescent protein (EGFP) was expressed under the control of the promoter of the neuronal glycine transporter GlyT2 (Zeilhofer et al. 2005). The transgenic strain was used to assist identification of glycinergic neurons during recordings. All experiments were undertaken in accordance with the Animal (Scientific Procedures) Act (UK) 1986. The appropriate statistical tests were performed as indicated in the Results sections.

2.1 Spinal cord preparation

Animals were anaesthetised with urethane 1.8 mg/kg I.P.. Following decapitation, spinal cords were extracted using standard techniques (Beato 2008). After anaesthesia was confirmed by absence of the hindlimb flexor-extensor reflex following pinching of the paw the animal was pinned down with the ventral side facing up. The ribcage was then removed to expose the heart so intra-cardiac perfusion could be performed. Intra-cardiac perfusion was performed with ice cold normal artificial cerebrospinal fluid (aCSF) of composition (in mM) 113 NaCl, 3 KCl, 25 $NaHCO_3$, 1 NaH_2PO_4, 2 $CaCl_2$, 2 $MgCl_2$ and 11 D-glucose. The use of intra-cardiac perfusion improved the quality of the slices, due to the protective effect of low temperature on the tissue, that, during the dissection procedure, is not supplied anymore through normal blood

circulation. After intra-cardiac perfusion the animal was decapitated and the limbs and any remaining skin or viscera were removed. The spine and any remnants of the ribcage were then moved to a dissection chamber filled with oxygenated ice cold aCSF. The spine was pinned down ventral side up and the spinal cord was exposed following a ventral laminectomy. The spinal cord was rapidly dissected out by cutting away connective tissue until the cord could be gently removed from the spinal column. Once freed, the cord was 'cleaned' of any remaining connective tissue. Preparations were abandoned if time from decapitation to the cord being ready for slicing was longer than 25 minutes as, within our age range, this resulted in sub-optimal slice preparations.

Extracted spinal cords were sliced in one of three ways depending on experimental protocol, either transverse, oblique or coronal. In all slice preparations the dorsal side of the cord was adhered to an agar block with tissue glue (Vetbond, WPI Scientific Instruments) and slices were cut in oxygenated ice cold solution containing (in mM) 130 K-gluconate, 15 KCl, 0.05 EGTA, 20 HEPES, 25 D-glucose , 3 kynurenic acid and pH 7.4 (Dugué et al. 2005) using a VT1000 vibrating microtome (Leica Microsystems). The choice of a high potassium solution enormously improved the quality of the slices, especially the rate of motoneurons survival when compared to the more commonly used sucrose substitute slicing solution. This is possibly due to the fact that during slicing many of the motoneurons dendrites are cut. Before they spontaneously seal, the inside of the cell is inevitably exposed to the external solution. By using a low chloride and high potassium solution, we match the normal intracellular milieu of the cells. On the contrary, the use of high sucrose solution would cause the entry of sucrose from the cut arborization. Since sucrose cannot be transported outside te cell, it would tend to increase the intracellular osmolarity and therefore lead to swelling of the membranes. The use of high potassium slicing solution has proved to be particularly effective in cerebellar preparation (Dugué et al. 2005) as well as in the spinal cord (Lamotte d'Incamps et al. 2012). Since, in the presence of high potassium, all neurons become depolarized at an equilibrium potential of $\sim 0\,\mathrm{mV}$, spikes are inactivated, thus preventing release of potentially toxic neurotransmitter. However, since at depolarized potential the glutamate transporters can reverse their action (Szatkowski et al. 1990), it is

necessary to block glutamate receptors with kynurenic acid. Also, excitotoxicity of calcium is prevented by using a calcium chelator (EGTA).

Straight transverse slices of thickness 400 µm were cut from the lumbar segments (L2-L5, see 2.1A). Oblique sections, also of400 µm thickness, were cut from the same lumbar segments at a 35° angle relative to the axis of the spinal cord by cutting an agar block to the required angle prior to gluing the cord to the agar as described above (see 2.1B). During spinal cord preparations for oblique slices, ventral roots were preserved to allow for antidromic stimulation of motoneurons, whose axons project obliquely from the spinal cord in the caudal direction. For coronal slices, the cord was glued to the agar block in the same way as for transverse slices but the agar block was glued horizontally to the base of the vibratome microtome and the dorsal horns cut away just dorsal to the ventral canal (see 2.1C). This preparation gives visual access to the dorsal motor nucleai (innervating digits muscle) as well as to the most dorsal parts of the ventral motor nucleus (innervating mostly the tibalis and gastrocnemius muscle).

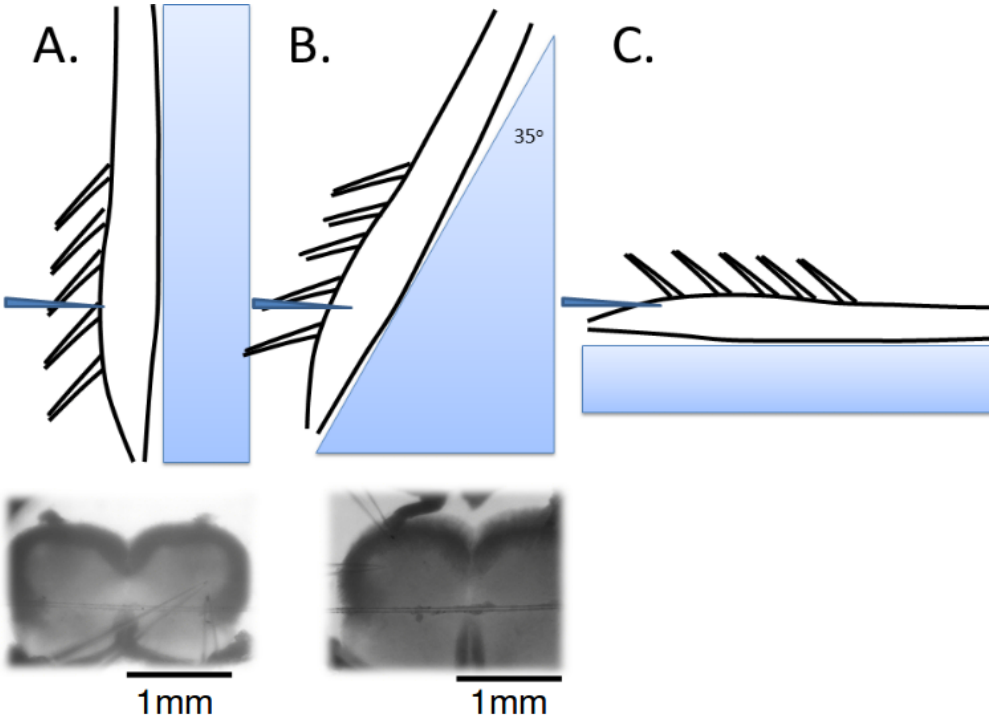

Figure 2.1: Illustration of spinal cord slicing methods. Diagram A shows a schematic illustration of a straight transverse slice with a infrared image of a transverse slice shown below. The diagram shows a spinal cord glue to a rectangular agar block and the relative position of the blade. Panel B shows a cord glued to an agar block cut, into a triangular shape, for the purpose of producing oblique slices. During oblique slice preparations every effort would be made to preserve ventral roots. An infrared image of an oblique slice is shown below diagram B and a preserved ventral root can be seen in the top left hand corner of the image. Diagram C shows a cord glued to a rectangular agar block, but positioned horizontally with respect to the blade, in order to cut away the dorsal horns.

After slicing tissue preparations were incubated at 37 °C in normal extracellular solution for approximately 45 minutes prior to experimentation. Experiments were performed at room temperature and slices were maintained by continuous perfusion of aCSF bubbled with a 95/5% O_2/CO_2 mixture at a rate of 5 ml/min to 8 ml/min.

2.2 Patch recordings

Whole cell voltage-clamp recordings were performed using an Axopatch 200B amplifier (Molecular Devices) and filtered with an eight-pole Bessel filter at 5 kHz. Both voltage and current signals were sampled at 50 kHz using an Axon 1440A interface device (Molecular Devices) and the data were acquired using Clampex 10 software (Molecular Devices).

Electrodes were pulled using a P-1000 Flaming/Brown micropipette puller (Sutter Instruments) from thick-walled borosilicate glass GC150F capillaries (Harvard Apparatus). Electrodes used to patch motoneurons for the purpose of voltage-clamp recordings were pulled to a resistance of $\sim 0.5\,\mathrm{M}\Omega$ and the tips fire polished to final resistance of $\sim 1.5\,\mathrm{M}\Omega$. Electrodes used to patch Renshaw cells were pulled to a resistance of $\sim 2\,\mathrm{M}\Omega$ and the tips fire polished to a final resistance of $3\,\mathrm{M}\Omega$ to $4\,\mathrm{M}\Omega$. Electrodes for loose cell attached stimulation of single cells were pulled to a resistance of $\sim 2\,\mathrm{M}\Omega$ and fire polished to a final resistance of $6\,\mathrm{M}\Omega$ to $7\,\mathrm{M}\Omega$.

Cells were visualised using infrared differential interference contrast (DIC) optics on an Eclipse E600FN (Nikon) with a $40\times$ water-immersion objective. For all voltage clamp recordings the series resistance ranged between $4\,\mathrm{M}\Omega$ to $10\,\mathrm{M}\Omega$ and was compensated by $60\,\%$ to $80\,\%$, if series resistance increased by more than $20\,\%$ the recording was abandoned. The typical motoneuron whole-cell capacitance of $\sim 200\,\mathrm{pF}$ and uncompensated series resistance of $1\,\mathrm{M}\Omega$ to $4\,\mathrm{M}\Omega$ gave a lowpass corner frequency of $0.2\,\mathrm{kHz}$ to $0.8\,\mathrm{kHz}$ which would filter currents. The typical Renshaw cell whole-cell capacitance of $\sim 30\,\mathrm{pF}$ and uncompensated series resistance of $1\,\mathrm{M}\Omega$ to $4\,\mathrm{M}\Omega$ gave a lowpass corner frequency of $1\,\mathrm{kHz}$ to $5\,\mathrm{kHz}$.

2.2.1 Paired recordings

In order to target EGFP positive interneurons, we used a custom built optical set up that allowed simultaneous visualization of cells with infrared (differential interference contrast) and fluorescence. We used a beam splitter that reflects the long wavelength (700 nm) infrared signal and transmitted the shorter

wawelength emitted by EGFP (510 nm). The emitted fluorescence was either directed to a high sensitivity camera (Qimaging, Retiga) or to a scanning confocal D-Eclipse C1 camera (Nikon). The simultaneous visualization (see Figure 2.2) was essential in obtaining a quick and unambiguous identification of green cells to be targeted for patching and allowed us to test for connectivity up to 3-4 cells every 5 minutes, while maintaining the recording from the post-synaptic cell.

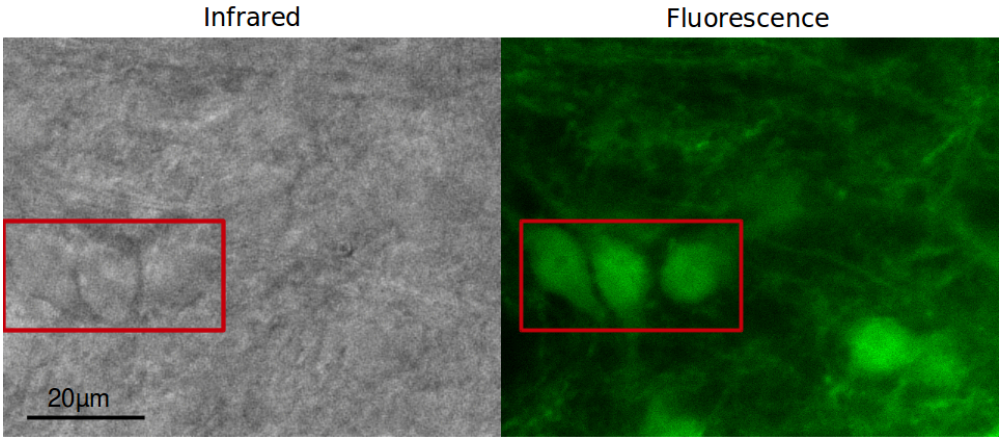

Figure 2.2: Simultaneous visualisation of eGFP positive interneuons with infrared and fluorescence images. The picture on the left shows an infrared image (taken with differential interference contrast) of cells in a lumbar slice taken from a P8 mouse. The picture on the right shows the same eGFP flourescence emitted by the same section of cells which allows visualisation of only the eGFP positive cells. Comparison of the infrared and fluorescence images allows identification of the eGFP postitive in the infrared image (see the red box in both images for an example).

Inhibitory interneuron to motoneuron paired recordings

Paired recordings of pre-synaptic inhibitory interneurons and post-synaptic motoneurons were performed in transverse slices to maximise the number of connections in each slice and therefore increase the chance of finding pairs of connected cells. Electrodes for post-synaptic motoneuron recordings were filled with an internal solution of composition (in mM) 140 CsCl, 4 NaCl, 0.5 $CaCl_2$, 10 HEPES, 5 EGTA, 2 Mg-ATP, QX-315 Br 3, pH 7.3 with CsOH, and osmolarity of 290−310 mOsm. High intracellular chloride improves the signal to noise

ratio by increasing the driving force for chloride across the cell membrane. This is particularly useful when recordings from motoneurons due to their large resistance resulting in large baseline noise. High intracellular chloride however does affect both glycinergic (Pitt et al. 2008) and GABAergic (Houston et al. 2009) currents through interactions with amino acids in the pore-lining region of the channels (Moroni et al. 2011) resulting in a prolonged decay phase of both types of IPSCs. However this intracellular solution does allow direct comparisons with previously published work by Jonas et al. (1998).

After establishing a stable whole cell patch on a motoneuron, a second electrode of $\sim 6\,\mathrm{M}\Omega$ resistance filled with normal aCSF was introduced into the Renshaw cell area (Alvarez and Fyffe 2007). Putative pre-synaptic neurons were patched in a loose cell-attached voltage-clamp configuration to stimulate the membrane and record evoked spikes (Barbour and Isope 2000). Neurons were stimulated using a $1\,\mathrm{V}$ to $1.5\,\mathrm{V}$ voltage step of $20\,\mu\mathrm{s}$ applied from an ELC-03X (NPI) amplifier.

Connected cells were identified by the presence of time locked motoneuron post-synaptic currents evoked by spikes in the pre-synaptic cell. Figure 2.3 shows a typical loose cell attached recoding in which extracellularly evoked and recorded spike induces an IPSC in a motoneuron. Typically 1 out of 100 tested interneurons was connected to the recorded motoneuron. After the pre-synaptic cell was identified the stimulating electrode was removed and the interneuron was patched whole cell with an electrode containing an internal solution of composition (in mM) K-gluconate 125, KCl 6, $CaCl_2$ 2, HEPES 10, Mg-ATP 2, pH 7.3 with KOH, and osmolarity of $290-310$ mOsm. In whole cell current-clamp configuration pre-synaptic cells were stimulated every $10\,\mathrm{s}$ using an ELC-03X amplifier (NPI) by application of the minimum positive current required to evoke an action potential reliably.

Motoneuron to Renshaw cell paired recordings

Paired recordings of pre-synaptic motoneurons and post-synaptic Renshaw cells were performed using oblique slices. EGFP positive cells were patched in a region ventro-medial to the motor nucleus (i.e. the 'Renshaw cell area' Al-

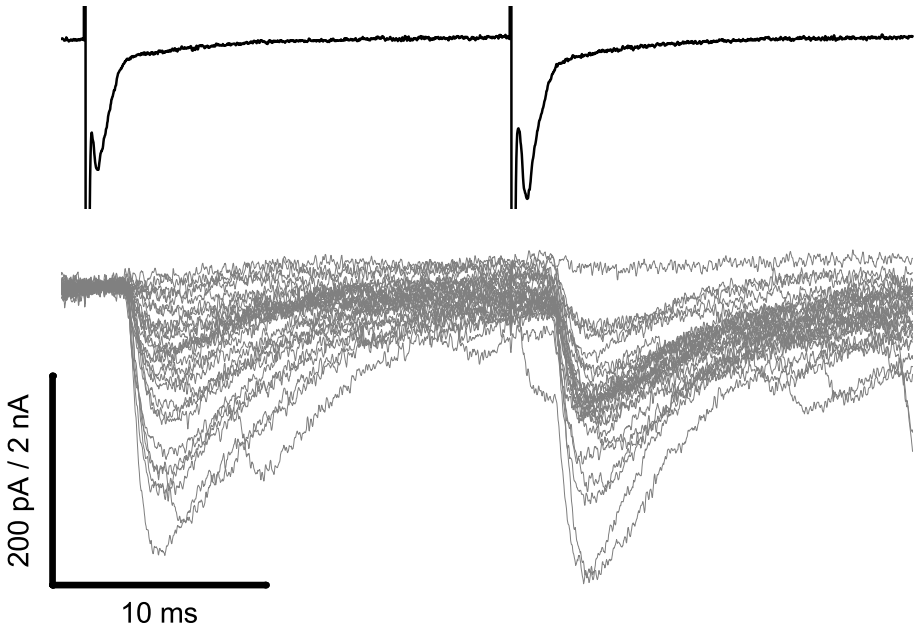

Figure 2.3: Paired recordings with extracellular loose cell-attached stimulation of an interneuron can be used to identify a connection with a motoneuron. The upper trace illustrates two extracellulary evoked spikes
(see Methods), clearly visible as downward deflections, from an interneuron patched in a loose cell-attached configuration. Post-synaptic responses of the motoneuron, illustrated in the lower trace, demonstrate a connection as IPSCs time-locked to the spikes. Following a 20 ms interval a second spike was evoked to potentiate the synapse and reduce the failure rate.

varez and Fyffe (2007)). Patched cells were identified as Renshaw cells by the presence of an evoked EPSC following ventral root stimulation. Renshaw cells were patched whole cell with $3\,\mathrm{M}\Omega$ to $4\,\mathrm{M}\Omega$ electrodes (produced as described above) filled with a K-gluconate based internal solution composed of (in mM) K-gluconate 125, KCl 6, $CaCl_2$ 2, HEPES 10, Mg-ATP 2, pH 7.3 with KOH, and osmolarity of $290-310$ mOsm.

After whole cell patch of a Renshaw cell an extracellular stimulation electrode filled with normal aCSF was introduced into the motor nucleus. As explained above, the putative pre-synaptic motoneuron was patched in the loose cell-attached voltage-clamp configuration and a spike was evoked by delivering

a short voltage step. A connection was identified in the same way as described above for interneuron to motoneuron paired recordings (see Figure 2.3). After identification of a pre-synaptic motoneuron the loose cell-attached stimulation electrode was carefully removed from the slice and the identified motoneuron re-patched whole cell. Pre-synaptic motoneurons were patched with an electrode fire polished to a final resistance of $\sim 3\,\mathrm{M}\Omega$ (slightly higher than that described for voltage clamp motoneuron recordings) in order to improve chances of a successful and stable patch. Motoneuron electrodes were filled with the same K-gluconate based solution used for pre-synaptic interneurons in the paired recordings described above. Pre-synaptic motoneurons were then held in whole cell current-clamp configuration and stimulated every $10\,\mathrm{s}$ using an ELC-03X amplifier (NPI) by application of the minimum positive current required to evoke an action potential reliably.

2.2.2 Ventral root stimulation

Ventral roots were stimulated as described by Lamotte d'Incamps and Ascher (2008) via a glass pippette adapted to the size of the ventral root ($60\,\mu\mathrm{m}$ to $100\,\mu\mathrm{m}$) filled with aCSF. An electrical current was applied using a DS3 constant current stimulator (Digitimer). Stimulus intensity ranged from $3.2\,\mathrm{mA}$ to $32\,\mathrm{mA}$ and stimulus durations varied between $20\,\mu\mathrm{s}$ to $500\,\mu\mathrm{s}$. Ventral roots were stimulated every $10\,\mathrm{s}$ at a frequency of $33\,\mathrm{Hz}$ unless otherwise stated in the text.

2.3 Quantal analysis

Estimates of quantal parameters were calculated from electrophysiological data using Bayesian quantal analysis (Bhumbra and Beato 2013; BQA,). BQA has several advantages over the more commonly used multiple probability fluctuation analysis (MPFA Silver 2003) that make BQA our preferred method. While MPFA only uses the mean and variance of the measured amplitude of synaptic currents, BQA estimates the quantal parameters from the whole amplitude distribution of observed events. The reduction of data sets to only the moments of

their distribution means that there is substantial loss of information contained in the data when performing MPFA. This is illustrated in Figure 2.4. Figure 2.4A shows peak amplitudes of 58 evoked IPSCs recorded at a single probability of release and the amplitude distribution of the same data set is shown below in figure 2.4B. The information taken from this data set in order to perform MPFA is shown in Figure 2.4C as a variance-mean plot. While the error associated with the mean is relatively small there is a considerable error associated with the variance ($350\,\text{pA}^2$ Fig.2.4C). The error associated with the variance is calculated as described by Silver (2003) (error of variance$= \sqrt{2/n-1}$) where n is the number of observations.) The error on the variance is particularly affected by the number of observations and since it cannot be assumed that long stable recordings will always be possible, especially during paired recordings, it is an error that is likely to confound MPFA estimates.

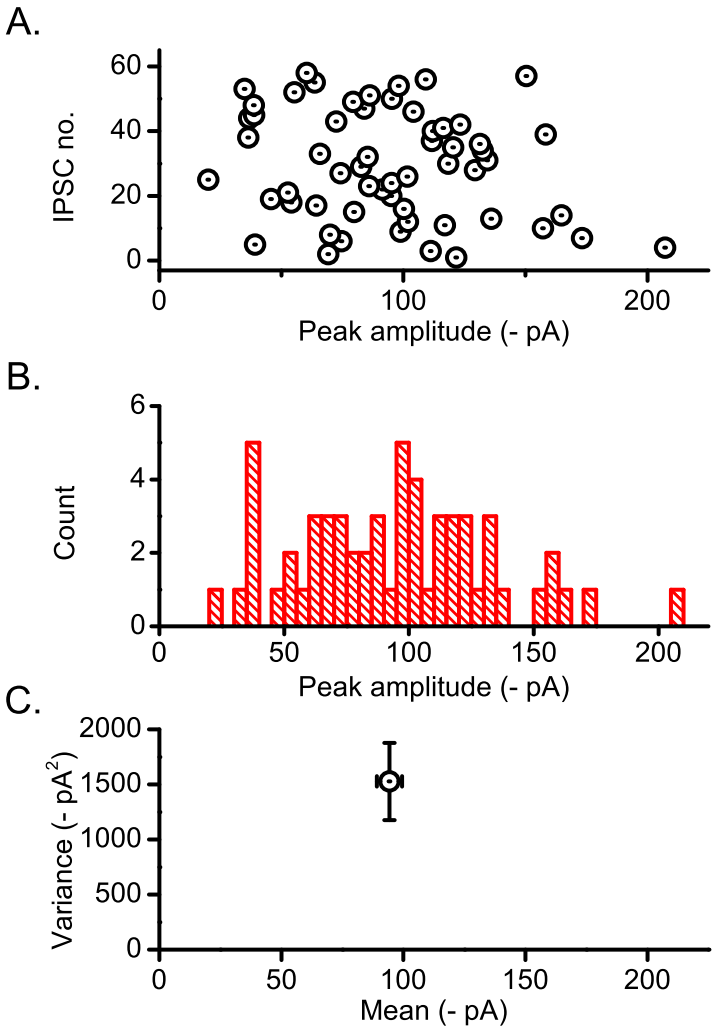

Figure 2.4: Example of data set used for quantal analysis. The graph in panel A shows a scatter plot of EPSCs recorded from a Renshaw cell evoked by ventral root stimulation. Panel B shows the amplitude histogram of the evoked response shown in graph A. Panel C shows the mean plotted against the variance of the data described above

MPFA requires a large number of observations at individual release probabilities, as well as recordings obtained at many different release probabilities in order to obtain an adequate parabolic fit. BQA on the contrary produces reliable estimates from recordings at only two probabilities of release with even from a small number (approximately 50) of observations for each probability (Bhumbra

and Beato 2013). Due to the difficulty in producing long stable recordings from our chosen cell types it is advantageous to use BQA instead of MPFA.

The most important advance that BQA provides over earlier quantal analysis methods is that it both models amplitude distributions (Korn et al. 1981) and allows incorporation of data recorded at multiple probabilities of release (Silver et al. 1998). Prior to the development of BQA these approaches were generally considered to be incompatible. In this methods section I will first describe the quantal likelihood function that BQA uses to model amplitude distributions at different release probabilities. Then after a brief explanation of the general concept of Bayesian analysis I will show how BQA uses Bayes' rule to incorporate the information from distributions that represent different release probabilities in the estimation of quantal parameters. The key step in this process is a re-parameterisation that allows for quantal parameters to be expressed as variables that are independent of probability of release p. While BQA can be modified to calculate any given set of parameters, here we use the same parameters originally used by (Bhumbra and Beato 2013). Our BQA analysis results in estimates of the quantal size q, the maximal response r (defined as the product of the number of release sites n and q) and the quantal coefficient of variations CV. From estimates of the quantal size and maximal response we can derive the number of release sites by dividing the latter by the former (i.e. $n = q/r$). The probability of release in any recording condition can be calculated by the quotient of the mean response size μ and the maximal response r (*i.e.* $p = \mu/r$).

2.3.1 Quantal likelihoods

The 'quantal likelihood function' describes the amplitude distribution of evoked responses x as a function of the set of parameters $\mathbf{\Phi}$ and is denoted by $\mathcal{Q}\left(x|\mathbf{\Phi}\right)$ that indicates the likelihood of observing the response x given the parameters $\mathbf{\Phi}$.

The $\mathcal{Q}$ function has to contain at least three elements. Firstly, a probability density function that describes the amplitude distribution of uniquantal events. Secondly, a probability mass function to describe the weighting coefficients

for the relative probabilities of observing $(1, 2, \ldots, n)$ numbers of vesicles released. Finally, a probability density function that describes the baseline noise. The three elements in our implementation are:

1. A continuous probability density function that models the amplitude distribution for a single successful quantal event. Here we use a gamma density function $\mathcal{G}(x|\gamma, \lambda)$ expressed with respect to the shaping parameter γ and the scaling parameter λ:

$$\mathcal{G}(x|\gamma,\lambda) = \frac{1}{\lambda^{\gamma}\Gamma(\gamma)} x^{\gamma-1} e^{\frac{-x}{\lambda}}, x, \gamma, \lambda > 0, \quad \Gamma(\gamma) = \int_0^{\infty} g^{\gamma-1} e^{-g} dg \quad (2.1)$$

   where g is the dummy variable of the integration and the quantal size can be expressed as the product of the parameters:

$$q = \gamma\lambda \quad (2.2)$$

   An example of a gamma probability density function ($\gamma = 11.1, \lambda =$9 pA) is shown in Figure 2.5A. The choice of a gamma function is dictated by several reasons. The first is that gamma distribution of uniquantal release gives a better description of data when compared with a gaussian model due to the possibility of gamma to account for the typical positive skew in the data (MacLachlan 1975, Robinson 1976b). In fact while intrasite variability gives rise to symmetrical distributions (Silver et al. 1996), there is no reason to assume symmetry for intersite variability (Robinson 1976b). The second is that for large values of γ the gamma distribution approximates a Gaussian therefore the gamma model can also describe Gaussian distributions although the opposite is not generally true. Finally, the convolution of multiple identical gamma probability density functions can be simply obtained by multiplication of the shaping parameters γ with the number of convolved components, similar to the convolution of multiple gaussian curves.

2. Assuming homogeneous probability of release we can use a simple binomial model to describe the probability of observing i successes from n quantal events.

$$\mathcal{B}(i|n,p) = \frac{n!}{i!(n-i)!}p^i(1-p)^{n-i}, 0 \leq i \leq n, \qquad 0 \leq p \leq 1 \tag{2.3}$$

An example of a binomial distribution describing six release sites of probability 0.35 is shown in 2.5B.

3. We used a normal probability density function $\mathcal{N}(x|0,\epsilon^2)$ where the mean is zero and the variance is ϵ^2 to model the the background noise.

$$\mathcal{N}(x|0,\epsilon^2) = \frac{1}{\sqrt{2\pi\epsilon^2}}e^{-\frac{x^2}{2\epsilon^2}}, \epsilon > 0 \tag{2.4}$$

ϵ^2 is calculated directly from raw traces as the variance of failures and is not estimated by BQA. An example of a normal probability density function of variance $625\,\text{pA}^2$ (standard deviation $25\,\text{pA}$) is shown in Figure 2.5C.

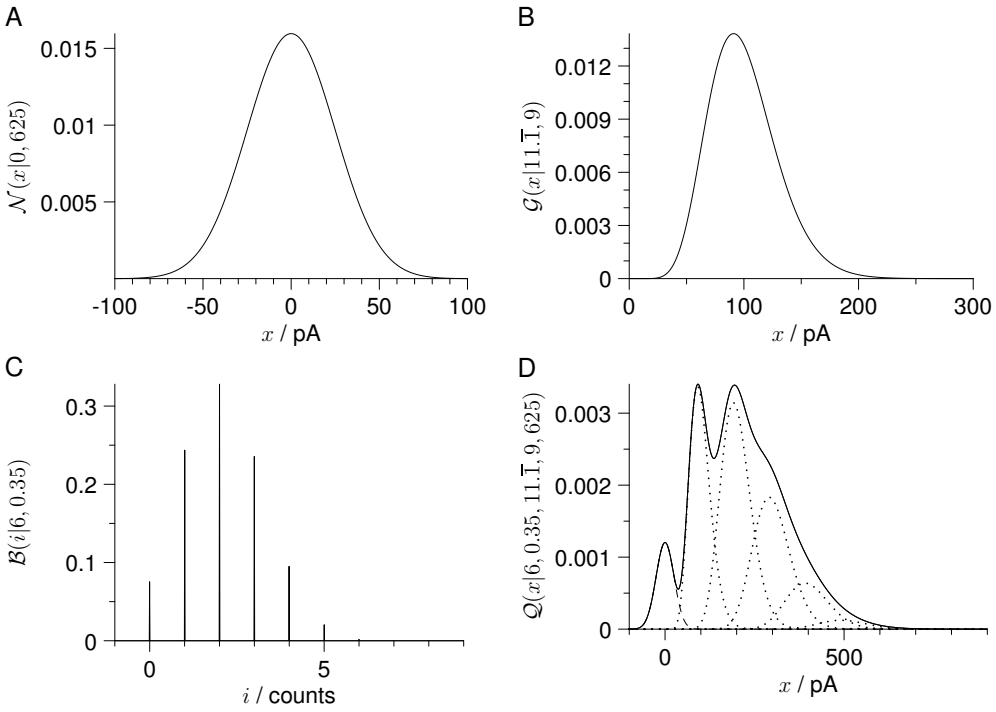

Figure 2.5: An illustration of the quantal likelihood function. Panel A shows an example normal probability density function (of mean 0, variance 625 pA^2 and standard deviation 25 pA) that is used to model baseline noise. Panel B shows an example gamma density function ($\gamma = 11.1, \lambda = 9$ pA) that is used to model the amplitude distribution of a single successful quantal event. Panel C shows a binomial distribution that describes the probability of observing i Bernoulli successes from six release sites each with a probability of release of 0.35. Finally, panel D illustrates the quantal likelihood function, as described by $Eq.2.5$, that combines the other three components described in this figure to model the probability distribution of a set of evoked responses. Figure adapted from Bhumbra and Beato (2013).

We can therefore combine these three elements to express the quantal likelihood function $\mathcal{Q}\left(x|n, p, \gamma, \lambda, \epsilon^2\right)$ with a gamma function to describe the release of single quanta, a binomial distribution to the describe multiple quantal events and a normal distribution to model background noise.

$$\mathcal{Q}(x|n, p, \gamma, \lambda, \epsilon^2) = \mathcal{B}(0|n, p)\mathcal{N}(x|0, \epsilon^2) + \sum_{i=1}^{n} \mathcal{B}(i|n, p)\mathcal{G}(x|i\gamma, \lambda) \qquad (2.5)$$

As the number of successes increases the additive effects of the the back-

ground noise become extremely small with respect to the size of multi-quantal events. We therefore excluded the additive effects of background noise from the summation. An example of the quantal likelihood function combining the three elements described above is shown in Figure 2.5D.

For individual sets of data recorded at a single release probability the joint likelihood $\mathcal{L}$ of the data $\mathbf{x}$ given the parameters of the quantal likelihood function above can be expressed as a product (assuming the data are independent and identically distributed).

$$\mathcal{L} = \prod_{\mathbf{x}} \mathcal{Q}(\mathbf{x}|n, p, \gamma, \lambda, \epsilon^2) \tag{2.6}$$

Using Equation 2.6 the quantal parameters can be obtained by standard likelihood maximisation procedures (Korn et al. 1981). However, when combining observations obtained with different levels of release probability, the requirement for identically distributed data is not met, because evoked responses recorded at different release probabilities would be described by different probability density functions. As a consequence, the likelihood values obtained from individual conditions, cannot be simply multiplied to obtain a 'global' likelihood value (Huzurbazar 1948).

Even though the numerical values of the likelihood in each condition are not normalized and thus arbitrary, they will still be proportional to the conditional probability distribution of the parameters given the data $f(\mathbf{\Phi}|\mathbf{x})$ (Fisher 1922). By defining c as a constant of proportionality the likelihood can be scaled to express the conditional probability density function.

$$f(\mathbf{\Phi}|\mathbf{x}) = c\mathcal{L} \tag{2.7}$$

The proportionality constant c will differ for each condition, but knowing its value for each condition would allow multiplication of each probability distribution (one per experimental conditions) to obtain a global probability distribution for the set of parameters conditional to the observed sets of data.

The values of c for each of the conditions will be be affected by the number of observations as well as by the integral of the likelihood calculated over the

whole parameter space. In the past it has been implicitly assumed that c is the same for all conditions. This assumptions gives equal weight to all conditions and lead to a global maximisation of the product of each likelihood, an approach that is often used for the fitting of single channel recordings to a kinetic model (see for instance Burzomato et al. 2004). This approach would bias the estimates towards highly tuned models that perform near-perfects fits to only a proportion of the data. A large peak in density would occur over a small volume of parameter space, the corresponding mass in probability would be small and thus could represent a highly improbable solution. Most importantly, different amplitude distributions observed at different release probabilities would give rise to different regions and volumes of likelihood peaks; since they would also differ in their likelihood integrals across parameter space, any attempt of global likelihood calculation by multiplication would be confounded.

It would therefore be incorrect to make any arbitrary assumptions about c and thus it is not possible to use maximum likelihood estimation for simultaneous fitting of data described by different probability distributions, as is the case with quantal analysis, for which in each recording condition, the values for quantal size and number of release sites are common across conditions, but the probability of release is not. With our approach, instead of relying on assumptions about c we calculate it directly using the standard rules of probability and Bayes' rules as described below.

2.3.2 Bayesian modelling

In order to describe Bayesian modelling briefly, consider A and B to be two propositions that may be either true or false. The joint probability of both being true $P\left(A, B\right)$ can be expressed with respect to the conditional probability $P\left(A|B\right)$, which represents the probability of A being true 'given' B is true, using a product according to the chain rule.

$$P(A, B) = P(B) \times P(A|B) \tag{2.8}$$

$P\left(B\right)$ can be obtained from the joint probability of $P\left(A, B\right)$ by summation over all possible outcomes for A according to the sum rule.

$$P(B) = \sum_{A} P(A, B) \tag{2.9}$$

The joint probability of $P\,(B, A)$ can be expressed in a similar manner as $P\,(A, B)$ is in Eq.2.8 by interchanging the terms A and B.

$$P(B, A) = P(A) \times P(B|A) \tag{2.10}$$

Since $P(A, B) = P(B, A)$ we can equate the right hand of Eq.2.8 and Eq.2.10

$$P(A) \times P(B|A) = P(B) \times P(A|B) \tag{2.11}$$

$$\text{therefore } P(B|A) = \frac{P(B) \times P(A|B)}{P(A)} \tag{2.12}$$

Equation 2.12 is Bayes' rule. BQA uses this rule to model the distribution of observed data $\mathbf{x}$ with respect to hypothetical parameters $\boldsymbol{\phi}$. Since both $\mathbf{x}$ and $\boldsymbol{\phi}$ represent numerical values rather than mutually exclusive events we use a probability density function f rather than discrete P values. By substituting A with the observed data $\mathbf{x}$ and B with the hypothetical parameters $\boldsymbol{\phi}$ we can use Equation 2.12 to represent a Bayesian model of our data and parameters.

$$f(\boldsymbol{\phi}|\mathbf{x}) = \frac{f(\boldsymbol{\phi}) \times f(\mathbf{x}|\boldsymbol{\phi})}{f(\mathbf{x})} \tag{2.13}$$

The Bayesian model shown above consists of four terms. The left hand side represents the outcome of BQA, namely, the probability distribution of the values of the parameters $\boldsymbol{\phi}$ given the observed set of data. This term is the 'posterior' and the position of its maximum in the parameter space determines the values of $\boldsymbol{\phi}$ that may best describe the data $\mathbf{x}$. The conditional probability of the data $\mathbf{x}$ given the parameters $\boldsymbol{\phi}$, $f(\mathbf{x}|\boldsymbol{\phi})$ is the likelihood of the observations given the set of parameters and can be calculated from the likelihood function described in Equation 2.5. The term $f(\boldsymbol{\phi})$ is an unconditioned probability and

can be interpreted as the probability distribution of the hypothetical parameters in the absence of data. In Bayesian statistics this is normally called 'prior' because its functional form is decided *a priori* and each of the modelled parameters may have its own prior. While this may appear to introduce an arbitrary assumption, in most applications the exact choice of priors has little effect on the outcome of the modelling as long as the choice of prior is 'non-informative'. 'Non-informative' priors may be chosen according to mathematical criteria that minimize the amount of information they represent by the shape of their distribution (Jaynes 2003) or functional form (Jeffrey's rule, Jeffrey 1998). For instance, if we were modelling the outcome of a series of coin throws, we could model it with a uniform prior centered at values of $P = 0.5$ for either head or tail (zero information). If the coin is not fair, the running of the experiment would gradually modify the posterior, biassing towards the more probable outcome (be it heads or tails).

The denominator term $f(\mathbf{x})$ is the 'probability of data' and is sometimes referred to as the 'evidence'. In analogy with Equation 2.9 we can express $f(\mathbf{x})$ as the sum of the joint probability of the parameters and the data $f(\mathbf{x}, \phi)$ over the whole parameter space. Since the parameters are continuous numerical values the summation is replaced by integration.

$$f(\mathbf{x}) = \int_{\boldsymbol{\phi}} f(\mathbf{x}, \boldsymbol{\phi}) d\boldsymbol{\phi} \tag{2.14}$$

The 'probability of data' is just a normalization constant that ensures unity in the integral of the posterior. The term $f(\mathbf{x}, \boldsymbol{\phi})$ can be expressed in a similar way to that described in $Eq.$ 2.10.

$$f(\mathbf{x}, \boldsymbol{\phi}) = f(\boldsymbol{\phi}) \times f(\mathbf{x}|\boldsymbol{\phi}) \tag{2.15}$$

We can therefore substitute $Eq.$ 2.14 into $Eq.$ 2.13 to express the normalization procedure as;

$$f(\boldsymbol{\phi}|\mathbf{x}) = \frac{f(\boldsymbol{\phi}) \times f(\mathbf{x}|\boldsymbol{\phi})}{\int_{\boldsymbol{\phi}} f(\boldsymbol{\phi}) \times f(\mathbf{x}|\boldsymbol{\phi}) d\boldsymbol{\phi}} \tag{2.16}$$

If we consider $f(\boldsymbol{\Phi}|\mathbf{x})$ to constitute the probability of two hypothetical pa-

rameters, ϕ_1 and ϕ_2, given the data (i.e. $\mathbf{\Phi} = (\phi_1, \phi_2)$), the posterior becomes the joint probability distribution $f(\phi_1, \phi_2|\mathbf{x})$. The posterior for the parameter ϕ_1 only, $f(\phi_1|\mathbf{x})$, can be evaluated by integrating the joint probability distribution over all the possible values of the parameter ϕ_2

$$f(\phi_1|\mathbf{x}) = \int_{\phi_2} f(\phi_1, \phi_2|\mathbf{x}) d\phi_2 \tag{2.17}$$

The advantage of this approach is that since we are dealing with probabilities and probability mass functions, the usual rules of probability apply. In particular, we can choose to reparametrize our distribution according to continuous functions of our initial parameters. We can express a set of parameters Ψ as a function of our previous set of parameters $\mathbf{\Phi}$ in the form $\Psi = F(\mathbf{\Phi})$ and that the function F is invertible, namely, there exists a function F^{-1} such that $\mathbf{\Phi} = F^{-1}(\Psi)$.

We can then reparametrize our posterior with respect to new parameters $\boldsymbol{\psi}$. The transformation in probability space can be evaluated by integrating over regions of probability space in which the initial and final parameters are constrained by the functional form $\mathbf{\Phi} = F^{-1}(\boldsymbol{\psi})$.

$$f(\boldsymbol{\psi}|\mathbf{x}) = \int_{\boldsymbol{\phi}=F^{-1}(\psi)} f(\boldsymbol{\phi}|\mathbf{x}) d\phi \tag{2.18}$$

We will use reparameterization to estimate quantal parameters from a data set containing observations recorded at different probabilities of release.

2.3.3 Quantal probabilities

We now consider a data set similar to the data recorded for quantal analysis with K number of conditions of release probability within the data X. X will be comprised of K vectors x_k ($k = \{1, 2, ..., K\}$) that may differ in number of observations. The model assumes that amplitude distributions will vary only as a result of differences in release probability p_k. We can represent the family of likelihoods $\mathcal{L}_k$ as the conditional probabilities of the data x_k given the parameters $\boldsymbol{\phi}_k$.

$$\mathcal{L}_k = f_k(\mathbf{x}_k|\boldsymbol{\phi}_k), \qquad k = \{1, 2, \ldots, K\} \tag{2.19}$$

Terms are subscripted with k as they correspond to different likelihoods associated with different release probabilities. Each likelihood term represents an unnormalised probability whose absolute value is entirely arbitrary unless it is multiplied by its respective scalar constant as described in Eq.2.7.

$$f_k(\boldsymbol{\phi}_k|\mathbf{x}_k) = c_k\mathcal{L}_k = c_k f_k(\mathbf{x}_k|\boldsymbol{\phi}_k) \tag{2.20}$$

Using Bayes's rule, expressed in Eq.2.12, the constants c_k can be substituted with the quotient of the two unconditioned probabilities (the 'prior' and the 'evidence'), giving

$$f_k(\boldsymbol{\phi}_k|\mathbf{x}_k) = \frac{f_k(\boldsymbol{\phi}_k)f_k(\mathbf{x}_k|\boldsymbol{\phi}_k)}{f_k(\mathbf{x}_k)} \tag{2.21}$$

The equation above illustrates that the product of every likelihood $f_k(\mathbf{x}_k|\phi_\mathbf{k})$ with the probability of the parameters in the absence of data $f_k\left(\boldsymbol{\phi}_k\right)$ (the prior) is proportional to each corresponding conditional probability of the parameters given the data $f_k(\boldsymbol{\phi}_k|\mathbf{x}_k)$(the posterior). The denominator terms $f_k(\mathbf{x}_k)$ (the evidence) are normalization scalars that can be evaluated as described above in Eq.2.14, giving

$$f_k(\boldsymbol{\phi}_k|\mathbf{x}_k) = \frac{f_k(\boldsymbol{\phi}_k)f_k(\mathbf{x}_k|\boldsymbol{\phi}_k)}{\int_{\boldsymbol{\phi_k}} f_k(\boldsymbol{\phi}_k)f_k(\mathbf{x}_k|\boldsymbol{\phi}_k)d\boldsymbol{\phi}_k} \tag{2.22}$$

In the BQA implementation used in this thesis we use the likelihood function shown in Eq.2.5 and assign priors based on the probability of release p_k, the total quantal coefficient of variation v and the number of release sites n, so $\boldsymbol{\phi}_k = (p_k, v, n)$. The variance of the background noise ϵ^2 that appears in the likelihood function is not evaluated as a parameter but it is calculated directly from the raw traces. Furthermore, in agreement with the binomial model of release, we assume that the probability of release p_k is proportional to the mean reponse μ_k. For each of the parameters $\boldsymbol{\phi}_k = (p_k, v, n)$ we choose

a prior probability function that is non-informative but incorporates the known constraints on each of the parameters. In particular, the coefficient of variation cannot be less than 0 and the probability of release is constrained in the range of $(0, 1)$. On the other hand, the number of release sites n has an obvious lower limit ($n = 1$) but no upper bound. Upper limits for n are therefore decided on a case by case basis by the user before analysis and analysis is re-run in cases where estimates of n tend towards the limit set by the user. For a detailed description of the rationale and choice of individual priors see Bhumbra and Beato (2013).

Our parameter space $\mathbf{\Phi}$ includes a variable that depends on the recording conditions, namely the release probability p_k. As a consequence, posterior distributions cannot be combined directly. Therefore, we resorted to a change of variables that removes the explicit dependency of individual posteriors from the probability of release by using the knowledge of the expression of the mean amplitude of synaptic responses as $\mu_k = nqp_k$. Our chosen new parameters are the quantal size q, the maximal response r and the gamma shaping parameter γ i.e. $\Psi = (q, r, \gamma)$. Since none of these parameters are dependent on release probability, we can define a probability density function that applies to all data sets recorded at different release probabilities. Our joint posterior $f\left(\Psi|\mathcal{X}\right)$ is thus proportional to the product of the posteriors expressed as a function of the transformed set of parameters

$$f(\boldsymbol{\psi}|\mathcal{X}) \propto \prod_{k=1}^{K} f_k(\boldsymbol{\psi}|\mathbf{x}_k) \tag{2.23}$$

The two distributions shown in Figure 2.6 A-B represent the individual posterior distributions for two different conditions of release probability ($f_k(\boldsymbol{\psi}|\mathbf{x}_k)$ with $k = 1$ and $k = 2$ corresponding to $p = 0.1$ and $p = 0.8$ respectively, using the notation employed above). Note that for simplicity we performed a summation over γ and thus are showing the posteriors as a function of two parameters only (q and r). As in Equation 2.23, the overall posterior $f(\boldsymbol{\psi}|\mathcal{X})$ is obtained from the product of the individual ones and is shown in 2.6 C.

Once a normalization is obtained (by dividing by the evidence), the posterior distributions for each individual parameter can be calculated by integrating

over the remaining parameters, giving rise to one unidimensional probability density for every parameter (see Figure 2.6 D-F). We obtain the estimates for q, r and γ from the medians of their individual posteriors. While we do not model the number of release sites n, probability of release p or coefficient of quantal variance CV directly we can calculate them using the estimates of parameters we have modelled. Since we define the maximal response as the mean response when probability of release equals one then $r = nq$, we can therefore use best estimates of r and q to calculate n (i.e. $n = r/q$). Similarly we can estimate the probability of release in any condition by dividing the respective mean response μ_k by the maximal response (i.e. $p_k = \mu_k/r$). Based on these estimates for n and q the model can be used to produce predicted distributions for any given p. An example of predicted distributions are shown overlaid on top of the amplitude distributions of raw data for two p conditions in Figure 2.6G-H. The coefficient of variation is defined by its relationship with the gamma shaping parameter $CV = \sqrt{1/\gamma}$. Therefore we now have estimates for the quantal parameters n, p and q as well as an estimate for the total quantal coefficient of variation CV derived from the entire data set using all the individual observations from recorded data.

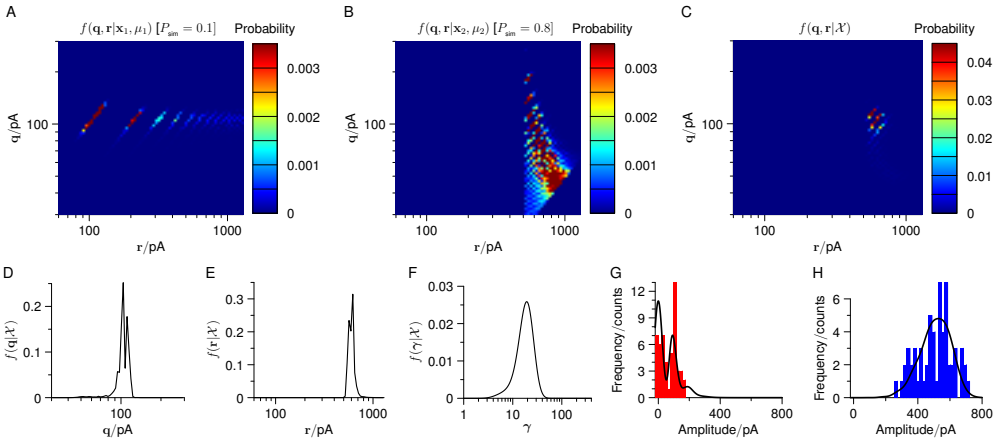

Figure 2.6: An illustrative example of BQA results using simulated data. Posterior distributions for the quantal size and maximal response, for a synapse of $q = 100$ pA and $n = 6$, in a low release probability ($p = 0.1$) and high release probability ($p = 0.8$) are shown in panels A and B respectively. The posterior distribution of a low p condition gives a good estimate of q but a poor estimate of r (panel A, whereas the posterior distribution of a high p condition give a good estimate of r but a poor estimate of q (panel B). Combining the two posterior distributions to produce a joint posterior, as shown in panel C, gives a good estimation of both r and q. Unidimensional posterior distributions calculated from the joint posterior can then be used to provide best estimates of quantal parameters. BQA produces estimates for q, r, and the γ shaping (from which the total quantal variance can be calculated). Distributions for each of these parameters is shown in panels D (q), E (r) and F (γ). Panels G and H show amplitude distributions of the data simulated in low and high probability respectively (bin width= 20 pA), with the profile of the amplitude distributions calculated from BQA estimates overlaid in black. This figure was adapted from Bhumbra and Beato (2013).

Chapter 3

Co-release of GABA does not occur at glycinergic synapses onto motoneurons in juvenile mice

3.1 Introduction

Fast inhibition in the CNS is mediated by the neurotransmitters γ-aminobutyric acid (GABA) and glycine. Anatomical studies have shown that GABA and glycine are both co-localised in nerve terminals in the spinal cord (Bohlhalter et al. 1994, Örnung et al. 1996, Taal et al. 1994, Todd et al. 1996). Co-release of GABA with glycine was first demonstrated by Jonas et al. (1998) who showed that a high percentage of miniature post-synaptic currents (mIPSCs) recorded from P6-10 rat motoneurons were mediated by both neurotransmitters. This evidence suggests that both neurotranmitters are packaged together, since mIPSCs are the post-synaptic response to a release of a single vesicle . Their observations were strenghtened by paired recordings between inhibitory interneurons and motoneurons that also displayed co-release (Jonas et al. 1998).

Co-release was later demonstrated in the brainstem and cerebellum of juvenile rats (O'Brien and Berger 1999, Dugué et al. 2005) and in the dorsal horn of adult rats (Chéry and De Koninck 1999). O'Brien and Berger (1999) showed that both GABAergic and glycinergic mIPSCs were present in hypoglossal mo-

toneurons by distinguishing them on the basis of their decay kinetics and modulation by pentobarbital. Dugué et al. (2005) showed that a single Golgi cell can produce pure GABAergic inhibition when projecting onto granule cells and pure glycinergic inhibition when projecting onto unipolar brush cells. They also showed that this is due to post-synaptic receptor specialization since GABA and glycine receptors immunoreactivity was differentially distributed among granule cells and brush cells, while the Golgi pre-synaptic terminals were positive for both the GlyT-2 transporter and for GAD, the enzyme responsible for GABA synthesis. The study by Chéry and De Koninck (1999) showed that lamina I neurons receive a mostly glycinergic input as inhibitory synaptic currents were abolished in the presence of strychnine. However, they were able to demonstrate an underlying GABAergic component by altering the kinetics of mIPSCs with application of the benzodiazepine flunitrazepam. It has also been demonstrated that GABA and glycine share a common vesicular transporter (Wojcik et al. 2006) which provides a mechanism for uptake of both neurotransmitters into the same vesicle and therefore supports evidence for co-release of the two neurotransmitters. A possible role has been suggested for GABA release at glycinergic synapses by Lu et al. (2008), who showed that GABA can act as a partial agonist on post-synaptic glycine receptors reducing the response size and speeding up the decay time of IPSCs.

There is evidence that in the dorsal horn co-release decreases during development and disappears after maturation of the spinal cord (Keller et al. 2001). In the ventral horn co-release is detected from most interneurons at a young age and selectively disappears only from Renshaw cells at around P9 (González-Forero and Alvarez 2005). The only electrophysiological evidence of co-release onto motoneurons comes from a study performed on 'mostly' P6-P8 rats (Jonas et al. 1998). This is an intermediate development stage in rats and at this age animals are not yet weight bearing. During development the subunit composition of glycinergic receptors changes with age and the $\alpha 2$ homomers found in newborn rats are replaced by $\alpha 1\beta$ heteromeric receptors in juvenile animals (at $\sim$P10 Malosio et al. (1991), Takahashi et al. (1992)). The key difference between these two receptors subtypes is that the decay kinetic of $\alpha 2$ homomers is slower than that of $\alpha 1\beta$ heteromeric receptors and thus dur-

ing later developmental stages glycinergic currents decay faster (Takahashi et al. 1992, Singer et al. 1998). The relatively long decay constants observed by Jonas et al. (1998) (16.3 ± 3ms at P5-P10) are more comparable with decay time constants reported by Takahashi et al. (1992) prior to the developmental shift (12.0 ± 5.7ms at P8) than with those recorded later in development (5.90 ± 2.2ms at P16). This suggests that the age range in which Jonas et al. (1998) conducted their experiments was still an early developmental stage for inhibitory connections in the spinal cord.

Anatomical studies show that Ia interneuron and Renshaw cell inputs onto motoneurons are mainly glycinergic ($> 80\%$). However a third of these glycinergic terminals are also immunoreactive for the GABA synthesis enzyme Glutamic Acid Decarboxylase (GAD, Alvarez et al. 2005). This suggests that while glycine is the dominant inhibitory neurotransmitters in the ventral horn there is the possibility that a small population of adult spinal cord ventral interneurons can co-release GABA with glycine.

The majority of experiments presented in this chapter have been conducted using mice between the ages of P8 and P14. This is still an intermediate developmental age range but by this time mice are already almost fully weight bearing. This age range was chosen as it is the latest developmental stage at which reliable recordings from motoneurons are still feasible.

The function of co-release of two different neurotransmitters is not entirely clear. If the two transmitters are co-detected, the differences in the deactivation kinetics of GABA and glycine would result in a fast peak and slow decay inhibitory response which may prolong the duration of inhibition at the post-synaptic cell. This would be similar to what has been shown at the excitatory motoneuron to Renshaw cell synapse where acetylcholine and glutamate are co-released (Lamotte d'Incamps and Ascher 2008) and activation of NMDA receptors prolongs the duration of otherwise short ACh mediated component of the post-synaptic response. On the other hand, if GABA receptors are not present at the post-synpatic membrane but are still co-released, GABA would only act as a partial agonist (Lu et al. 2008) and the effect of co-release would be to shorten the windows of inhibition.

The main aim of the experiments in this Chapter is to determine if GABA

is released from pre-motor glycinergic interneurons in the mouse spinal cord and if this has any detectable effect on motoneuron inhibition. In particular we addressed the following two questions:

- Are GABA and glycine co-detected at inhibitory synapses onto motoneurons?
- Are GABA and glycine co-released by premotor synaptic terminals?

3.2 Methods

3.2.1 Spinal cord preparation and patch recordings

Transverse, coronal and oblique slices (for ventral root stimulation experiments) as well as aCSF were prepared as described in the General Methods section. Whole cell patch recordings of motoneurons were performed as described with a caesium chloride based intracellular solution in the patch pipette (see General Methods for full composition). This is a high chloride internal solution and was chosen to improve the signal to noise ratio of IPSC recordings. However the high chloride solution also prolongs the decay phase of both glycinergic and GABAergic currents (Pitt et al. (2008), Houston et al. (2009), see General Methods). As a consequence, the decay time we observed does not reflect the decay time observed in physiological chloride, but it does allow direct comparison of results with previously published work by Jonas et al. (1998).

Extracellular stimulation was delivered via an electrical current through a patch pipette filled with normal aCSF using a constant current DS3 isolated stimulator (Digitimer). After patching a motoneuron in transverse slices, the stimulation electrode was manoeuvred within the ventral region of Rexed lamina VIII, in the Renshaw cell area until a response could be elicited. Having established the minimum intensity required to evoke inhibitory post-synaptic currents (IPSCs) reliably, the stimulus strenght was fixed at $\sim 1.5\times$ threshold. For experiments performed on the coronal preparation, the stimulation electrode was placed in the ipsilateral lateral white matter at least two or three

segments rostral or caudal to the motoneuron which was always recorded from the dorsolateral motor nucleus of L5.

3.2.2 Pharmacology

Where specified in the text, aCSF contained 3 mM kynurenic acid (Sigma) to block glutamatergic excitatory transmission and isolate inhibitory currents. Strychnine (0.3 µM to 2 µM, Sigma) and SR-95331 (5 µM, Sigma) were bath applied via the perfusion system to respectively isolate both GABAergic and glycinergic IPSCs. Diazepam (1 µM, Sigma) was applied as specified in the text to potentiate the effect of GABA binding onto $GABA_A$ receptors (resulting in larger IPSC amplitudes and longer decay time constants) (Gallager 1978).

In neurons glutamate is the precursor that is used by glutamic acid decarboxylase (GAD) to synthesize GABA (Mathews and Diamond 2003). Glutamate is either transported into cells by vesicular glutamate transporters (VGLUTs) or synthesized from glutamine by glutaminase. GABA can also be transported directly into cells by GABA transporters (GATs). In a subset of experiments we reduced pre-synaptic GABA content by disrupting GABA synthesis and blocking GABA re-uptake into cells. Glutamine uptake was blocked using α-(methylamino) isobutyric acid (MeAIB, 4mM Varoqui et al. 2000; Sigma). Glutamate uptake was blocked DL-threo-β-benzyloxyaspartic acid (Shimamoto et al. 1998; TBOA,1 µM, Tocris) and synthesis of GABA from glutamate by GAD was inhibited by isoniazid (De Koninck and Mody 1997; 20 mM, Sigma). GABA re-uptake into cell was blocked using nipecotic acid (2 mM, Tocris). During application of isoniazid, 1 µM CGP-55845-HCl was applied for the duration of the entire experiment to block activation of metabotropic $GABA_B$ receptors that could have confounding effects on the measured post-synaptic currents.

In experiments where miniature inhibitory post-synaptic currents (mIPSCs) were recorded,0.5 µM tetrodotoxin (Tocris) was perfused after a whole-cell patch was established. This concentration of tetrodotoxin was maintained during control recordings but reduced to 0.2 µM during drug application. At least 50 sweeps, of duration 9 s, were recorded for each condition. After the control period, the agents 5 µM SR-95531 or 0.3 µM strychnine were included in the

perfusate to isolate glycinergic or GABAergic mIPSCs respectively.

3.2.3 Concentration jumps

Any direct effect of the GABA-depleting agents on glycine receptors was tested by performing concentration jump experiments on recombinant rat $\alpha 1\beta$ glycine receptors, the adult isoform. Receptors were expressed in HEK293 cells using standard culture and transfection procedures (Burzomato et al. 2003). Concentration jumps were performed in an extracellular solution of composition (in mM) 102.7 NaCl, 20 Na gluconate, 2 KCl, 2 $CaCl_2$, 1.2 $MgCl_2$, 10 HEPES, 14 D-glucose, 15 sucrose, and 20 TEACl, pH adjusted to 7.4 with NaOH (osmolarity $\sim$320 mOsm). Pipettes were filled with a high chloride solution containing (in mM): 107.1 KCl, 1 $CaCl_2$, 1 $MgCl_2$, 10 HEPES, 11 EGTA, 20 TEACl, and 2 MgATP.

Outside-out patches were pulled and manoeuvred towards a theta tube, of tip diameter of 15 µm, mounted on a piezo-stepper (Burleigh Instruments). During control conditions one barrel contained normal extracellular soltuion (nECS) and the other contained nECS with the addition of 1 mM glycine. At least 5 fast applications of the glycine containing barrel lasting 1 ms were performed interleaved with 10 s periods for recovery. During testing of the GABA-depleting agents (*i.e.* isoniazid, MeAIB, TBOA, and nipecotic acid) the tested drug was added to both barrels (so one contained nECS with GABA-depleting drug and the other nECS with GABA-depleting drug and 1 mM glycine). Fast applications were then performed in the same way as described during control experiments. The patch was first allowed to equilibrate to the new solution containing the GABA-depleting drug before testing. Effects of fast application in control and test conditions on responses were measured using the changes in the peak current.

3.2.4 Analysis of inhibitory currents

Successfully evoked IPSCs were discriminated offline using Clampfit 10.2 (Molecular Devices) whereas mIPSCs were detected using WinEDR 3.2.4

(Strathclyde Electrophysiology Software). Analysis of currents was performed using MATLAB 7 (MathWorks). Both evoked IPSCs and mIPSCs were subjected to exponential fitting analysis. Events were excluded for exponential fitting analysis if their amplitude was less than 3 standard deviations of the baseline noise, if there were overlapping events within 50 ms, or if the asymptotic decay did not reach 90% of the current peak. The Levenberg-Marquardt least-squares iterative algorithm was used to fit one or two exponential components to the decay phase of each post-synaptic current from 95% to 5% of peak amplitude:

$$\hat{I}_1(t) = I_0 + Ae^{-\frac{t}{\tau}}$$
$$\hat{I}_2(t) = I_0 + A_1 e^{-\frac{t}{\tau_1}} + A_2 e^{-\frac{t}{\tau_2}}$$

The fit was selected on the basis of the F-test statistics for the two curves with $F > 4.8$ as a the threshold for favoring the second. Since the decay constants were normally distributed, they were amenable to parametric test statistics. Comparisons across treatments were undertaken using one-way ANOVA F statistics, with *post-hoc* tests based on Student's t statistics employing Bonferonni's correction for multiple comparisons. Summary data are presented as mean $\pm$ S.E.M.

Since mIPSCs were always recorded in the presence of kynurenic acid, inward currents could only have resulted from GABAergic or glycinergic events. We thus quantified the overall inhibitory drive for each sweep by evaluation of the integral of the entire current trace per unit of time. Using pharmacological isolation of GABAergic or glycinergic events, we used the integral to estimate their relative contributions to overall inhibitory drive.

Prior to integral estimation however we first corrected for slow baseline drifts. We used a low-pass filter at 0.5 Hz that cancelled completely the fast-rising events associated with synaptic activity and subtracted the result from the original signal to obtain a drift-free trace. Since the subtraction could impose a non-zero centre for the baseline, it was necessary to eliminate any offsetting effects on the integral evaluation by a further subtraction of this bias.

We estimated the bias using the mode of the data, which was evaluated by convolution with a Gaussian kernel of a standard deviation $\sigma n^{-0.3}$, where n is the size and σ^2 is the variance of the data (Bhumbra and Dyball 2010).

3.3 Results

3.3.1 GABA and glycine are not co-detected in evoked IPSCs

Motoneurons receive strong, mainly glycinergic, inhibition from spinal cord interneurons. It has been shown that at an intermediate stage of development in rats (P6-7) approximately 44% of inhibitory events are mixed GABAergic and glycinergic responses (Jonas et al. 1998). It is however unclear whether co-detection and co-release are maintained during development with some evidence suggesting that GABAergic components disappear during maturation (Keller et al. 2001). In this study spinal cords were extracted from P8-14 mice. While this is a similar age range to the rats used by Jonas et al. (1998) it constitutes an important difference between the studies. Mice motor development occurs earlier than it does in rats and while P6-7 mice are already weight bearing, rats do not become weight bearing until about P12. The experiments in this study are therefore performed at a later developmental stage than those reported by Jonas et al. (1998).

We started by obtaining a set of paired recordings between glycinergic interneurons (identified through expression of EGFP under the control of the GlyT2 transporter) and motoneurons in transverse slices taken from the L5 region of the spinal cord.

In control conditions the evoked IPSC (eIPSC) decays were best fitted by a single exponential component (3.3 ± 0.3 ms, n=4). This decay time constant agrees with purely glycinergic currents which are typically 3 ms to 7 ms. This observation is in contrast to Jonas et al. (1998) who in 10 out of 11 interneuron-motoneuron pairs found eIPSC decays were best fitted with two exponential components, a fast putative glycinergic component and a slower

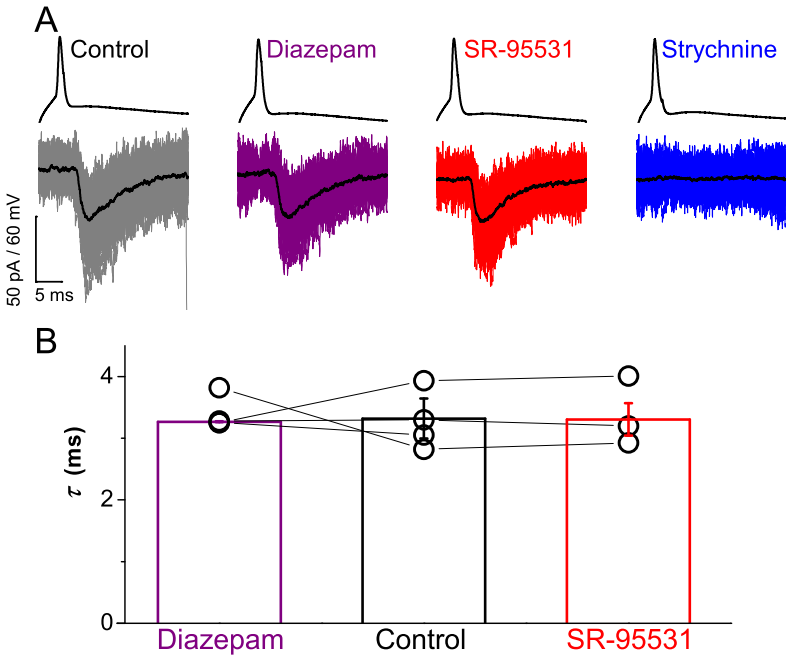

Figure 3.1: Paired recordings showed no contribution of GABA to evoked IPSCs. Traces in A illustrate responses from a connected pair representing a single spike elicited in the interneuron above and the evoked IPSCs recorded from the motoneuron below with the mean current overlayed in black. Bath application of neither 1 µM diazepam (purple) nor 5 µM SR-95531 (red) modulated the time constant of evoked IPSCs whereas 2 mM strychnine (blue) abolished all responses. Group data from four connected pairs are represented in graph B, which illustrates no significant effect of diazepam (purple) or SR-95531 (red) on the time constant (see text). Error bars indicate mean ± S.E.M.

putative GABAergic component (it should be noted that decay times were generally slower in the study by Jonas et al. (1998) due the developmental stage of the animals used in their recordings, see introduction). Our results suggest that in these synapses GABA is not co-detected with glycine. However because of high baseline noise when recording from motoneurons (due to low input resistance and high capacitance of the cell) and the similar time course of mature glycine and GABA currents (5 and 10ms respectively, González-Forero and Alvarez 2005, Chéry and De Koninck 1999) it is possible that GABA currents could go undetected due to their small amplitude and the difficulty in separating out the two components in the IPSC.

We therefore applied 1μM diazepam to enhance any putative GABAergic component that might be below threshold for detection in control conditions. Diazepam is known to increase the peak amplitude of GABAergic IPSCs and prolong their decay time to 50 ms (Chéry and De Koninck 1999). If $GABA_A$ receptors are present at the synapse but in a very low density compared to glycine receptors application of diazepam would help distinguish the smaller GABAergic response from the larger glycinergic response by increasing the GABAergic response size and duration. It is also possible that $GABA_A$ receptors are mainly extrasynaptic (Chéry and De Koninck 1999) and therefore, following release, would be exposed to a much lower concentration of neurotransmitter than those receptors found at the post-synaptic density. Application of diazepam in this situation would result in a larger $GABA_A$ receptor response to smaller concentrations of GABA and thus could allow detection of IPSCs originating from extrasynaptic receptors. Following diazepam application we applied SR-95531, a specific $GABA_A$ receptor antagonist to abolish any GABA mediated eIPSC component.

Figure 3.1B shows group data for the four connected pairs. In three out of four pairs one-way ANOVA statistics showed no statistically significant effect on the decay time constant ($F \leq 0.11, P \geq 0.523$). In one pair the test statistic was significant ($F = 19.3, P < 0.001$) due to a small decrease in the time constant in the presence of diazepam ($\tau = 3.2 \pm 0.1$ms)compared to control ($\tau = 3.9 \pm 0.1$ms, $t = 4.64, P < 0.001$). However a decrease in time constant is inconsistent with the effect of Diazepam which should enhance and prolong the GABA component of evoked IPSCs. Blocking $GABA_A$ receptors with SR-95531 had no effect on the decay time of evoked currents ($\tau = 3.3 \pm 0.3$ms, $n = 3$) thus confirming the lack of a GABAergic response in the evoked ISPCs.

While the decay time constant of eIPSCs did not change during either of the drug treatments we consistently observed a decrease in the mean amplitude of synaptic events to $93 \pm 8\%$ of control in the presence of diazepam and $82 \pm 11\%$ of control during SR-95531 application. This observation however cannot be attributed to the action of the drugs for two reasons. Firstly, diazepam should increase both the duration and strength of a GABAergic IPSC and therefore an increase in amplitude would be expected. Secondly, slow run down of response

is common in prolonged paired recordings (see for example, Diana and Marty 2003). A similar $5 - 20\%$ decrease in amplitude over an hour of recording has been observed in a separate set of paired recordings in which no drugs were applied (Bhumbra, Beato, personal communication). This small but progessive decrease in amplitude over time prevented detailed analysis of the effect of diazepam and SR-95531 on eIPSC amplitudes.

The lack of a GABAergic component in the paired recordings suggests that GABA is not co-released with glycine onto motoneurons. Since it has been reported that transmission from Renshaw cells onto motoneurones is mediated by both transmitters in adult cats (Schneider and Fyffe 1992) we recorded recurrent inhibitory currents originating from Renshaw cells. Slices were cut at a $35\,^{\circ}$ angle with ventral roots preserved to maintain motor axons exiting the slice (see General Methods). Ventral root stimulation elicited antidromic spikes in all the motoneurons that had axons in the preserved rootlet, giving rise to the activation of all Renshaw cells postynaptic to these motoneurons. Renshaw cells are inhibitory interneurons that receive excitatory inputs from motoneurons collateral fibres and then synapse back onto motoneurons in the same motor pool (see Introduction). The eIPSCs recorded from motoneurons are therefore composed of inhibitory inputs from multiple cells and thus we were able to sample a large number of the inhibitory synapses formed by a distinct class of pre-synaptic cells.

There is some evidence of a postnatal shift from GABAergic to glycinergic inhibition in the spinal cord (Gao et al. 2001, Ma et al. 1993, Tran et al. 2003, Ma et al. 1992). As previously mentioned, the co-release demonstrated by Jonas et al. (1998) was probably observed at an earlier developmental age than our paired recordings. It is therefore possible that younger mice would still exhibit co-release of GABA with glycine and that the lack of co-release in our paired recordings is due to the increased maturity of the animals that were used in the present study. We therefore recorded ventral root evoked IPSCs from motoneurons in slices obtained from both neonatal (P0-3) and juvenile (P9-10) animals to investigate if co-release is present in younger spinal cords at the Renshaw cell to motoneuron inhbitory synapse.

In neonatal animals an inhbitory component of eIPSCs was still present

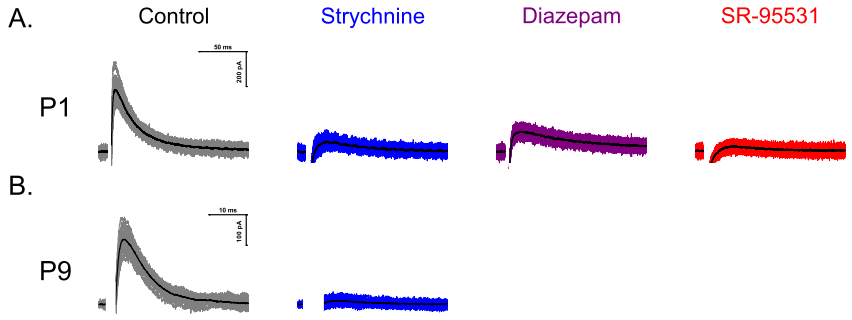

Figure 3.2: Whole cell motoneuron recordings showing neurotransmitter composition of Renshaw cell inhibition in neonatal and juvenile animals. Recurrent inibition of motorneurons was evoked by stimulation of ventral rootlets in oblique slices of the lumbar region of the spinal cord (see Methods). Motoneurons were recorded in voltage-clamp at 0 mV with a low Cl^- solution in the pipette to isolate inhibitory currents. In neonatal animals (figure A) a GABAergic component was still present after the block of glycine receptors by 0.3 µM strychnine. This GABAergic component was enhanced by addition of 1 µM diazepam and abolished in the presence of 5 µM SR-95531. Strychnine completely abolished eIPSCs in slices obtained from P9 animals (panel B).

after addition 0.3 µM strychnine (figure 3.2A). This component was potentiated in the presence of 1 µM diazepam and blocked by addition of 5 µM SR-95531 suggesting the current was indeed GABAergic (figure 3.2A, n=6). In juvenile animals inhibitory responses following ventral root stimulation were completely abolished after addition of strychnine suggesting that at this age inhibtion is purely glycinergic (figure 3.2B, n=5). We can therefore conclude that while in immature animlas GABA is co-released with glycine and co-detected at the Renshaw cell to motoneuron synapses, during development (and already at P8-P10) the GABA component disappears from the recurrent IPSC originating from Renshaw cells.

Paired recordings were peformed in transverse slices in order to maximise the chance of finding interneuron to motoneuron connections and recordings with ventral root stimulations were performed in similar slices cut at a 35° angle to preserve motoneuron axons. Therefore, the recordings described above were all performed on synapses orginating from interneurons projecting onto motoneurons within the same segment. Work by Liu et al. (2010) suggests that axon terminals from transverse and ascending/descending projections may dif-

fer in neurotransmitter content or are apposed to post-synaptic membranes with different receptor composition. To ensure our results were not biased towards transverse pure glycinergic connection we used a coronal preparation to investigate IPSCs evoked by extracellular stimulation of ascending and descending fibres.

In seven recordings motoneuronal IPSCs evoked by stimulating ascending or descending projections were all best fit with a single exponential in control conditions ($n = 223$) and in the presence of diazepam ($n = 223$). The average time constant across all sweeps and cells was $\bar{\tau} = 5.8 \pm 0.9$ ms. The short mean time constant and lack of second component to the exponential fits are consistent with purely glycinergic IPSCs. The lack of any effect on eIPSCs during application of diazepam or SR-95531 confirmed that co-detection of GABA with glycine does not occur at these connections. A representative example of eIPSCs during drug treatments is shown in Figure 3.3A. Application of $1\,\mu$M strychnine completely abolished responses which further supports the conclusion that these eIPSCs are purely glycinergic.

Group data for the seven motoneurons are illustrated in Figure 3.3B. Paired t-test statistics evaluated from the average fitted time constant for each cell across all seven motoneurons confirmed no significant effect on the decay kinetics of evoked IPSCs by diazepam ($\tau = 6.1 \pm 0.9$ms, $t = -1.51, P = 0.183$) or SR-95531 ($\tau = 5.7 \pm 1.0$ms, $t = -1.04, P = 0.346$). Analysis of the recordings obtained from coronal preparations thus indicated that there is no detectable GABAergic component in IPSCs evoked by simulation of ascending or descending projections.

It is known that $GABA_A$ receptors containing β and $\gamma 2$ and either $\alpha 4$ or $\alpha 6$ subunits show no affinity for diazepam (Wisden et al. 1991, Hadingham et al. 1996, Knoflach et al. 1996) and therefore if these GABA receptor subtypes were present post-synatpically their response would not be potentiated during diazepam application. To investigate putative GABAergic components of currents mediated by diazepam-insensitive $GABA_A$ receptors, evoked responses from four motoneurons were recorded in transverse slices during bath application of 200 nM THDOC. Group results are shown in Figure 3.3C. In comparison to control conditions ($\tau = 5.5 \pm 0.3$ ms), paired t-test statistics showed no signif-

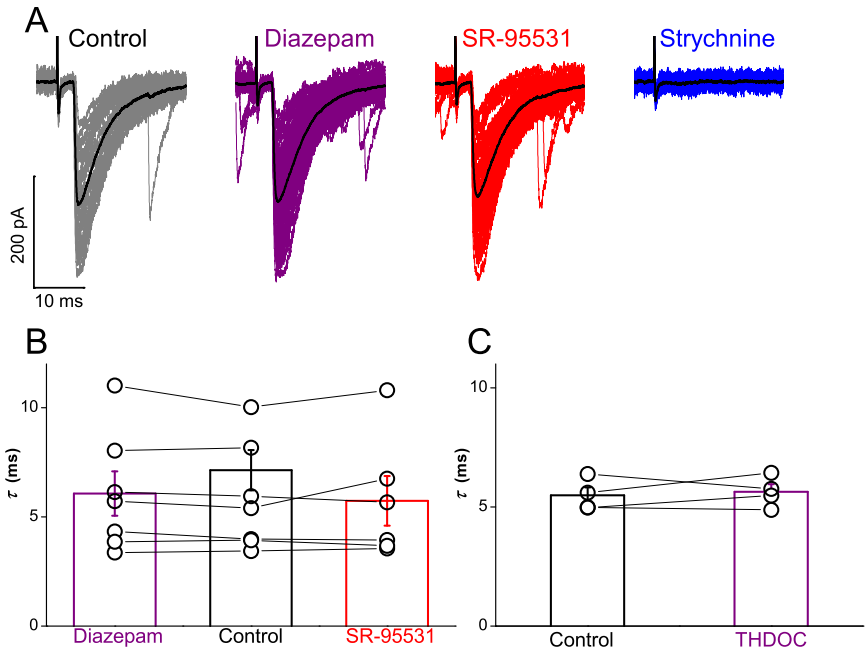

Figure 3.3: Extracellular stimulation of ascending and descending projections showed no contribution of GABA to evoked IPSCs. Traces in A illustrate responses of a motoneuron with the mean current overlayed in black. Bath application of neither $1\,\mu$M diazepam (purple) nor $5\,\mu$M SR-95531 (red) modulated the time constant of evoked IPSCs whereas $2\,\mu$M strychnine (blue) abolished all responses. Group data shown in graph B, illustrates no significant effect of diazepam (purple) or SR-95531 (red) on the time constant (see text). Graph C shows no significant effect of 200 nM THDOC(purple) on the time constant of responses evoked in transverse slices.

icant effect of THDOC on the time constant ($\tau = 5.6 \pm 0.3$ ms, $t = -0.47$, $P = 0.672$).

3.3.2 GABA and glycine are not co-detected in miniature IPSCs

While our initial results have shown there is no GABAergic component to IPSCs evoked from glycinergic neurons there is a possibility that our limited sample of inhibitory inputs onto motoneurons has comprised only a specific subpopulation of purely glycinergic inputs. We therefore recorded spontaneous

miniature inhibitory post-synaptic potentials (mIPSCs) from motoneurons in the same age range as the paired recordings above (P8-P10). mIPSCs are the post synaptic response to the spontaneous release of a single vesicle and can therefore occur at any of the synaptic contacts. Their properties are representative of all the synaptic inputs impinging onto the recorded motoneurons. By recording mIPSCs we are no longer selecting for a limited sub-populations of synapses (as is the case for evoked IPSCs) but we are sampling the largest possible number of synaptic contacts.

In control conditions (with only excitatory transmission blocked) both GABAergic and glycinergic mIPSCs were observed. All miniature events with a stable baseline and an inter-event interval long enough to allow full restoration to baseline were selected and fitted with one or two exponential components. All events were best fit with a single component (see Methods) suggesting that "mixed" responses were either rare or below our detection threshold.

Miniature events were recorded from seven motoneurons, 5 µM SR-9553 was applied in six recordings and 1 µM diazepam in four. Exponential fitting analysis of all recorded mIPSCs showed currents were best fit with a single exponential in control conditions ($n = 1398$) and in the presence of diazepam ($n = 992$). The averaged time constant fitted for all mIPSCs $\bar{\tau}$ recorded in control conditions was 6.0 ± 0.9ms. The fast time constant and lack of a second component to the exponential fits is consistent with purely glycinergic miniature currents. Assuming that both glycine and GABA are released, the mean decay time of all the fitted mIPSCs would be an average of both their decay times, weighted by their relative frequency. Therefore, diazepam would be expected to prolong the mean τ by potentiating any GABAergic response while SR-95531 would make the mean τ faster because it would block the slower GABAergic component. A representative example of the effects of 1 µM diazepam and 5 µM SR-9553 on mIPSCs recorded from a motoneuron are shown in 3.4A and shows very little effect of either drug on mIPSCs. Group data showing mean relative amplitude of currents compared to control and mean fitted time constant across all recordings is shown in 3.4B. The relative mean amplitude was not changed in the presence of SR-95531 ($99.1 \pm 6.9\%$) or diazepam ($99.4 \pm 5.0\%$). There was also no significant effect on the mean fitted time constant with di-

azepam (6.2 ± 1.3ms, paired $t = -0.57, P = 0.607$) or SR-95531 (5.9 ± 0.8ms, paired $t = 0.50, P = 0.618$).

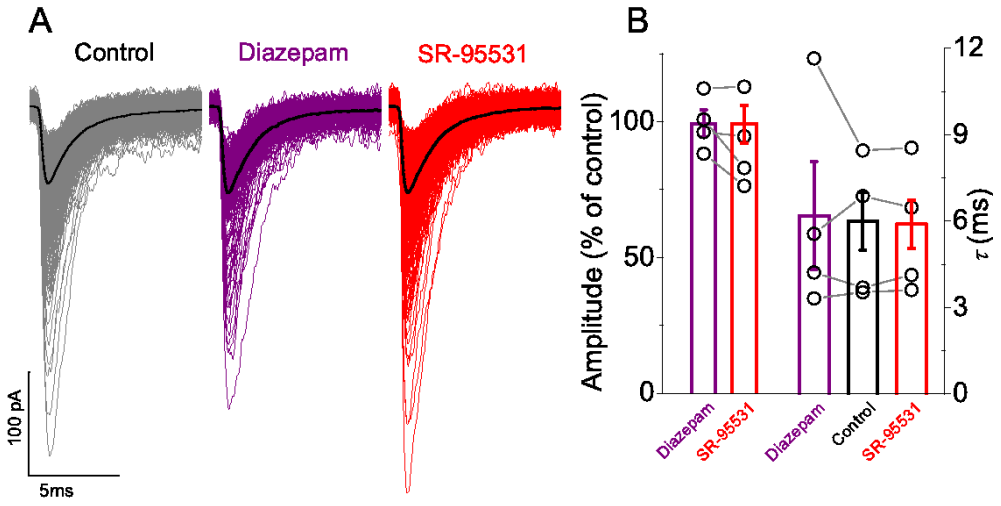

Figure 3.4: Effect of diazepam and SR-95531 on decay time and amplitude of motoneuron mIPSCs. Traces in A illustrate mIPSCs recorded from the motoneuron with the mean current overlayed in black, demonstrating no detectable effect of the two agents. Group data from all recorded motoneurons are represented in graph B, which illustrates no significant effect of 1 µM diazepam (purple) or 5 µM SR-95531 (red) on the relative amplitude or time constant of mIPSCs.

The lack of effect of diazepam and SR-95531 suggests that release of mixed GABA and glycine vesicles either does not occur or is at least very rare. These results also suggest that contribution of GABA to the post-synaptic response is low compared to glycine. The lack of an effect of SR-95531 on the fitted τ also indicates that only a small proportion of events were GABAergic. We therefore wanted to quantify the overall proportion of GABAergic and glycinergic inhibition by measuring the total charge transfer onto motoneurons due to each inhibitory component.

Motoneuron mIPSCs were recorded in the presence of either 5 µM SR-95531 (to block all GABA currents) or 0.3 µM strychnine (to block all glycinergic currents). As a measure of the contribution of each inhibitory component the integral of the recorded traces was calculate (see Methods). Figure 3.5A shows SR-95531 has almost no effect on amplitude or frequency of events whereas

strychnine almost completely abolished all events. In all seven experiments strychnine caused a significant reduction in the integral size. In three experiments mIPSC occurrence was completely abolished while in the other four activity was significantly suppressed (to $24.9 \pm 4.1\%$ Figure 3.5B). SR-95531 however did not alter the overall inhibitory drive in five cells ($99.0 \pm 6.4\%$ of control) and resulted in a significant reduction in only one recording (to $45.0 \pm 25.7\%$ Figure 3.5B).

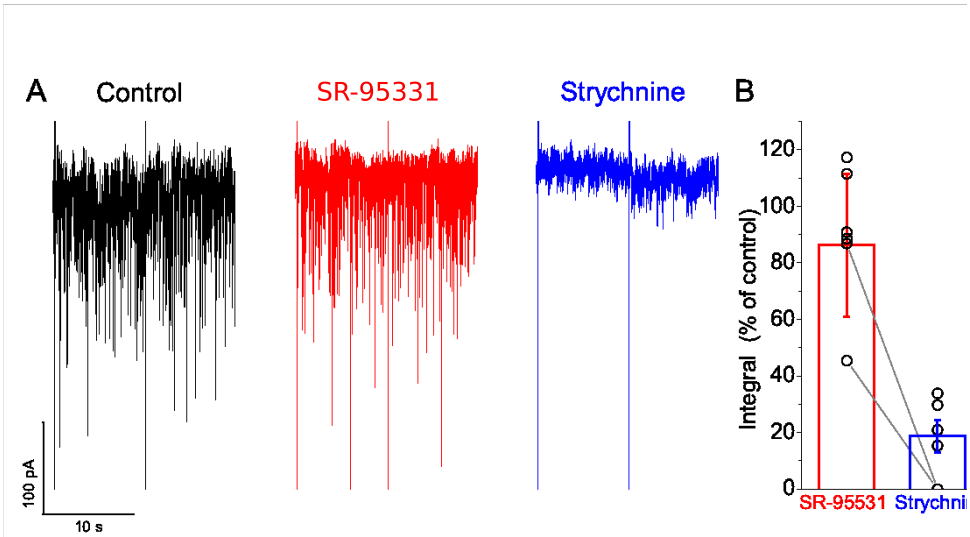

Figure 3.5: Effect of SR-95531 and Strychnine on charge of motoneuron mIPSCs. Example traces of motoneuron mIPSCs recorded in control (black),5 µM SR-95531 (red) and 0.3 µM strychnine (blue) are shown in A. The large downward deflections are the truncated responses to voltage steps that were delivered every 10 seconds to monitor the series resistance.Group data illustrated in graph B, which shows that overall inhibitory drive is not significantly affected by SR-95531 (red) but substantially attenuated by strychnine (blue) and abolished in some cases.

3.3.3 GABA depletion did not affect evoked IPSCs

The results so far show that GABA is not co-detected with glycine at synapses onto motoneurons. However, it is possible that GABA is co-released but there are no post-synaptic GABA receptors. GABA could still have a post-synaptic effect on glycine receptors acting as a partial agonist (Lu et al. 2008). We tested

this possibility by altering the pre-synaptic vesicle content through interfering with GABA synthesis or re-uptake into pre-synaptic terminals.

In neurons GABA is synthesised from glutamate by GAD, and glutamate is either transported into cells or synthesised from glutamine by glutaminase. Therefore we used the glutamine uptake blocker α-(methylamino) isobutyric acid (MeAIB,4mM Varoqui et al. 2000; Sigma), the glutamate uptake blocker DL-threo-β-benzyloxyaspartic acid (Shimamoto et al. 1998; TBOA,$1\,\mu$M, Tocris) and the GAD inhibitor isoniazid (De Koninck and Mody 1997; $20\,$mM, Sigma) to deplete upstream GABA substrates and directly inhibit its synthesis from glutamate. GABA uptake into cells was blocked using nipecotic acid ($2\,$mM).

Motoneuron IPSCs were evoked by inserting a patch pipette containing aCSF into the Renshaw cell region and using it as a stimulator to excite inhibitory neurons. During application of all four GABA depleting drugs a fast reduction of extracellular eIPSC amplitudes was observed (70% within 5 minutes, not shown). This fast action is incompatible with an effect on metabolic processes and is more likely to be due to direct action on post-synaptic glycine receptors. Therefore we performed tests on recombinant $\alpha 1\beta$ receptors (the mature isoform of glycine receptors in the spinal cord) using fast concentrations jumps (see Methods) to determine which GABA depleting agent had the smallest direct effect on glycinergic receptors. The response to a 1 ms 1 mM pulse of glycine was measured in control conditions and after pre-incubation with each one of the four drugs above and co-application of the same concentration of glycine. Nipecotic acid was shown to reduce mean amplitudes by $29.0 \pm 4.2\%$ (n=7) and MeAIB by $25.5 \pm 3.9\%$ (n=7) and TBOA by $34.4 \pm 9.8\%, n = 5$ (n=5, figure 3.6). Isoniazid however only reduced glycinergic current amplitudes by $14.0 \pm 3.0\%, n = 5$ (n=5, figure 3.6).

As isoniazid only had a modest direct effect on glycinergic currents we used it as a tool to reduce vesicular GABA. We therefore first had to confirm that isoniazid could deplete or reduce the amount of pre-synaptic GABA. IPSCs were evoked by extracellular stimulation in the presence of $1\,\mu$M strychnine, blocking any glycinergic currents and isolating GABAergic responses.

Evoked GABAergic IPSC traces recorded over the course of 50 minutes show a steady reduction in current amplitude (Figure 3.7A-C). The decrease

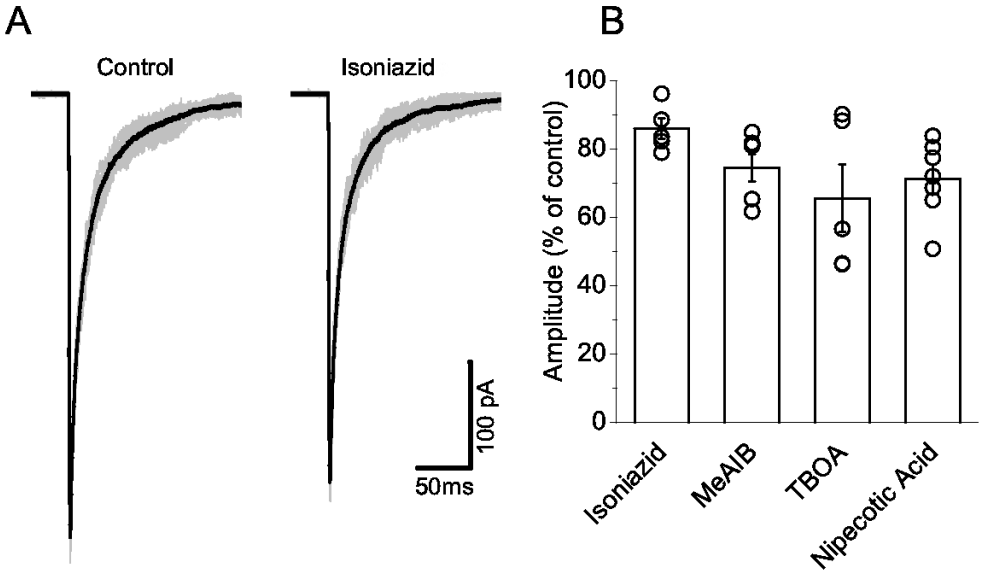

Figure 3.6: Fast concentration jump experiments showed that isoniazid administration produced the least attenuation in current among the GABA depleting agents. Traces in A illustrate an example in which a small reduction in the current is observed in the presence of 20 mM isoniazid. Graph B illustrates isoniazid attenuated the current to the least extent (see text) compared to 4 mM MeAIB,1 µM TBOA, and 2 mM nipecotic acid.

(shown in figure 3.7D) occurred over a 30 min to 40 min period, which suggests that it was not due to direct action onto post-synaptic receptors (which would be much faster) but instead was due to a pre-synaptic reduction of vesicular GABA content. GABAergic IPSC amplitudes were reduced in all cases with an average reduction of $61 \pm 5\%$ after 40 minutes in the presence of 20 mM isoniazid (Figure 3.7E, n= 4).

After determining that isoniazid does indeed deplete vesicular GABA (which is in agreement with observations by De Koninck and Mody 1997), experiments were performed to determine if changing the pre-synaptic inhibitory neurotransmitter content to favour glycine loading would have any effect on glycinergic IPSCs. Therefore, isoniazid was applied in the presence of 5μM SR-95531 while recording extracellular eIPSCs. This blocked any $GABA_AR$ responses leaving only glycinergic IPSCs. Lu et al. (2008) have shown that GABA acts as a weak partial agonist at glycine receptors. Therefore if GABA is being co-released with glycine isoniazid should gradually deplete GABA from pre-synaptic termi-

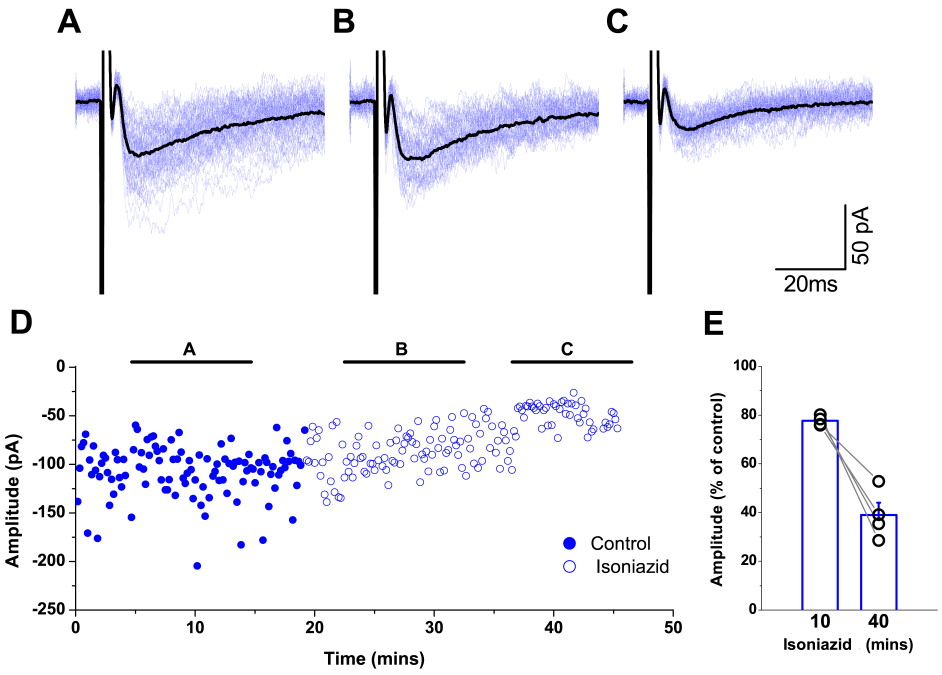

Figure 3.7: Application of 20 mM isoniazid depleted vesicular GABA over a period of 30 min to 40 min. In the presence of 1 µM strychnine, IPSCs were evoked by extracellular stimulation. The traces illustrate an example of a recording of post-synaptic responses during the control period (trace A) and two epochs following isoniazid superfusion (traces B and C). Mean responses are overlayed in black. Graph D plots the changes in amplitude, illustrating the time periods corresponding to A–C, and shows a gradual but substantial reduction in current. The group data represented in graph E illustrates that evoked IPSCs in all motoneurons were progressively attenuated during the ~ 40 minutes of isoniazid superfusion.

nals thus removing GABA's effect as weak partial agonist on glycine receptors. This would result in an increase in amplitude and reduction in decay time constant of evoked IPSCs as released glycine would no longer be competing with GABA for glycine receptor binding sites.

In the presence of isoniazid glycincergic eIPSC amplitudes did not increase in size (Figure 3.8A-D) as would be expected if GABA was initially being co-released. However, a fast reduction of $13.5 \pm 6.6\%$ was observed in the first ten minutes after application of isoniazid (Figure 3.8D). This agrees with the observed direct effect of isoniazid on glycine receptors (Figure 3.6). Mean IPSC amplitude did not decrease further and was still $15.8 \pm 7.6\%$ less than control

after one hour (Figure 3.8C). IPSC decay time constant showed no significant change in the presence of isoniazid (5.8 ± 0.8ms in control to 5.8 ± 0.8ms after one hour, paired $t = -0.05$, $P = 0.963$, $n = 6$). This suggests that little or no GABA is co-released with glycine at the observed synapses as depletion of pre-synaptic GABA by isoniazid has no effect on the amplitude or decay time constants of evoked glycinergic IPSCs.

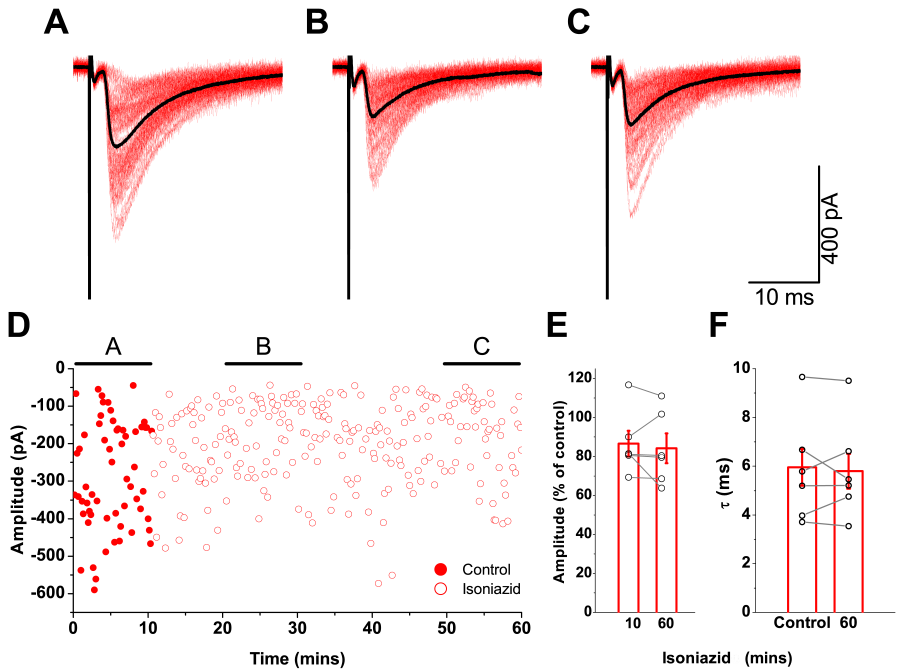

Figure 3.8: Effects on glycinergic IPSCs by application of 20 mM isoniazid were not compatible with vesicular GABA depletion. The traces illustrate an example of a recording of post-synaptic responses during the control period (trace A) and two epochs following isoniazid superfusion (traces B and C). Mean responses are overlayed in black. Graph D plots the changes in amplitude, illustrating the time periods corresponding to A–C, and shows a modest but rapid reduction in current. The group data for all motoneurons shows that the attentuation of evoked IPSCs (graph E) after one hour was no greater than that observed after ~ 10 minutes, and that isoniazid superfusion had no systematic effect on the decay time constant (graph F).

3.3.4 Glycine loading did not affect evoked IPSCs

Depletion of GABA from vesicles did not produce any effect on amplitude or kinetics of post-synaptic responses, we therefore conducted experiments to determine if increasing the proportion of vesicular glycine had any effect on IPSCs. In order to favour glycine uptake into vesicles paired recordings were performed in which the pre-synaptic terminal was loaded with $20\,\text{mM}$ glycine. Changes in the neurotransmitter content of pre-synaptic vesicles would be detected as a progressive change in post-synaptic response over time after establishing a whole cell configuration for the interneuron. Trains of 1000 spikes at $50\,\text{Hz}$ were delivered every 10–$15\,\text{minutes}$ to deplete vesicles in the pre-synaptic cell.

Shifting pre-synaptic release to favour glycine over GABA did not cause any detectable effects on eIPSCs (Figure 3.9, $n = 4$). There was no appreciable effect on the decay constant, with a mean in control of 4.8 ± 0.4ms and of 4.6 ± 0.4ms ~ 45 minutes after establishing the whole cell configuration (Figure 3.9C). After an hour of patching with high intracellular glycine in the patch pipette, there was also almost no change in the mean amplitudes of IPSCs ($98.9 \pm 11.7\%$ of control, Figure 3.9D). The lack of any effect on amplitude or decay time suggests that even if any GABA was present in the pre-synaptic terminal, it was not in sufficient quantities to be detected.

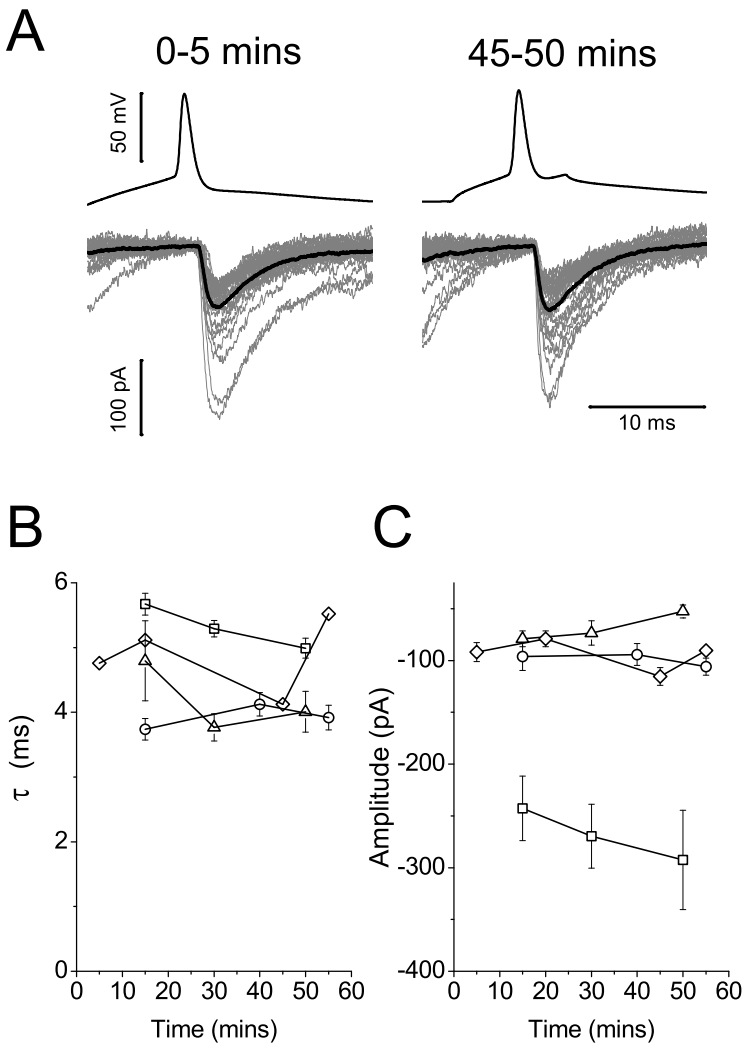

Figure 3.9: Loading the pre-synaptic cell with 20 mM glycine during paired recordings resulted in no progressive changes in post-synaptic responses. Traces in A illustrate an example of inter-neuronal spikes and motoneuronal responses for the first 5 minutes and 45 minutes after rupturing the membrane of the pre-motor interneuron. Group data ($n = 4$) is illustrated graphically to show changes in the decay constant (B) and amplitude (C), neither of which showed systematic changes during the course of the loading of glycine into the pre-synaptic vesicles.

3.4 Discussion

The data in this chapter shows that GABA is most likely not co-released with glycine from glycinergic pre-motor interneurons in the spinal cord and that even

if it is, the concentration released is too low to cause a detectable post-synaptic effect. This contrasts with the previously mentioned study by Jonas et al. (1998) that showed co-release of GABA and glycine from pre-motor interneurons in neonatal rats. However, there are two important differences between their study and the work presented here that could explain this disparity. In their study Jonas et al. (1998) used rats in an age range from P5-P10 (although mostly P6-7) whereas we used P8-14 mice. Due to the difference in the relative stages of motor development between these two age groups this is possibly the key reason for the differing results. A rat aged P5-10 is only capable of producing a pivoting motion (Altman and Sudarshan 1975) whereas by P8-14 mice can already crawl and move short distances. Therefore, Jonas et al. (1998) possibly observed a transient phenomenon occuring at an early developmental stage that is not present in the adult spinal cord.

There is a postnatal shift in the ventral horn from GABAergic to glycincergic inhibtion. Studies have previously shown that the frequency of pure GABAergic IPSCs decreases post-natally (Gao et al. 2001) as does GABA and GAD immunoreactivity (Ma et al. 1993, Tran et al. 2003) and $GABA_A$ receptor expression levels (Ma et al. 1992). If this shift continues into later postnatal stages it is possible that the lack of co-release observed in this study is more representative of functional inhibition in the adult spinal cord. Indeed data shown in Figure 3.2 suggests that this could very well be the case as experiments conducted on tissue from neonates exhibited a GABAergic eIPSC component the same experiments conducted on juvenile spinal cord tissue did not.

At early developmental stages GABA may have a an important regulatory role. GABA has been shown to mediate spontaneous oscillations in the spinal cord (Wu et al. 1992) and retina (Sernagor et al. 2003), and its depolarizing effect during development is thought to be an essential trophic factor during neuronal circuit maturations (Owens and Kriegstein 2002). It is therefore possible that mixed GABA and glycine events could also have some early developmental significance for the maturation of the motor control in the spinal cord.

In order to identify glycinergic interneurons we used transgenic mice in which EGFP is expressed under control of the gene encoding for the neuronal glycine transporter. This is obviously another difference between our study and

the study by Jonas et al. (1998) however it is unlikely this could account for the disparity in results. The level of protein expression of GlyT-2 has been shown to be similar in wild type and transgenic animals (Zeilhofer et al. 2005) and therefore it is unlikely co-expression of EGFP would affect vesicle filling at glycinergic terminals.

During paired recordings the intracellular content of pre-synaptic interneurons would have been dialysed over time due to diffusion of the intracellular pipette solution. There is a possibility that this slow alteration of intracellular content could have affected the relative vesicular content of GABA and glycine leading to purely glycinergic currents post-synaptically. However if it was the case then at least initially during recordings (before dialysis could realistically have affected vesicular content) we should have observed a double exponential decay similar to that described by Jonas et al. (1998) but a slower component was never observed. Neither were double exponential decays observed during analysis of mIPSCs and in those experiments intracellular content of pre-synaptic cells was not dialysed. Similarly evoking IPSCs by extracellular stimulation does not have any effect on the intracellular composition of pre-synaptic cells and the time constant of eIPSCs was stable over time and never exhibited a slow second exponential component.

In a subset of paired recordings a run-down of $10 - 20\%$ in the amplitude of synaptic responses was observed. This is likely due to washing out of intracellular components that are essential for efficient vesicle filling (Diana and Marty 2003). The extent of run-down (when present) was only associated with the duration of the recording and not with drug treatment.

Our results show that in juvenile mice the majority of inhibitory input onto lumbar motoneurons is glycinergic (Figure 3.5). It is possible that GABA is still co-loaded into vesicles with glycine but if this was the case either GABA-receptors are not present post-synaptically or GABA is released in too low a concentration to have a detectable effect on post-synaptic glycine receptors. If GABA receptors were present post-synaptically then we would have observed a subset of mIPSC (and some eIPSCs) with a second slow GABA component, especially after potentiating of the GABA response by diazepam (Figures 3.4, 3.1 and 3.3). Similarly if vesicular GABA content was too low to have an effect

on post-synaptic glycine responses then either GABA depletion (Figures 3.7 and 3.8) or loading of the pre-synaptic vesicular loading with glycine (Figure 3.9) should have had an effect on IPSC time courses but neither did.

The role of many inhibitory pre-motor interneurons in the ventral horn of the spinal cord is not fully understood. Recent work has suggested that inhibitory synapses may be sufficient for generation of locomotor activity as following genetic ablation of glutamatergic transmission locomotor-like activity can still be induced pharmacologically (Talpalar et al. 2011). It has also been shown that a genetically identified subclass of inhibitory interneurons that express the transcription factor Engrailed1 (termed V1, Talpalar et al. 2011) and comprise also Renshaw cells and Ia inhibitory interneurons regulate the speed of rhythmic locomotor output (Gosgnach et al. 2006) indicating a role for inhibitory interneurons that goes beyond the simple distribution of alternated rhythmic inputs to antagonist motor pools.

Pre-motor synapses were some of the earliest central synapses to be described and as the last modulatory input onto motor output before the neuromuscular junction could have an important role in fine control of movement. A better understanding of how they effect motoneuron activity would be useful not just in understanding motor control but also could still provide important information about basic neurophysiology and neuronal computation.

Chapter 4

Motoneuron to Renshaw cell excitatory synapse

4.1 Introduction

While the neurotransmitter composition of the motoneuron to Renshaw cell synapse has been well characterised (see Introduction chapter and Lamotte d'Incamps and Ascher 2008) there is still much to be learned about the level of connectivity between the two cell types. Anatomical studies have been useful in determining the post-synaptic receptor density but they have so far not been able to make conclusive estimates of the number of motoneuron to Renshaw cell connections (Alvarez et al. 1999, Lagerbäck et al. 1981).

The aim of the present study is to estimate the quantal parameters of this synapse and to determine the convergence of motoneurons onto Renshaw cells by analysing data from both paired recordings and those made during ventral root stimulations. This will give us a measure of the efficacy of synaptic transmission and an insight into the possible effect of firing in motoneuron pools on Renshaw cell activity.

4.2 Methods

Lumbar slices were obtained from P8–10 mice, in which the enhanced green fluorescent protein (EGFP) is expressed under the control of the promoter of the neuronal glycine transporter GlyT2 (Zeilhofer et al. 2005). Slices were cut obliquely at a 35° angle and ventral rootlets preserved during dissection. EGFP positive neurons located ventro-medial to the motoneuron nucleus where patched whole cell and confirmed as Renshaw cells by the presence of an evoked EPSC after ventral root stimulation. Dissection and slicing methods as well as protocols for paired recordings, whole-cell patch recordings and ventral root stimulation are described in detail in the General Methods.

4.2.1 Charge transfer calculation

Ventral root stimulation of Renshaw cells often resulted in excitatory postsynaptic currents (EPSCs) with multiple peaks (see Figure 4.6). It was therefore not possible to use peak amplitude as a measure of the size of the response as this would result in an ambiguous measure of EPSC size and incorrect estimates of quantal parameters. We therefore calculated the total charge of each response as this allowed for inclusion of currents occurring with a different latency with respect to the stimulation. This was done by selecting the entirety of the EPSC, beginning at a stable baseline prior to the currents rise and ending once the EPSC had once again reached baseline (or the next stimulus had begun), taking the sum of all the samples over this period and multiplying by the total number of samples. We then converted this to charge (Coulomb,C) by multiplying by the sampling interval (because $Q = \int_{t_0}^{t_n} I dt$ where t_0 is the start time and t_n is the end time).

However, in a subset of experiments due to high spontaneous activity in higher extracellular calcium concentrations it was not possible to measure the charge of responses as it would consistently include a high proportion of EPSCs that were not evoked. To allow for comparison of estimated quantal size between results produced from current and charge measurements it was necessary to convert peak amplitude estimates to charge. In experiments where

only mean peak amplitude could be measured the charge of response was measured (as described above) in low calcium where spontaneous activity was lower due to a lower probability of release and thus does not interfere with the measurement of charge. Peak amplitude and charge measurements from low calcium recordings were then plotted against each other and a linear fit made to calculate a conversion factor (see 4.1A). This method of conversion was validated using data sets where there was only a single evoked EPSC peak and low spontaneous activity in all calcium concentrations. Quantal sizes estimated using the measured charge of responses were compared with quantal sizes estimated using peak amplitude and then converted to charge. No significant difference was observed (ranksum $z = 0.0947$, $P = 0.925$, see Figure 4.1B).

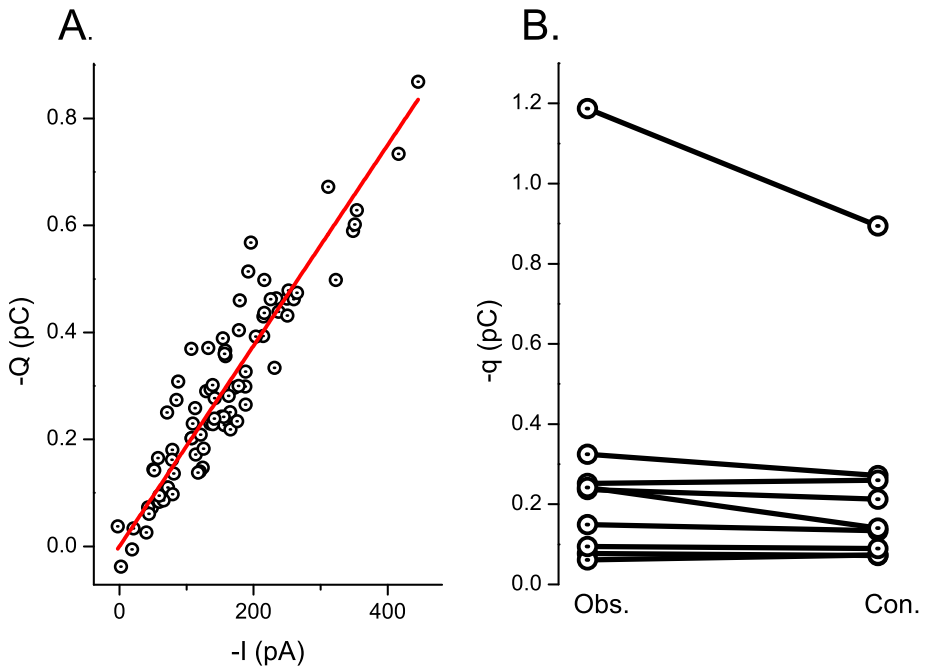

Figure 4.1: Illustration of current to charge conversion. The graph in panelA shows a scatter plot of measured charge against measured current with a linear fit overlaid in red. Panel B shows a comparison of quantal size in charge taken either from analysis done using charge as a measure of the size of response (Obs.) or from analysis that used peak amplitude as a measure of response size and then converted to charge using the method describe above.

4.2.2 Stimulus artefact subtraction

Following identification of Renshaw cells, the duration and intensity of ventral root stimulation was adjusted to find the maximal response. The choice of applying a maximal stimulation was dictated by the need of evoking a spike in as many motoneurons as possible, therefore maximising the excitatory input onto the recorded Renshaw cell. Ventral root stimulation that evoked a maximal response resulted in a stimulus artefact that we were unable to reliably reduce and varied in duration between 0.2 ms to 4 ms. Since evoked post synaptic responses occurred 1 ms to 2 ms after the stimulus it was necessary to subtract the stimulus artefact from traces to determine the 'true' PSC amplitudes. This was done in one of two ways depending on whether or not there were failures (i.e. stimulus with no response) in the experimental condition. Where an experimental condition resulted in 3 or more failures and the stimulus artefact was stable throughout the recording an averaged trace was made from all the failures. This averaged failure trace was then subtracted from the data (figure 4.2A). Averaging of traces and subtraction from data was done using pClamp (Molecular Devices). Failures were discriminated from successes using Pyclamp (a software suite developed by G.S.Bhumbra and available at http://sourceforge.net/projects/pyclamp/) by producing scatter plots of several parameters (rise time, decay time, amplitude, Fourier coefficients and the first principal components) of all the responses and then identifying clusters that contained failures. If there were no failures in a condition then a region of the trace subsequent to the stimulus but prior to the response was selected and a single or double exponential curve fitted to the region (figure 4.2B). In these conditions a fitted curve was produced for each sweep and therefore, unlike when subtracting the averaged failure trace, stability of the artefact was not critical, since an exponential fit was obtained for each response and the subtracted fit matched the time course of the artefact of each response. In conditions with no failures both fitting and subtraction were done using Pyclamp.

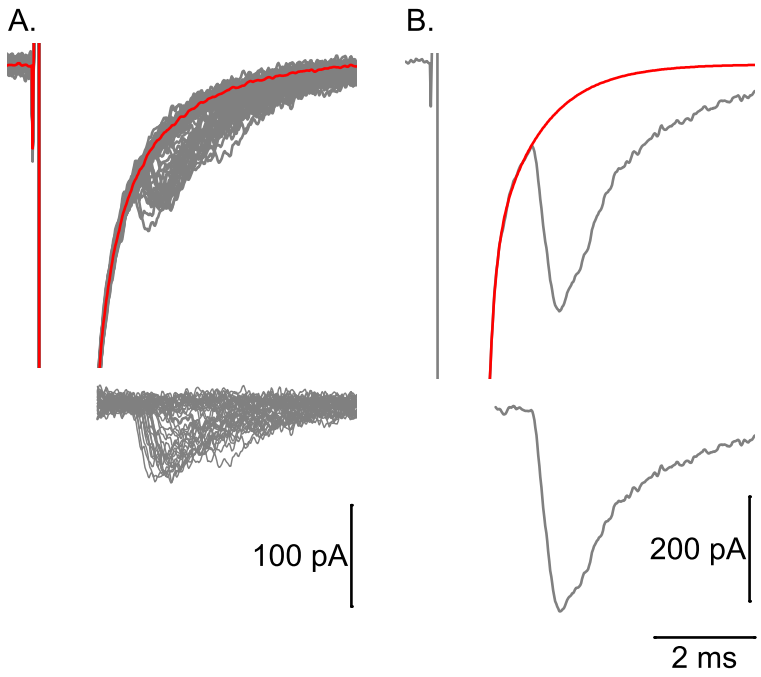

Figure 4.2: Subtraction of stimulus artefact. Panel A shows subtraction of a stimulus artefact in an experimental condition with failures and a stable artefact shape. The top trace shows traces before subtraction in grey with an averaged failure trace overlaid in red. The bottom trace in figure A shows the traces after subtraction of the averaged failure trace. The trace in panel B shows artefact subtraction in a condition where there were no failures. The top trace shows a trace prior to subtraction with an exponential fit of the stimulus artefact overlaid in red. The trace below shows the trace after subtraction of the fitted curve from the data. Both examples were taken from the same data set.

4.3 Results

4.3.1 Quantal analysis of paired motoneuron to Renshaw cell recordings

First described by Renshaw (1946) the motoneuron-Renshaw cell recurrent inhibitory circuit has atracted the interest of neuroscientists for decades since its discovery (Alvarez and Fyffe 2007). Despite the large amount of work done to describe the circuit and its function there are still some very basic questions about the synapses that compose this recurrent inhibitory loop that need to be

answered. Recent studies have thoroughly characterised the neurotransmitter composition of the motoneuron to Renshaw cell excitatory synapse (Lamotte d'Incamps and Ascher 2008, Lamotte d'Incamps et al. 2012). However there is still little known about the degree of connectivity between the motoneurons and Renshaw cells. This is important information if we wish to understand the impact of recurrent inhibition on motoneuron firing. In order to further characterise this synapse we performed BQA on data obtained from paired motoneuron to Renshaw recordings. This will give us estimates of the number of functional release sites, quantal size and probability of release thus giving us a measurement of the efficacy of the motoneuron to Renshaw cell synapse

In order to allow for Renshaw cell identification, paired recordings were made in oblique slices cut at a 35° angle with a section of ventral root preserved to maintain motoneuron axons exiting the slice. EGFP positive (and therefore glycinergic) cells located in a region ventro-lateral to the motor nucleus were considered putative Renshaw cells. Once patched, the cells were confirmed as Renshaw cells by the presence of an EPSCs in response to ventral root stimulation. Pre-synaptic motoneurons were found by evoking spikes in individual motoneurons with a loose cell attached electrode until a post-synaptic response was observed in the Renshaw cell. The pre-synaptic motoneuron was then patched, held in a current clamp configuration and 4 spikes were evoked by current step at a frequency of $33\,\mathrm{Hz}$ every 10 seconds(see figure 4.3).

Paired whole cell recordings of Renshaw cells and pre-synaptic motoneurons were made at a number of different calcium concentrations to vary the probability of neurotransmitter release and allow for estimation of the quantal parameters. A representative example of a paired motoneuron-Renshaw cell recording in $1\,\mathrm{mM}$, $2\,\mathrm{mM}$ and $4\,\mathrm{mM}$ extracellular calcium is shown in Figure 4.3A-C. In the example traces increasing calcium concentrations increased the mean current amplitude of all evoked Renshaw cell EPSCs. In low calcium EPSCs potentiated across all four stimulations whereas in control conditions the mean response depressed after the second stimulation and in high calcium depressed after the first.

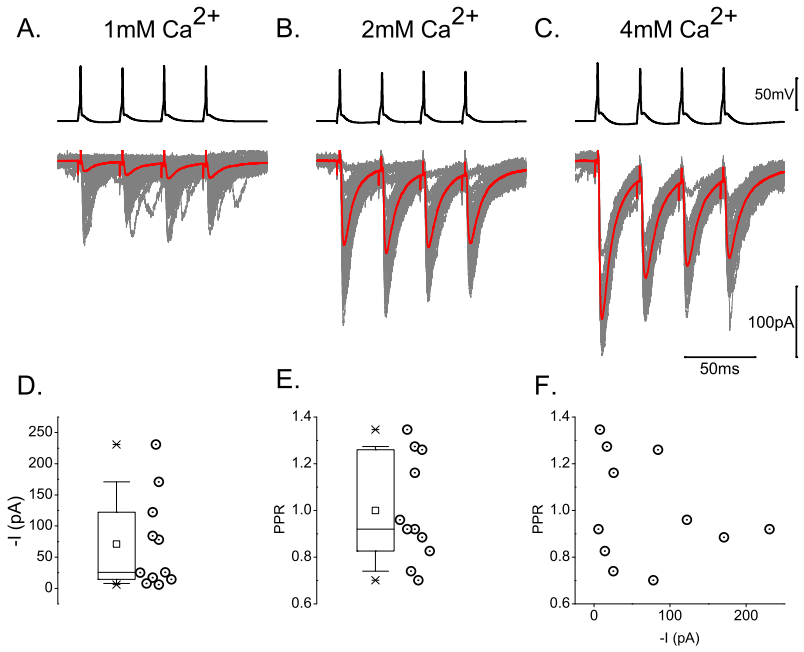

Figure 4.3: Paired recordings showing Renshaw cell response to stimulation of a single pre-synaptic motoneuron. Traces in A-C show trains of 4 motoneuron spikes evoked at a frequency of 33 Hz above response EPSCs recorded from a post-synaptic Renshaw cell with mean current overlaid in red. The probability of neurotransmitter release increases with increasing extracellular calcium concentration as the size of Renshaw cell EPSCs increases from 1 mM calcium to 4 mMCa and the mean current changes from potentiating at all four reponse in 1 mM calcium to depressing after the 2nd at 2 mM calcium and depressing after the 1st at 4 mMCa. Group data showing mean current and paired pulse ratio in control conditions (2 mM calcium) is displayed as whisker and box plots in D and E. The box plots show the interquartile range and median, outliers are shown as whiskers and the mean is displayed as square plot point. A scatter plot showing paired pulse ratio plotted against mean current is shown in F.

Group data for paired motoneuron-Renshaw cell recordings are shown in Figure 4.3D-F (n=11). The average mean current amplitude in control was -70.1 ± 22.9pA. In control conditions in 4 out of 11 paired recordings the EPSC potentiated from 1st to the 2nd stimulation (paired pulse ratio ranging from 1.16 to 1.27) while the majority of synapses observed were depressing (paired pulse ratio ranging from 0.7 to 0.92). There was no significant correlation between paired-pulse ratio and the mean current (Spearman's $r = -0.2$, $p = 0.558$).

Figure 4.4 illustrates BQA of the recordings shown in Figure 4.3. An example motoneuron spike and the first response of a Renshaw cell to a train of motoneuron spikes in 1 mM, 2 mM and 4 mM extracellular calcium are shown in 4.4A-C. Averaged Renshaw cell EPSC responses are overlaid in red.

BQA produces probability distributions for quantal size (*q*), maximal response (*r*) and the gamma shaping parameter (γ) from which estimates of the quantal parameters are derived (Figure 4.4D-F). The medians of the distributions for quantal size and maximal response are used to provide best estimates for q and r (figure 4.4 D-E). The quotient of the best estimate of the maximal response ($r = -253.2$) over the best estimate of quantal size ($q = -49.5$) gives the estimated number of release sites ($N = 5.1$). The shaping parameter γ gives an estimate of the quantal coefficient of variation (CV) because the coefficient of variation of a gamma probability density function is defined by the inverse of the square root of the gamma shaping parameter (i.e. CV$= 1\sqrt{\gamma}$, $\gamma = 11.9$, CV$= 0.29$). The posterior probability distributions for all the parameters have a sharp peak and extend over a very limited range, indicating a good estimate of the parameters, with a very narrow error band.

Histograms showing the current amplitude distributions in different calcium conditions are displayed in Figure 4.4G-I. Amplitude distributions calculated from BQA estimates are shown overlaid in black. Since the final BQA estimates are calculated from the entire data set, including observations at all release probabilities, the overlaid distributions are entirely independent of the binned amplitude distributions shown in the histograms. A close association of the calculated distribution with the experimental distribution indicates that our calculated parameters provide a good description of the observed data.

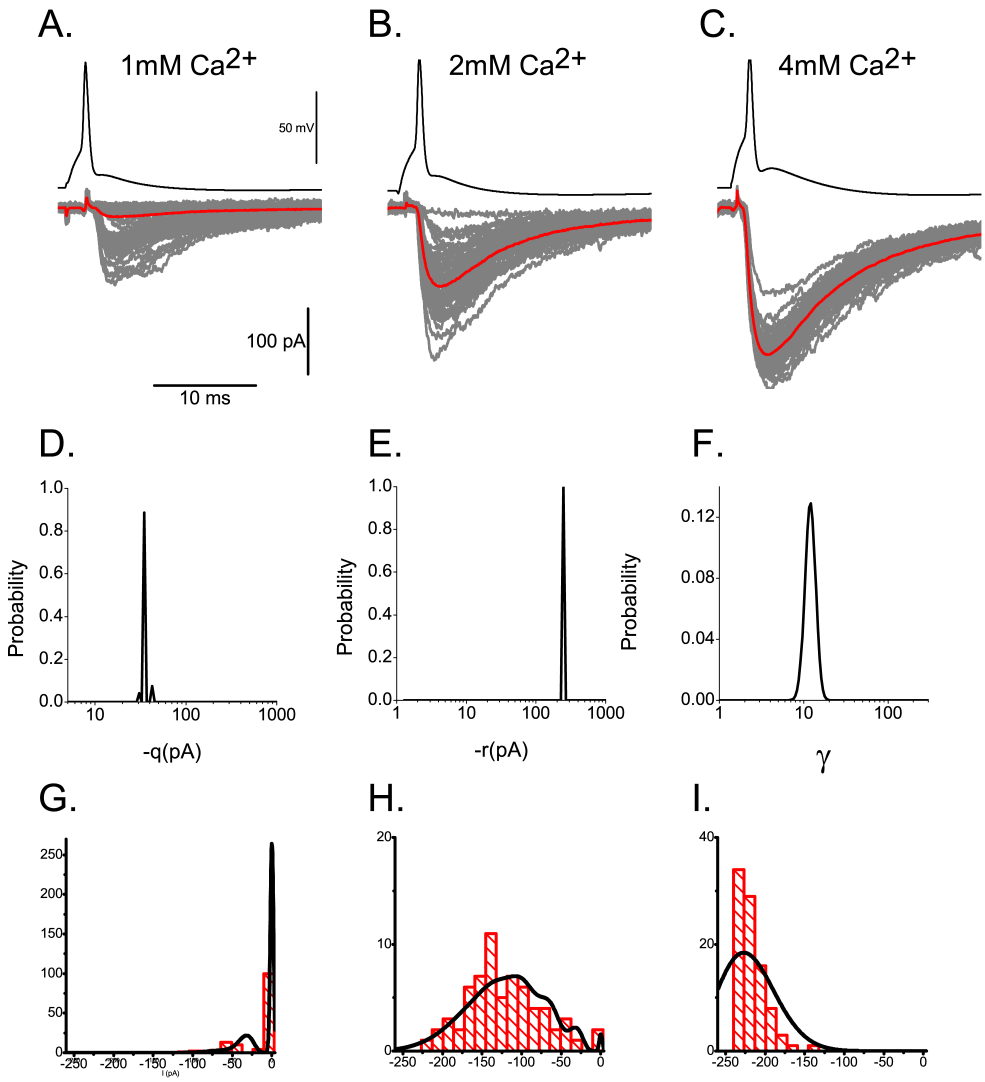

Figure 4.4: Quantal analysis of a connected motoneuron to Renshaw cell pair. An illustration of a paired recording in 1 mM, 2 mM and 4 mM extracellular calcium is shown in panels A-C. A motoneuron spike is shown in black above response Renshaw cell EPSCs in grey with an average response overlaid in red. Results of BQA are shown as probability distributions for quantal size (q) , maximal response (r) and the gamma scaling factor (γ) in panels D-F respectively. The quotient of the maximal response over the quantal size is used to calculate an estimated number of functional release (N) and the inverse of the square root of the gamma scaling factor gives an estimate of the quantal coefficient of variation(CV). Amplitude distributions for the same conditions described by graphs A-C are shown in panels G-I respectively. The predicted distribution calculated from BQA estimates for n, p and q for each of these conditions is shown overlaid in black (panels G-I).

Group results from all eleven paired motoneuron-Renshaw cell recordings that were suitable for quantal analysis are shown in Figure 4.5. Best estimates for quantal size were calculated directly from probability distributions produced by BQA as the median of the distribution (figure 4.5 A). The estimates for the number of functional release sites (figure 4.5B) were calculated using best estimates for the quantal size and maximal response (i.e. $N = r/q$). Quantal coefficients of variation (figure 4.5C) were calculated from the gamma scaling factor produced by BQA (as described above). Probability of release was calculated by dividing the mean response to the first spike in control (2 mM) extracellular calcium by the best estimate of the maximal response (i.e. $p = \bar{I}/r$ where $\bar{I}$ is mean amplitude of the response and $r = Nq$). Plotting the paired pulse ratio of the first two responses in control conditions against probability of release (4.5E) showed no significant correlation (Spearman's $r = -0.2636$, $P = 0.435$). Estimates of the failure rates in control conditions were calculated from the probability of failure to release ($p_{fail} = 1 - p_{success}$) and the best estimate of the number of release sites (failure rate $= p_{fail}^{N}$). Estimated failure rates were compared with the failure rate observed during recordings and no statistically significant difference was found (sign-rank $z = 1.689$, $P = 0.091$). This is validation of the BQA estimates as the observed failure rate is not used at all during BQA and therefore is independent of the quantal estimates from which the estimated failure rate is calculated.

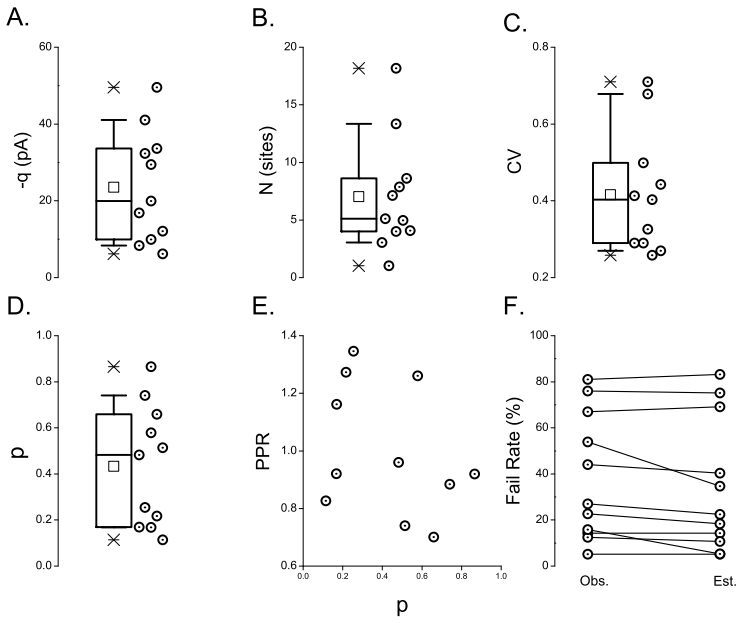

Figure 4.5: Group data showing quantal parameters of the motoneuron to Renshaw cell synapse obtained from paired recordings. Whisker and box plots of quantal size (q), the number of functional release sites (N), quantal coefficient of variation (CV) and probability of release in control conditions (p) are shown in panels A-D respectively. A scatter plot of paired-pulse ratio plotted against probability of release is shown in panel E. Observed failure rate plotted against failure rate estimated from BQA results is shown in panel F.

These estimates provide information about the properties of the synapse between individual motoneurons and Renshaw cells. However, multiple motoneurons are known to project onto a single Renshaw cell (Cullheim et al. 1977, Cullheim and Kellerth 1981). While it is important to know the extent of the conductance change associated with a single motoneuron input to a Renshaw cell, the overall response of Renshaw cells to firing in motoneurons will be dependent on how many individual motoneurons contact a single Renshaw cell. In order to understand the transmission properties of the recurrent inhibitory circuit it is thus necessary to know the degree of convergence of motoneurons onto Renshaw cells.

4.3.2 Quantal analysis of Renshaw cell ventral root stimulation recordings

Stimulation of the ventral root antidromically excites all motoneurons with axons still present in the root (which is probably the majority of motoneurons in the slice). This means that EPSCs recorded from Renshaw cells in response to ventral root stimulation are the summation of excitatory inputs from all excited motoneurons. Quantal analysis of ventral root stimulation response provides a measure of the quantal parameters of the combined inputs from all motoneurons in the slice projecting onto the recorded Renshaw cell and therefore it can lead to an estimate of the number of motoneurons impinging on a single Renshaw cell.

Evoking EPSCs in Renshaw cells by ventral root stimulation often resulted in current amplitude traces with multiple peaks. During ventral root stimulation motoneurons with axons projecting from the slice into the root are stimulated antidromically. However, motoneurons belonging to the same nucleus, as well as synergistic motoneurons, are known to be connected by excitatory synapses (Gogan et al. 1977). As a consequence, there is another population of motoneurons post-synaptic to those firing antidromically that also fire after ventral root stimulation but do so with a longer latency with respect to the stimulus. This results in different populations of motoneurons firing with different latencies depending on whether they are excited antidromically or orthodromically (see Figure 4.6). Since antidromic spikes are followed by a long lasting (20-30 ms) after hyperpolarization, it is unlikely that an antidromic spike could be followed by an orthodromic one. We verified this possibility by performing loose cell-attached recordings from motoneuron and delivering maximal stimulation to the ventral root in a set of experiments performed on oblique slices. In all the recorded motoneurons(n=10, data not shown), spikes could be evoked either antidromically (identified by the short and consistent latency of $\sim 1\,\text{ms}$) or orthodromically (characterized by large jitter and a latency of $> 4\,\text{ms}$), but a sequence of antidromic-orthodromic spike was never observed in the same motoneuron. This is most likely due to the refractory period after the action potential in antidromically stimulated motoneurons preventing repeated firing.

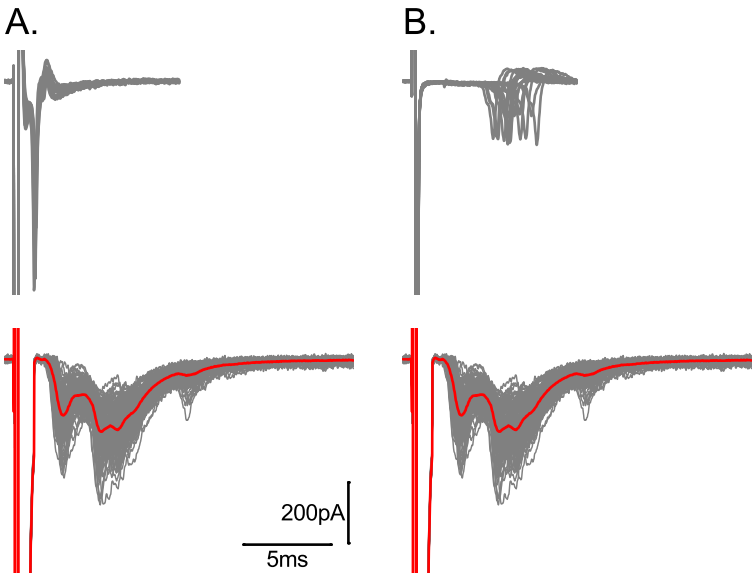

Figure 4.6: Example traces showing loose cell attached recordings of motoneurons firing either antidromically (A) or orthodromically (B).The traces shown below are an example of Renshaw cell EPSCs evoked by ventral root stimulation (n.b. both sets of traces show the same recording). The multiple peaks evident in the Renshaw EPSCs correspond to responses from motoneurons firing either antidromically or orthodromically as shown in the loose cell attached recordings above. (the difference in spike size between A and B is due to differences in the seal between the two cells recorded in loose cell-attached

There was therefore a subset of experiments in which the multi-peaked Renshaw cell response to ventral root stimulation meant that peak amplitude would be an ambiguous measurement of the size of evoked responses. In fact, by analyzing for instance the early peak (as in the example of Figure 4.6), one would exclude the currents originating from the motoneurons who fire later (presumably orthodromically). As a consequence, the estimate of quantal parameters would include only early (antidromically) firing motoneurons, leading to an underestimate of the number of functional release sites. We therefore calculated the total charge of responses (see Methods) which allowed us to incorporate the multiple peaks into our measurement of the size of the response

and give a correct estimation of quantal parameters. The size of Renshaw cell response and quantal size in these ventral root stimulation experiments is therefore reported in coulomb (pC).

A representative example of Renshaw cell responses to ventral root stimulations is shown in Figure 4.7A-B. Similar to the paired recordings protocol, the ventral root was stimulated 4 times at a frequency of 33 Hz every 10 s. In the example traces shown in Figure 4.7A-B the size of response increased with higher extracellular calcium (Figure 4.7A-B). At low (1 mM extracellular calcium concentrations the mean response potentiated across all four stimuli. While at higher (2 mM) extracellular calcium concentrations the mean response depressed after the stimulus. Group data showing the mean charge of the response and the paired pulse ratio (between the first and second response to ventral root stimulation) in control conditions are shown in Figure 4.7C-D. A plot of paired pulse ratio against mean charge showed significant correlation between the two variables (Spearman's $r = -0.846$, $P = 0.001$).

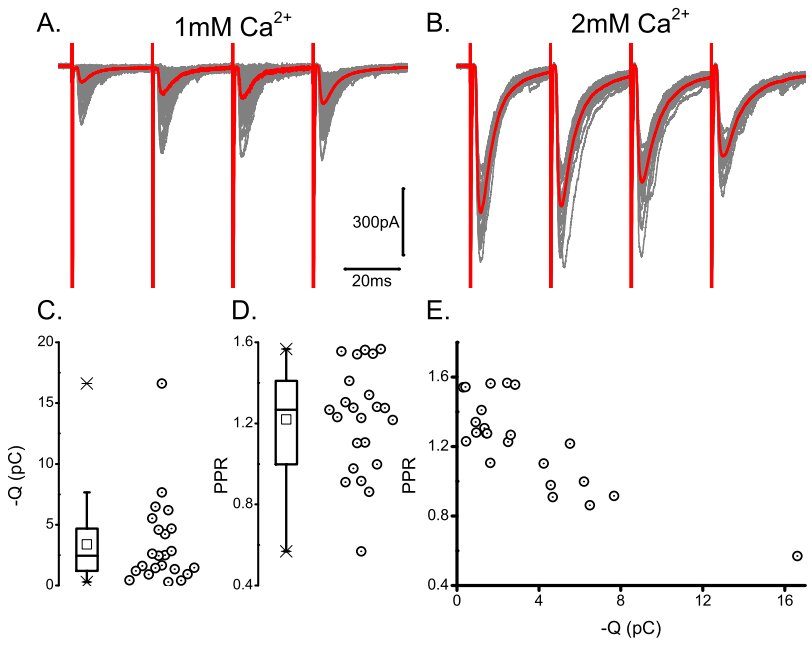

Figure 4.7: Excitatory post-synaptic currents in Renshaw cells evoked by ventral root stimulation. Traces in A and B show Renshaw cell EPSCs following ventral root stimulation in 1 mM and 2 mM extracellular calcium. Individual responses are shown in grey with an averaged trace overlaid in red. Group data for mean charge and paired pulse ratio are shown as whisker and box plots in C and D respectively. A scatter plot showing charge transfer against paired pulse ratio is shown in E.

An illustration of BQA of Renshaw cell ventral root stimulation recordings is shown in Figure 4.8. Traces shown in figure 4.8A and B show the first response to ventral root stimulation in 1 mM and 2 mM extracellular calcium. Probability distributions produced by BQA for the quantal size (q), the maximal response (r) and the gamma scaling factor (γ) are shown in Figure 4.8E-G respectively. The median of distributions provide best estimates for quantal size and the maximal response, and from these the number of release sites (n) is calculated ($n = r/q$). The inverse of the square root of the gamma scaling factor is used as an estimate of the quantal coefficient of variation ($CV = 1\sqrt{\gamma}$, $\gamma = 4.42$, $CV = 0.475$). Histograms showing charge distributions of traces shown in Figure 4.8A and B are shown in F and G. The black line overlaid on top of the histograms is a distribution of charge calculated from estimates of

the quantal parameters derived from BQA results. The quantal parameters estimated by BQA are independent on individual probability distributions as they are calculated from the entire data set which comprises all recorded probabilities of release. The overlaid distribution and amplitude distributions for individual release probabilities are therefore independent of each other and a close association between the estimated distribution and the observed experimental distribution are consistent with a valid estimation of quantal parameters.

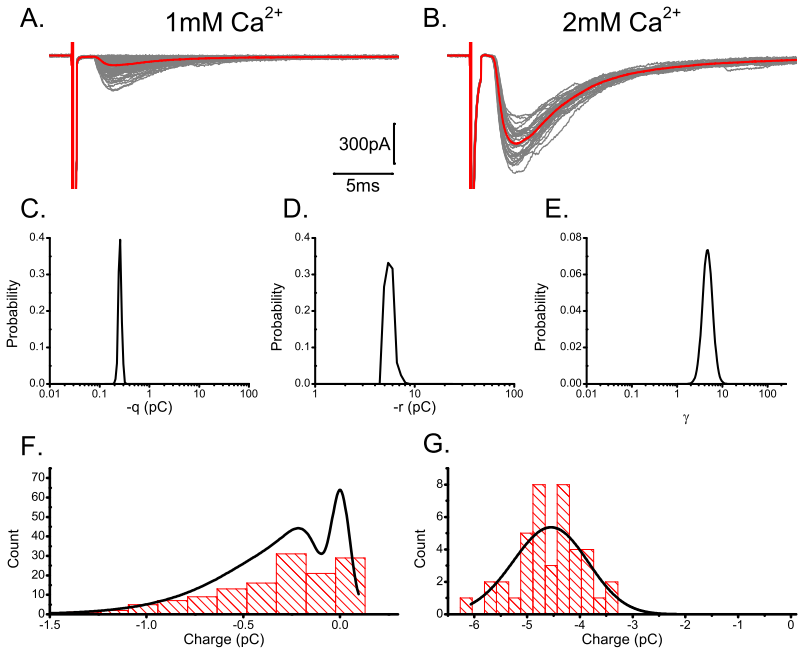

Figure 4.8: Illustration of experimental data and results of BQA. Example traces of the first response from ventral root stimulation in low (1 mM) and control 2 mM extracellular calcium concentrations are shown in panel A and B respectively. BQA yields probability density distributions for quantal size, the number of release sites and a gamma scaling factor which are shown in panels C-E. Histograms showing the amplitude distributions of those EPSCs are shown below in red (panels F and G). Estimated amplitude distributions calculated from BQA results are shown overlaid in black.

Figure 4.9 shows BQA estimates for all Renshaw cell ventral root stimulation recordings that were suitable for analysis ($n = 23$). The data were split into three groups depending on the type of analysis that could be performed: in one set of experiments ($n = 8$) double or multiple peaks were observed in the post-

synaptic response, due to synapses formed from a mixed population of motoneurons, some firing antidromically and some firing orthodromically. In these cases, only measurement of total charge could be taken. In a second subset ($n = 9$), the evoked EPSCs had a single well defined peak, indicating that the recorded Renshaw cell was connected only to motoneurons firing antidromically. In these cases both charge and peak amplitude measurements could be used to derive the quantal parameters. In this subset of experiments, BQA was performed for both measures and the estimates derived for n and p were not significantly different (see below). In a third group of experiments ($n = 6$) the frequency of spontaneous events was high, leading to a contamination of the tail of the evoked response. In those cases, peak amplitude measurements were used. In order to compare the quantal size obtained from these 'amplitude only' measurements, we used the responses recorded in low calcium. In these conditions of reduced probability of release, spontaneous events were infrequent and therefore did not interfere with measurement of charge. As described in the Methods, we measured both amplitude and charge for the same data set and used them to calculate a conversion factor from current ampere to charge coulomb. The same conversion factor was then used to translate the mean peak amplitude measured in high Calcium into a charge measurement. Similarly, we converted to charge the q and r parameters obtained from BQA.

In the group data presented in Figure 4.9 n, p and CV (panels B, D and C respectively) are taken from estimates calculated using the charge where possible and from peak amplitude where not possible. Mean quantal size of all experiments was -0.22 ± 0.23pC. The mean number of release sites was 31 ± 3.5 and the mean probability of release was 0.49 ± 0.03. Paired-pulse ratio of the first two responses in control conditions showed a strong correlation with probability of release (Spearman's $r = -0.846$,$P < 0.001$, figure 4.9E).

Figure 4.9F shows a comparison between failure rates calculated from estimates of quantal parameters made using charge or peak amplitude (failure rate $= p_{fail}^{N}$) with those observed during recordings. There was no significant difference between observed failure rate and those estimated using charge as a measure of response (sign-rank $z = -0.88$, $P = 0.397$) nor between observed failure rate and those estimated from those estimated using

peak amplitude as a a measure of response (sign-rank $z = -1.29$, $P = 0.198$).

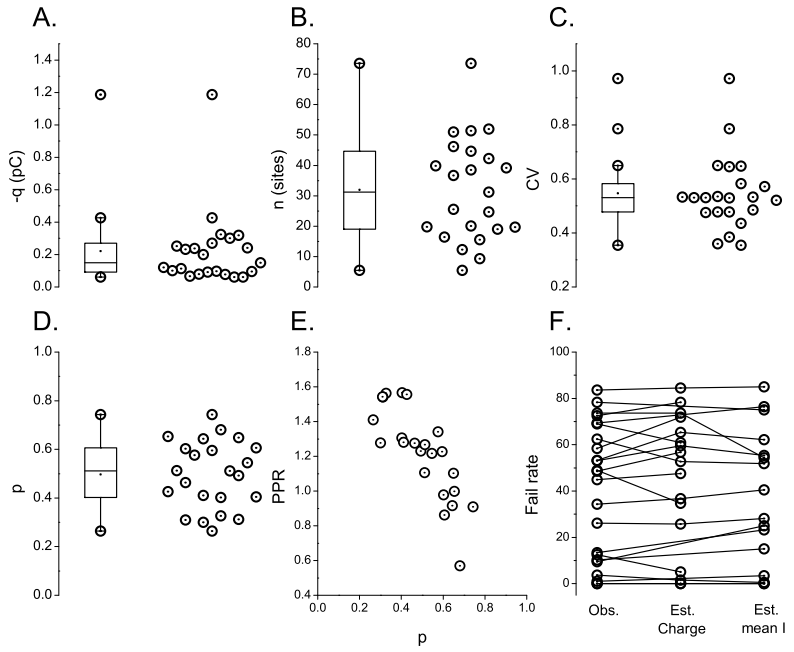

Figure 4.9: Group data of BQA estimates from Renshaw cell ventral stimulation recordings. Box-and-whisker plots for the number of release sites, quantal size, quantal coefficient of variation and probability of neurotransmitter release are displayed in panels A-D. A scatter plot of paired-pulse ratio against probability of release is shown in panel E. A comparison of observed failure rates, failure rate calculated from from BQA estimates derived using the charge of the response and failure rate calculated from BQA estimates derived using the mean current amplitude of the response is shown in panel F.

Figure 4.10 shows a comparison of estimates for number of functional release sites and probability of release as well as failure rates for experiments in which both the charge and peak amplitude could be used to measure the size of response($n = 9$). There was no significant difference in the estimates of the number of functional release sites (sign-rank $z = 1.54$, $P = 0.124$) or probability of neurotransmitter release (sign-rank $z = -0.84$, $P = 0.401$). There was also no significant difference between observed failure rates and those calculated from quantal estimates derived from the charge (sign-rank $z = -1.18$, $P = 0.237$) or those calculated from quantal estimates derived from peak cur-

rent amplitudes (sign-rank $z = 0.085$, $P = 0.933$).

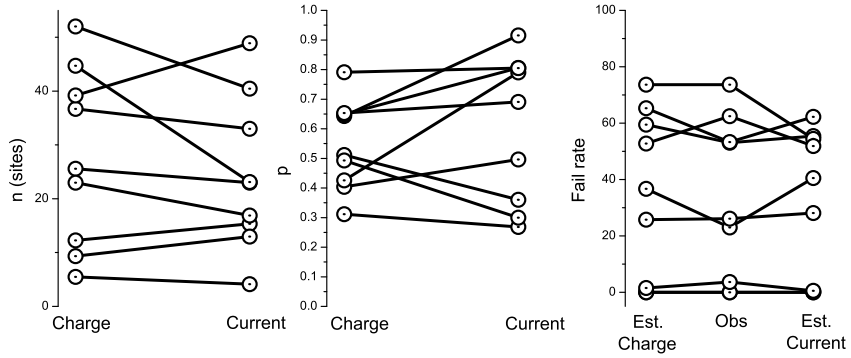

Figure 4.10: Comparison of quantal estimates calculated using either charge or current peak amplitude as a measure of the size of response. Plots comparing estimate for number of release sites and probability or release are shown in panels A and B respectively. A comparison of failure rates calculated from estimates of quantal parameters with failure rates observed during recordings is shown in panel C.

In the eight experiments in which, due to multiple peaks in evoked EPSCs, only charge could be measured we also measured peak amplitude of the initial peak (see Figure 4.11A for an illustrative example). This peak amplitude measure was then used to estimate quantal parameters so a comparison could be made between the number of release estimated using the whole response (by measuring the charge) and only part of the response (by measuring peak amplitude). The peak amplitude measurement should give lower estimates for n as it should be sampling from a smaller number of release sites, excluding most of the EPSCs originating from orthodromically excited motoneuron, occurring at a longer latency with respect to the stimulation.

While the number of release sites estimated from peak amplitude and charge were not significantly different (sign-rank $z = 1.5$, $P = 0.1235$) in all but one of the eight multi-peak experiments there was a lower estimate of n using peak amplitude compared with charge (Figure 4.11B). Probability of release however was significantly greater when calculated from quantal estimates derived from measurements of peak amplitude (sign-rank $z = 2.52$, $P = 0.011$, Figure 4.11C). Since probability of release is calculated using the mean response and the maximal response it is therefore reliant on estimates of quantal

size and number of release sites ($r = nq$). A significantly different p therefore indicates that measurement of only the peak does result in significantly different estimates of quantal parameters from using the charge.

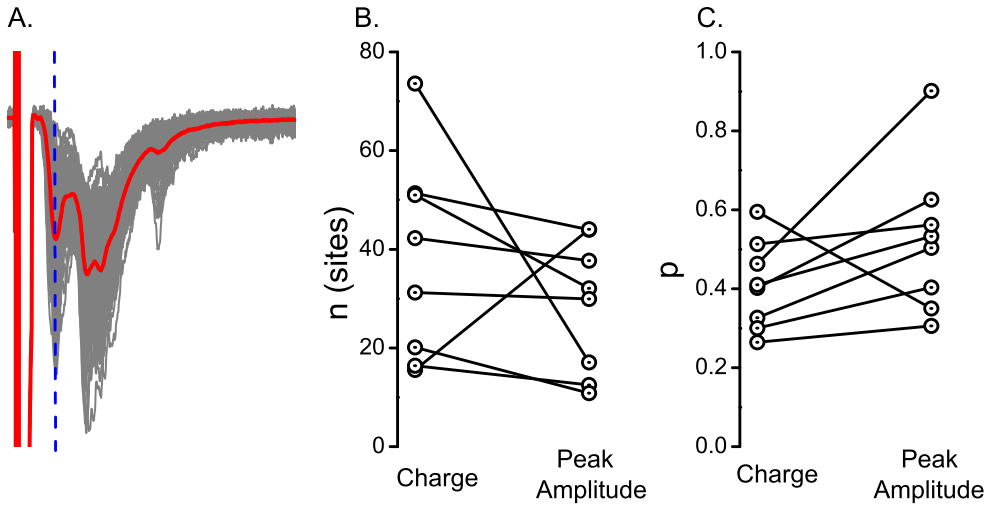

Figure 4.11: Comparison of quantal estimates from experiments with multi-peaked evoked EPSCs obtained from charge and peak amplitude measurements. Panel A shows an example traces of multipeaked response (mean trace overlaid in red) with a blue dotted line placed over the first peak to illustrate where mean peak amplitude was measured. A comparison of estimates for number of release sites and probability of release calculated using charge and peak amplitude are shown in panels B and C respectively.

4.3.3 Effect of motoneuron firing on evoked Renshaw cell EPSCs

Estimates of the quantal parameters shown above give us information about the properties of the motoneuron to Renshaw cell synapse and a measurement of the degree of convergence of motoneurons onto Renshaw cells. However, to understand the role of this synapse in the recurrent inhibtory circuit it is necessary to know how a pre-synaptic spikes is translated into changes in the post-synaptic potentials and in particular what is the effect of repetitive firing has on the post-synaptic response. To investigate the reliability of synaptic transmission we performed paired recordings with both cells recorded in current-clamp

configuration and spikes evoked in the motoneuron by current step. Figure 4.12 shows examples of two paired recordings where Renshaw cells were recorded in both voltage and current-clamp configurations and pre-synaptic motoneurons were recorded in current-clamp. In Figure 4.12A the EPSCs, shown in the top trace, evoked by spikes in the pre-synaptic motoneuron are small (mean current of first response is -18.8 ± 2.2 pA) but are still able to evoke induce firing on the second or fourth stimulus (Figure 4.12A bottom trace). While Figure 4.12B shows another pair in which spikes in evoked in the pre-synaptic motoneuron evoked large EPSCS (-223 ± 3.9 pA, top trace) and here action potentials are reliably induced on the first and third stimulus. The after-hyperpolarising potentials of the spikes evoked by the first and third stimuli is probably responsible for the lack of response on the second and fourth stimulus (Figure 4.12B bottom trace).

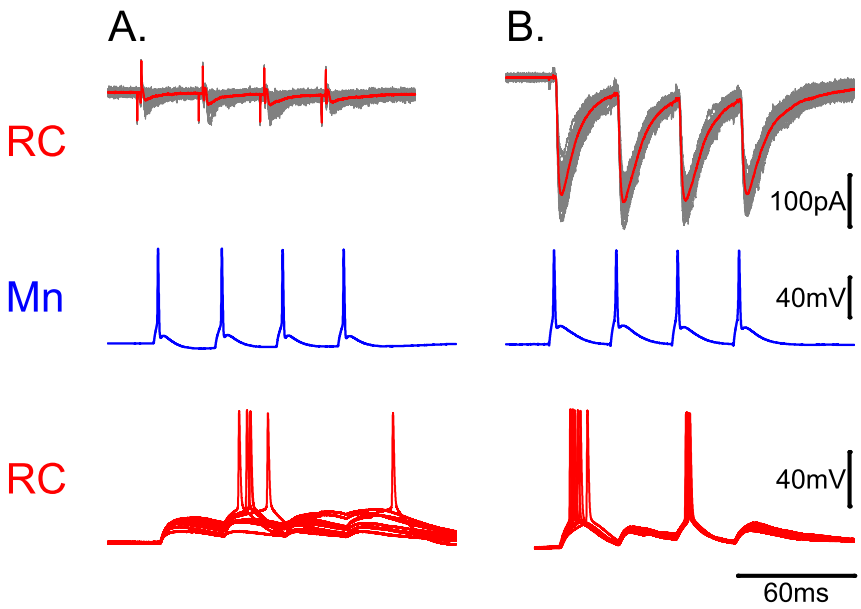

Figure 4.12: Reliability of synaptic transmission at the motoneuron to Renshaw cell synapse. Panels A and B show recordings from two different motoneuron to Renshaw cell pairs. The top traces in both panels show example traces of Renshaw cell EPSCs recorded in voltage-clamp evoked by four spikes in the pre-synaptic motoneuron induced at a frequency of 33 Hz. The bottom traces show current clamp recordings from the same Renshaw cell that was recorded in voltage clamp for the top traces. EPSPs are evoked by spikes induced in the pre-synaptic and result in action potentials in the post-synaptic cell after the second and fourth stimulus in panel A and first and third stimulus in panel B.

The ability of the motoneuron to evoke an action potential even in a relatively small synapse (as shown in Figure 4.12A) suggests that this is a very reliable synapse. During different motor tasks, motoneurons can fire at a very broad frequency range, from the primary range (15-30 Hz) to the secondary high frequency range (50-80 Hz). We therefore conducted experiments to evaluate the effect of different motoneuron firing frequencies on evoked response in the Renshaw cell. After whole-cell patch of Renshaw cells ventral roots were stimulated 20 times at a frequency of $3, 10, 33, 50$ or 100 Hz every 10 seconds. Group data in Figure 4.13A shows faster stimulation frequency results in greater depression of evoked EPSCs. Paired pulse ratio of evoked EPSCs between the

first and second pulse was similar across all frequencies (Figure 4.13B). Group data for each frequencies across all cells were fitted with a single exponential decay to determine the asymptotic value for depression at different frequencies. Motoneuron firing at 3 and 10 Hz caused relatively modest depression to 77% and 64% of the first EPSC respectively (Figure 4.13C). Frequency of firing 33 Hz and greater reduced evoked EPSCs to less than half the initial response (45% at 33 Hz, 44% at 50 Hz and 38% at 100 Hz Figure 4.13C).

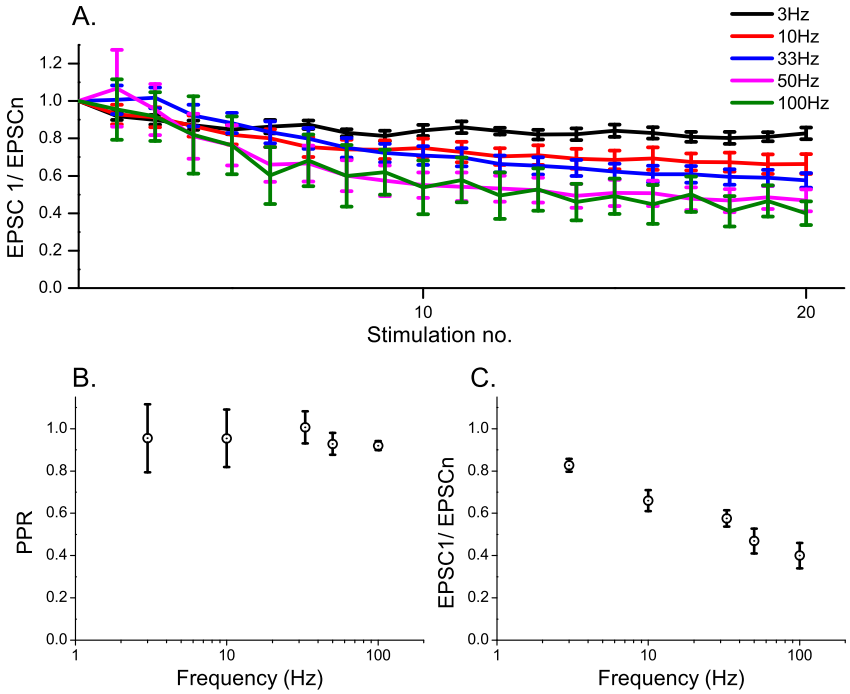

Figure 4.13: Effect of motoneuron firing frequency on depression of Renshaw cell evoked EPSCs. Panel A shows group data showing the effect paired pulse ratio at each stimulus number across different frequencies of stimulation ($n = 4$ for 100 Hz, $n = 7$ for 50 Hz, $n = 8$ for 3 Hz, $n = 9$ for 10 Hz and $n = 13$ for 33 Hz). Panels B and C show paired pulse ratio against frequency of stimulation for the second stimulus and the 20th stimulus respectively.

4.3.4 Reciprocal connections between motoneuron and Renshaw cells

It is known that Renshaw cells receive excitatory input from motoneurons that are in the same motor pool as the motoneurons they innervate and inhibit. It is therefore possible that a population of Renshaw cells receive excitatory input from and deliver an inhibitory output onto the same motoneuron. During paired recordings we tested for reciprocal connections by holding the 'post-synaptic' motoneuron in voltage clamp at 0 mV (in order to isolate inhibitory currents) and the 'pre-synaptic' Renshaw cell in current clamp, then induced action potentials in the motoneuron by current step. If the cells had a reciprocal connection we would see evoked IPSCs in the motoneuron recording. Out of 18 cells tested for a reciprocal connection only 3 pairs featured both an excitatory and inhibitory connection. An illustrative example of a reciprocal connection is shown in Figure 4.14.

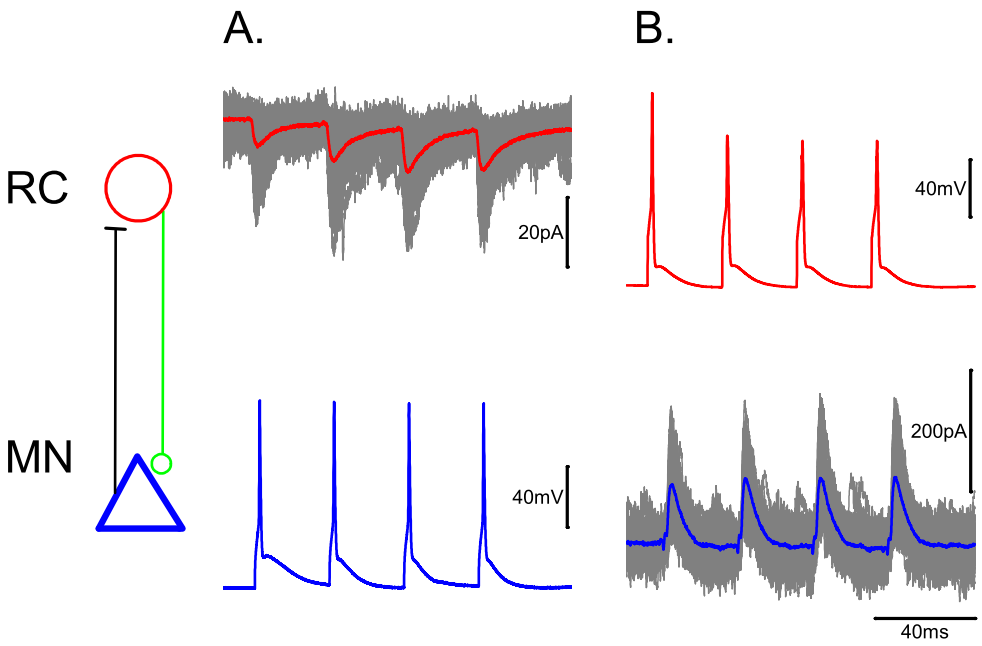

Figure 4.14: Recording of a reciprocal connected pair. In panel A the Renshaw cell and motoneuron are in the same configuration as the paired recordings described in the quantal analysis experiments. Action potentials are evoked in the motoneuron which is held in current-clamp configuration (bottom blue trace) and evoked EPSCs can be seen the Renshaw cell recorded in voltage-clamp configuration (top grey traces with average trace overlaid in red). The recordings in panel b show recordings from the same cells but this time the action potentials are evoked in the Renshaw cell which is held in current clamp (top red trace) and the evoked IPSCs are recorded from the motoneuron held in voltage-clamp (bottom grey traces with averaged trace in blue). A diagrammatic scheme of reciprocally connected cells is shown on the left hand side of the figure with the Renshaw cell in red and motoneuron in blue. An excitatory connection from the motoneuron to Renshaw cell is shown as a black line and the inhibitory Renshaw cell to motoneuron projection is shown as a green line.

4.4 Discussion

4.4.1 Number of release sites

The data presented in this chapter show estimations of the quantal parameters of the motoneuron to Renshaw cell synapse, both between single cells and between multiple motoneurons and a single Renshaw cell. Importantly this gives

the first estimate of the functional number of release sites at the motoneuron to Renshaw cell synapse and the degree of convergence between motoneurons and Renshaw cells. Anatomical studies have previously given estimates of roughly $50 - 100$ motoneurons contacting each Renshaw cell (Alvarez et al. 1999). This is likely to be an overestimate as it assumes that the density of cholinergic contacts observed at the soma and proximal dendrites will be the same at distal projections. It is also a indirect measure of contacts as it is based on staining techniques that could include cholinergic contacts that are not necessarily functional synapses. The data in this chapter shows the mean number of functional release sites estimated from paired recordings was $n = 6.5 \pm 1.15$ (Figure 4.5B) and from ventral root stimulation was $n = 31.9 \pm 3.5$ (Figure 4.9B). From these results we can estimate that in slice preparations an average of ~ 6 motoneurons synapse onto each Renshaw cell. This is comparable with an observation made by Lagerbäck et al. (1981) in an anatomical study of cat motoneurons who noted "4 boutons from one (Motoneuron) collateral were observed in synaptic contact with one single post-synaptic neuron". While Lagerbäck et al. (1981) did not positively identify Renshaw cells, post-synaptic neurons were assumed Renshaw due to anatomical position and morphology. A limiting factor in our own estimates is of course the size of the slice preparation. Our slices were $400\,\mu m$ thick and therefore it is possible that some connections will have been lost during cutting. However this would lead to an underestimate of the number of release sites calculated from both paired and ventral root stimulation data and therefore our estimation of motoneuron to Renshaw cell convergence may still be valid.

4.4.2 Quantal size and probability of neurotransmitter release

Quantal size and probability of release should be shared parameters between the paired and ventral root stimulation data sets since the paired recordings are simply a smaller sample of the release sites observed during ventral root stimulation. Indeed, no significant difference was found between the two data sets for quantal size (rank sum $z = 0.516$, $P = 0.606$) and probability of re-

lease (rank sum $z = -0.737$, $P = 0.461$). This is convincing evidence that the paired recordings are a representative sample of motoneuron to Renshaw cell synapses in this slice preparation. BQA estimates were more generally validated by the lack of significant difference between observed failure rates and those calculated using estimated quantal parameters (see Results). Failure rates can be calculated from estimates of quantal parameters but are neither an input nor output of BQA. The agreement of failure rates observed during recordings with those predicted by quantal parameters estimated by BQA is therefore a convincing validation of BQA results.

Studies of the neuromuscular junction (NMJ) in the crayfish (Bittner 1968, Atwood and Bittner 1971, Frank 1973, Cooper et al. 1996, Parnas 1972) and frog (Bennett et al. 1986, Robitaille and Tremblay 1987; 1991) have shown heterogeneity in probability of release between synapses. It is therefore possible that p is not uniform across all release sites at the motoneuron to Renshaw cell synapse. In this study our BQA assumed homogeneity of p and therefore the p reported is an average probability that desrcibes p across all release sites. It has been shown that p at pyramidal cell synapses can vary depending on post-synaptic cell identity (Koester and Johnston 2005). This has also been shown to be the case in other cell types (Rosenmund et al. 1993, Murthy et al. 1997). It is therefore possible that post-synaptic cell identity can act as a determinant of probability of release and therefore p would likely vary between central motoneuron synapse and peripheral motoneuron synapse. Even though we have not calculated p at individual synapses, if there was a considerable difference between p at motoneuron to Renshaw cell synapse and p at the NMJ it would possibly be evident while comparing the average p for each of these connections. While there have been no studies that have estimated the probability of neurotransmitter release at the mouse NMJ, experiments by Christensen and Martin (1970) estimated probability of release at the rat neuromuscular junction in low Calcium concentration (1.5 mM) to be 0.12 ± 0.05. Studies of the frog NMJ have estimated that the probability of neurotransmitter release at an extracellular calcium concentration (1.8 mM) similar to our control (2 mM) to be between 0.32 and 0.65 (Miyamoto 1975). Both these estimates are in agreement with our estimation of p in control ($\bar{p} = 0.47 \pm 0.03$, 2 mM) and low ($\bar{p} = 0.14 \pm 0.05$,

1 mM) extracellular calcium. While this certainly does not preclude the possibility of a wider range of p across motoneuron to Renshaw cell synapses it does suggests that both connections have similar synaptic fidelity. In fact given the lack of significant differences between estimates of p in paired and ventral root recordings does imply that p is relatively uniform between connections.

4.4.3 Role of recurrent inhibition

Eccles et al. (1954) initially suggested that the primary role of Renshaw cells and recurrent inhibition was simply to prevent excessive firing of motoneurons. However as our understanding of the complexity of spinal cord circuitry has advanced the role of recurrent inhibition has become less certain (see Windhorst 1996, Hultborn 2006, Windhorst 2007; for extensive reviews on the subject). It is now known that Renshaw cells receive inputs from neurons that are not α-motoneurons and therefore cannot be regarded as only part of simple feedback circuit (Alvarez and Fyffe 2007). Studies in the cat by Brooks and Wilson (1958) suggested that Renshaw cells act to 'localize' the stretch reflex thus aiding the control of fine movement. This however is in disagreement with later findings that muscles involved in fine movement are not subject to recurrent inhibition (Illert and Kümmel 1999). Since Renshaw cells are also know to project onto group Ia interneurons it has been suggested that they could have a role in limiting the excitatory effects group Ia neurons have on motoneurons (Katz and Pierrot-Deseilligny 1999). It has also been suggested that the purpose of Renshaw cells is to provide an 'efferent copy' of motor output that estimates the muscle activation generated by neural excitation (Loeb et al. 1989). Studies of the human spinal cord have suggested that recurrent inhibition acts as a variable gain regulator of motor output by varying inhibition depending on the intensity of muscle use (Hultborn and Pierrot-Deseilligny 1979).

Renshaw cells have been shown to be rhythmically active during fictive locomotion (McCrea et al. 1980, Nishimaru et al. 2006, Pratt and Jordan 1987) and while their role is not clear it does appear that they are not involved in the generation of rhythmic firing (Pratt and Jordan 1987). Reduction of Renshaw cell activation by application of a cholinergic antagonist during locomotion results

in an increase in motoneuron firing (Noga et al. 1987) suggesting they could reduce motoneuron firing during locomotion. However the same study (Noga et al. 1987) also showed no loss of inter-burst membrane hyper-polarisation nor an increase in burst duration in burst duration during inhibtion of Renshaw cell activity.

While an overall role for recurrent inhibition in motor control is still uncertain what is clear is that the motoneuron to Renshaw cell synapse is an exceptionally reliable step in the recurrent inhibitory circuit. Studies by Ross et al. (1975; 1976) showed that stimulation of single motoneurons can evoke firing in Renshaw cells and drive Renshaw cell firing up to a frequency of 60 Hz. The convergence of ~ 6 motoneurons onto each Renshaw cell therefore suggests that it is very unlikely that within synergistic motoneuron pools connected Renshaw cells would fail to fire during muscle contraction. This could be considered to be in agreement with the suggestion that Renshaw cells act as an 'efferent copy' of motor output as it can be concluded that the motoneuron to Renshaw cell synapse exhibits high fidelity of transmission and therefore Renshaw cell activity would follow motor neuron output very closely. Our data has also shown that at calcium concentrations of 2 mM evoked EPSCs will depress even at low frequencies of motoneuron firing (27% depression at 3 Hz) and are reduced more that half a frequencies of 33 Hz and above (see Figure 4.13). Studies of recurrent inhibition in humans have shown that while weak muscle contraction results in strong recurrent inhibition, strong muscle contraction results in weak recurrent inhibition (Hultborn and Pierrot-Deseilligny 1979). Synaptic depression at the motoneuron to Renshaw cell synapse could have a role in reducing the strength of recurrent inhibition during repetitive firing. This could be functionally useful during intensive use of muscles where recurrently inhibiting motoneuron firing would be counter-productive.

The role that Renshaw cells and recurrent inhibition play in the control of motor output remains unclear but is certainly more complex than Eccles et al. (1954) first suggested when describing the circuit over half a century ago. The data presented here provides further evidence of the strength and reliability of the motoneuron to Renshaw cell synapse. The synaptic depression observed very early during repetitive stimulation (Figures 4.3 and 4.7) also suggests that

this synapse could be important for modulation of recurrent inhibition. The relatively high p and n, combined with the estimated motoneuron to Renshaw cell convergence and the comparable p of central synapses observed here and peripheral observed in other studies suggests that Renshaw cell activity is likely to be a direct copy of motoneuron activity. Recently developed viral staining techniques are beginning to elucidate the structure of neuronal pre-motor architecture (Stepien et al. 2010). This information along with the quantal parameters presented in this chapter will hopefully help to inform future modelling studies that will be able to more fully realise the complexity of spinal cord circuitry and finally suggest a conclusive functional role for Renshaw cells.

Chapter 5

General Discussion

Sir Charles Sherrington famously described motor output as the 'final common pathway' of the nervous system. Motor control and coordination follow a complex pathway, from initiation by 'higher functions' to the fine control of motoneuron firing by local neuronal circuits. This makes motor control an invaluable subject of study for understanding neurophysiology both at a cellular and network level. Historically, the study of motoneurons and their projections has given great insights into how the nervous system works. Seminal studies of the spinal cord provided the first evidence for chemical neurotransmission (Fatt and Katz 1951) and for the quantal nature of neurotransmitter release (Fatt and Katz 1952).

Understanding the premotor circuitry of the spinal cord however presents a number of challenges. One important factor is that the ventral horn lacks any clear neuroanatomical structure. This prevents easy identification of interneuron cell types purely by morphology and position. In contrast, the dorsal horn cytoarchitecture is characterized by functionally different types of neurons that project specifically to different lamina (Wall 1967). In the ventral horn, it is necessary to rely on genetic tools and electrophysiological criteria to identify interneuron subtypes. Many of the experiments in this thesis use a genetically modified mouse to identify inhibitory interneurons and electrophysiological criteria to identify Renshaw cells. Another difficulty that has slowed the progress of understanding spinal neuronal networks in the ventral horn is the difficulty in

maintaining healthy in vitro slice preparations from adult animals. While recordings from adult spinal cord slices (for example, Husch et al. 2011, Mitra and Brownstone 2012) have been recently reported, the majority of electrophysiological studies of the ventral horn made use of neonatal tissue preparations. This, as will be discussed later in this chapter, is still an early developmental stage and possibly not a true representation of the adult spinal cord.

In this thesis we have extended the normal age range of in vitro recordings (most commonly P1-P7) to animals up to P14 of age. At this age level, we have been able to obtain consistently healthy tissue and to perform long duration electrophysiological recordings. While obtaining slices from older animals is feasible, our targeted visual patch recordings would have been impossible due to the extensive degree of myelination, that starts around P10 and makes the ventral horn completely non transparent (even to infrared light) by P14. The poor optical access is particularly severe in the ventromedial region near the motor nuclei, where most motoneurons axon collaterals branch to contact the Renshaw cells. While the mouse is certainly not fully mature by P14, the maturation of ventral spinal cord does occur much earlier than that of other CNS regions. Functional maturation of motor circuitry is evident at P8 when animals are already weight bearing and capable of sustained locomotion. The chloride reversal has already switched from a depolarising to a hyperpolarising potential, and the expression of the chloride extruding potassium-chloride co-transporter type 2 (KCC2) is complete by P6 (for a comparative analysis of the development of various regions on the CNS (see the comprehensive review by Dehorter et al. 2012). Similarly, a shift from GABA to predominantly glycine mediated inhibition in the ventral horn commences already at P1 (Gao et al. 2001), before reaching a steady-state by P9-P15 in the rat ventral horn ((González-Forero and Alvarez 2005), and even earlier in the mouse (Bhumbra et al. 2012).

This thesis contains two major results that increase our knowledge of the local neuronal network that governs motor control at the lumbar level of the mouse spinal cord. Firstly, we have shown that synaptic inhibitory inputs on motoneurons are mainly glycinergic. This contrasts with previous work that has shown co-release of GABA with glycine onto spinal motoneurons at a sim-

ilar age range in the rat (Jonas et al. 1998). Secondly, we have determined the quantal parameters at the excitatory motoneuron to Renshaw cell synapse and estimated the degree of convergence of motoneurons onto Renshaw cells. Both findings will be instrumental in the understanding of the general principles governing the control of motor output through synaptic inhibition and through local recurrent feedback circuits.

I have already discussed the more specific aspects of this thesis in the individual chapters and I will now broaden the scope and discuss the results within a more general context of spinal cord circuity. First by looking at the transmission of GABA and glycine throughout development and considering the implications of a purely glycinergic inhibition of motoneurons. Then by discussing recurrent inhibition and how the new data on the motoneuron to Renshaw cell synapse may inform us about its functional role.

5.1 GABA and glycine transmission during early development of the spinal cord

GABA synthesis and glycine expression occur around the same time during development at $\sim$E12.5 (Ma et al. 1992, Allain et al. 2004; 2006). A study of the mouse embryonic spinal cord by Allain et al. (2004) showed that GABA maturation follows a rostrocaudal gradient, occuring first at brachial levels at E11.5 and then in the lumbar regions a day later. Immunoreactivity spreads from ventromedial to ventrolateral regions and subsequently decreases in those same areas while increasing in the dorsal cord (Allain et al. 2004). Between E12.5 and E16.5 glycine population parallels that of GABA (Allain et al. 2004) albeit a with a 24 hours delay (Allain et al. 2006). It is interesting to note that in their study, Allain et al. (2006) also showed that at E13.5 and E17.5 about a third of neurons located the ventral area are immunoreactive for both GABA and glycine. Following the embryonic period, a transition from GABA to moslty glycine mediated signalling occurs (Gao et al. 2001, Kotak et al. 1998, Nabekura et al. 2003).

GABA and glycine play an essential role during embryonic development,

since they are both mediators of spontaneous patterned activity. Excitation waves are a common feature of the early developmental stages of all parts of the nervous system (Ben-Ari 2001, Penn and Shatz 1999). Spontaneous activity during early development is important for the differentiation of neuronal phenotypes, for axon growth (Mattson and Kater 1987, Mattson et al. 1988), for the formation of synapse and for the initiation of signalling processes (Moody 1998, Moody and Bosma 2005, Spitzer 2006). Organized motor patterns are spontaneously generated in the embryonic spinal cord of the chick (Bekoff 1992, Milner and Landmesser 1999, O'Donovan 1999), rat (Ren and Greer 2003) and mouse (Hanson and Landmesser 2003, Myers et al. 2005), in intact preparation as well as in organotypic slices (Ballerini et al. 1999). At early prenatal stages GABAergic and glycinergic signalling are depolarizing, due to high intracellular chloride levels (Ben-Ari et al. 1989) and can trigger Ca^{2+} influx, bring the cells closer to threshold for firing (Dehorter et al. 2012) and even induce action potentials *per se* (Ben-Ari et al. 1989, Reichling et al. 1994, Obrietan and van den Pol 1995). During embryionic development, the functional role of GABA and glycine is excitatory (Ben-Ari et al. 1989). In fact, in the embryonic rat spinal cord at E14.5-15-5 spontaneous motor activity can be entirely abolished by blockade of glycine transmission and greatly reduced by blockade of GABA (Nishimaru et al. 1996). After E15.5 however the expression of the Na^{2+}-K^{+}-$2Cl^{-}$ cotransporter isoform 1 (NKCC1), which takes up chloride ions (Alvarez-Leefmans et al. 1988, Rohrbough and Spitzer 1996, Russell 2000), is reduced and the reversal for chloride moves away from the spike threshold and towards the resting potential of the cells (Delpy et al. 2008). At birth, GABA and glycine currents reverse close to the resting potential in the rat (Takahashi 1984, Jean-Xavier et al. 2006, Stil et al. 2009) and mouse (Stil et al. 2011) due to the increase in expression of KCC2 and decrease in expression of NKCC1, that results in progressive lowering of the intracellular chloride levels (Stil et al. 2009; 2011).

5.2 Co-release of GABA and glycine

Slow GABAergic currents are more effective than fast glycinergic currents at triggering transient increases in calcium (Gao et al. 1998, Xie and Ziskind-Conhaim 1995). The longer time course of GABA mediated currents could be important in a development stage during which motoneurons are not capable of repetitive firing (Xie and Ziskind-Conhaim 1995), becuase GABA receptors activation could keep the membrane potential closer to threshold for longer, thus favouring the propagation of spontaneous bursts. As mentioned previously, a subset of neurons in the ventral side of the embryonic spinal cord co-localise GABA and glycine (Allain et al. 2006). Gao et al. (2001) showed also that before birth around 25% of inhibitory synaptic activity is mixed GABA and glycine. Indeed, embryonic motoneurons express $GABA_A$ receptors at a higher density than glycine (Gao and Ziskind-Conhaim 1995) but after birth this situation is reversed and there is a large increase in both size and frequency of glycine currents (Gao et al. 2001). It is possible that such bias towards GABAergic transmission aids the development of neuronal networks by prolonging the effect of chloride mediated depolarizing currents.

However, after birth the animals gain control of movement and slowly acquire the refined tuning and coordination of each muscle. In this thesis I have shown that inhibitory transmission onto motoneurons in weight bearing mice is mostly mediated by glycine. This is consistent with the progressive speeding up of synaptic inhibition that is observed in the spinal cord (as well as in other parts of the brain). In fact, following birth, both GABA and glycine receptors undergo a developmental shift in subunit composition. For instance, $\alpha 2$ homomeric glycine receptors are replaced by $\alpha 1\beta$ heteromers, whose decay kinetics is much faster (Malosio et al. 1991). A similar shift occurs for GABA receptors (Fritschy et al. 1994). The reduction of GABA mediated and the increase in glycine mediated synaptic transmission marks another shift towards a regime of faster synaptic currents. In this context, it is possible that the co-detection of GABA observed by Jonas et al. (1998) corresponds to an intermediate stage in the development of inhibitory transmission. By performing experiments at a later stage of development, we have in fact shown not only that co-detection

GABA and glycine does not occur, but also that the vast majority of inhibitory synaptic currents onto motoneurons are solely mediated by glycine. Our results have been recently supported by evidence coming from in vivo recordings in adult mice (B. Alstermark, personal communication), showing that glycine is virtually the only inhibitory neurotransmitter active at lumbar motoneurons. It is tempting to speculate that the speeding up of the time course of inhibition during development goes in parallel with the ability of the animals to perform more complex motor tasks, requiring the fine tuning and coordinated movements of more limbs and joints. Since GABA and glycine share a common vesicular transporter, it is still possible that the two transmitter are packed together in the same vesicles. Lu et al. (2008) showed a surprising effect of co-release of GABA and glycine at a MNTB synapse, where only glycine receptors are present. In fact, co-released GABA acts as a partial agonist at glycine receptors, reducing response size and speeding up the decay time by a factor of 2. This gives rise to glycinergic currents with decay times as fast as 1-2 ms at physiological chloride and temperature. Such precise timing of inhibition is necessary to detect small interaural differences, that allows the localization of sound. By contrast, at least in the spinal cord, we have shown that even if vesicles were filled by both glycine and GABA, the level of GABA is not sufficient to produce detectable effects on the time course of post-synaptic currents. However, our methods for altering the putative GABA/glycine ratio within the vesicles (blocking GABA synthesis or loading the pre-synaptic terminal with glycine) may not give rise to a shift in the ratio that is sufficient to observe an effect at the post-synaptic level.

5.3 Glycinergic inhibition of motoneurons

As discussed above, the decay time of inhibitory currents onto motoneurons decreases with age. This is due to a shift in receptor subunit composition as well as to a more general shift from slow GABAergic transmission to faster glyicnergic synapses. In a juvenile animal, the decay time course of glycine current can be as fast as 2 ms to 3 ms, when measured with intracellular physiological

chloride at room temperature (Pitt et al. 2008). At physiological temperature, this can be further reduced to $\sim 1-2$ ms. It is thus an apparent paradox that such a fast inhibition could affect cells like motoneurons, whose capacitance exceeds 300 pF and whose input resistance is extremely low ($\sim 10-20$ MΩ). In fact, the activation of a glycinergic synapse, considering the low input resistance of a motoneuron and the small driving force for chloride, would have little or no effect on the membrane potential. However, inhibition operates more by 'shunt' than by effective hyperpolarization. In fact, the activation of an inhibitory synapse gives rise to a large change in conductance at its location (Gidon and Segev 2012, Bhumbra et al. 2014). This further decreases the resistance of the cells, dramatically reducing the effect of simultaneously incoming excitatory inputs. The fast time constant of motoneurons ($\sim 2-4$ ms) is indeed optimal for maintaining the timing of inhibition since the duration of the synaptic conductance change will be faithfully reflected in the time course of the changes in the cell membrane conductance. Fast inhibition may thus allow fine tuning of the motoneuron activity that would not be possible with prolonged inhibition. In fact, fast and coordinated motor actions not only require balance between the intensity of excitation and inhibition, but also a precise timing in their sequence. Such a timing can be better achieved through a short, rather than a long lasting inhibitory action. It is therefore possible that GABA transmission at motoneurons is simply a developmental occurrence and that glycinergic transmission is in general preferable for control of motoneuron excitability in the adult spinal cord.

5.4 The motoneuron-Renshaw cell recurrent inhibitory circuit

As previously discussed motoneurons and Renshaw cells form a well defined recurrent inhibitory circuit in the ventral horn of the spinal cord that has been the subject of many studies (see the Introduction chapter as well as Chapter 4 and Alvarez and Fyffe 2007). Despite having gained considerable knowledge of the architecture of this circuit, we still do not have a quantitative description

of the individual synapses that form the circuit, nor a full understanding of the role of Renshaw cell mediated motoneuron inhibition. A study, complementary to the work presented in Chapter 4, (Bhumbra et al. 2014) describes in detail the electrophysiological and anatomical features of the Renshaw cell to motoneuron inhibitory synapses, in a similar way to the study of the motoneuron to Renshaw cell excitatory synapse presented in this thesis. As their study yields important information when considering the recurrent inhibitory circuit as a whole, I will briefly discuss their relevant results before discussing the excitatory synapse described in Chapter 4.

5.4.1 The Renshaw cell to motoneuron inhibitory synapse

Studies of recurrent inhibition in cats have previously suggested that Renshaw cells have a limited capacity to inhibit motoneurons. Renshaw cell synaptic contacts are located on motoneuron dendrites, further from the soma than Ia inhibitory interneurons whose synapses are located on or near the soma (Burke et al. 1971, Maltenfort et al. 2004). Windhorst et al. (1978) suppressed Renshaw cell firing by administering cholinergic antagonists and observed only a modest increase in motoneuron activity. A study of the effect on recurrent IPSPs on motoneuron impedance suggested Renshaw cells cause a similarly modest effect on motoneuron excitability (Maltenfort et al. 2004).

However, direct measure of the strength of the Renshaw cell to motoneuron synapse in the mouse by Bhumbra et al. (2014) proved that Renshaw cells can effectively inhibit motoneuron firing. Figure 5.1 demonstrates that a single action potential in a pre-synaptic Renshaw cell can inhibit motoneuron firing for up to ~ 5 ms, which is similar to the actual time course of the glycinergic synaptic conductance. Previous studies suggesting Renshaw cells cannot produce effective inhibition of motoneuron firing have mostly relied on peripheral nerve stimulation of homonymous (Hultborn et al. 1988) and heteronymous (Lindsay and Binder 1991, Maltenfort et al. 2004) motoneuron pools. This method synchronizes spikes within motoneuron pools, a pattern of activation that would not be expected during the execution of normal motor tasks. Furthermore, it is well known that homonymous motoneurons are connected by both gap junc-

tions and chemical synapses (Gogan et al. 1977). Synchronous stimulation of a large number of motoneurons would therefore result in the simultaneous activation of both excitatory and inhibitory recurrent pathways and the effect of Renshaw cell inhibition would be unclear due to the confounding effect of the recurrent excitation. The recording of a synapse between single cells, isolated from the rest of the circuit, provides direct measurement of the extent of inhibition exerted by a single Renshaw cell onto the motoneuron it contacts (Figure 5.1).

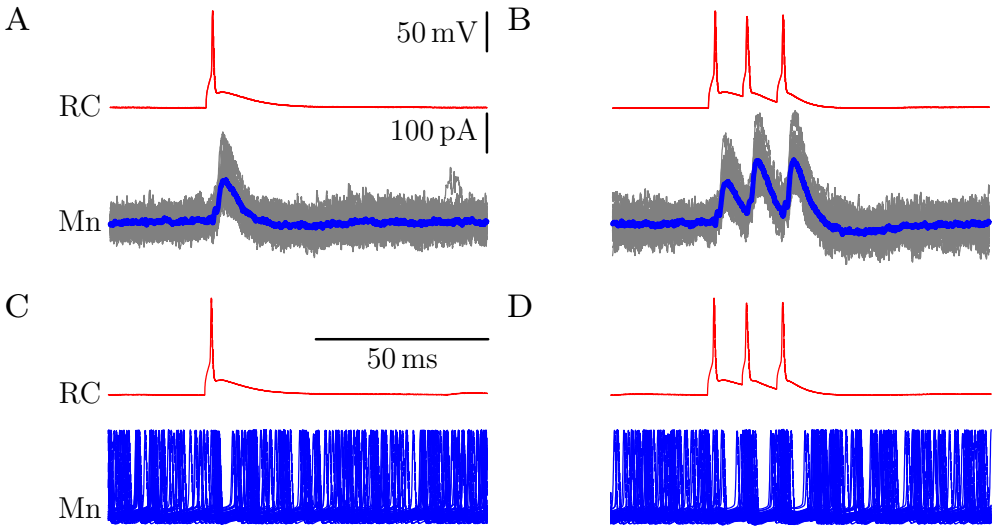

Figure 5.1: Inhibition of repetitive motoneuron firing by a single Renshaw cell. Panel A shows an action potential induced in a Renshaw cell held in a current-clamp configuration (shown in red) and the evoked IPSC in a connected motoneuron held in a voltage clamp configuration (individual traces shown in grey with the average trace overlaid in blue). The same configuration of cells is shown in panel b but three spikes are induced in the Renshaw cell at a frequency of 33 Hz. Panels C and D show the effect of spiking in the pre-synaptic Renshaw cell during repetitive of the post-synaptic motoneuron (which is held in a current-clamp configuration). The Renshaw cell can be seen to effectively inhibit motoneuron firing for a duration that is similar to the duration of the evoked synaptic currents shown in panels A and B.

The study by Bhumbra et al. (2014) also estimated the quantal parameters of single Renshaw cell to motoneuron synapses and found the number of release sites to be ~ 6 and the mean probability of release was 0.3. While this is not a high probability of release, the large number of individual contacts (6-10)

makes the synapse extremely reliable, with a low failure rate and giving rise to a large change in the conductance of the post-synaptic cell (Bhumbra et al. 2014). The large paired pulse facilitation (paired pulse ratio of 1.87) leads to increased inhibition during repetitive motoneuron firing. This is likely to be functionally relevant to the role of the circuit and suggests that recurrent inhibition may increase with the intensity of muscle contraction.

5.4.2 The motoneuron to Renshaw cell excitatory synapse

The results in Chapter 4 described the quantal parameters of the synapse between motoneuron and Renshaw cells. Quantal estimates showed that the motoneuron-Renshaw cell synapse has a mean probability of release of ~ 0.5 and mean number of release sites between individual cells of 6.5 ± 1.15. This suggests that it is likely to be a very reliable synapse. In fact, when connected pairs were recorded both in current clamp (Figure 4.12) even for contacts that elicited small IPSCs, action potentials were often induced in the Renshaw cell following one or two spikes in the pre-synaptic motoneuron. In agreement with our observation, extracellular recordings of Renshaw cells by Ross et al. (1975) showed that action potentials could be generated by stimulation of single motoneurons (also demonstrated in our preparations and shown in Figure 4.12) and that motoneuron firing can drive Renshaw cell activation up to a frequency of at least 40 Hz (Ross et al. 1976). Renshaw cells are even able to dynamically reflect motor output and Renshaw cell activity can follow motoneuron firing over a frequency range similar to that of physiological motoneuron firing (Christakos et al. 1987).

While the knowledge of the parameters governing the individual synapses (both excitatory and inhibitory) in the recurrent inhibition circuit is the first essential building block necessary to gain an understanding of the operation of the circuit, this knowledge alone is not sufficient for determining the actual response of each element of the circuit during physiological patterns of activation. It is clear that the overall effect of Renshaw cells on motoneurons and vice versa will be dependent on the degree of convergence of one type of cell onto the other. With the results presented in Chapter 4 we report the first mea-

surement of the degree of convergence of motoneurons onto Renshaw cells suggesting that on average ~ 6 motoneurons project onto each Renshaw cell. One possible caveat is that the degree of convergence was determined in a slice preparation, where inevitably, some of the connections are lost due to the limited thickness of the tissue. However, since a single synapse is often powerful enough to elicit a post-synaptic spike, even if ~ 6 motoneurons is an underestimate, it is still unlikely that any post-synaptic Renshaw cells will fail to fire during motoneuron activity.

The degree of convergence was calculated using the number of release sites estimated from ventral root stimulation recordings as the total number of motoneuron contacts onto a given Renshaw cell, and the number of release sites estimated using data from paired recordings as the number of contacts between individual cells. The quotient of these two estimates therefore gives an estimate of the total number of motoneurons that project onto each Renshaw cell. When stimulating the ventral root, most motoneurons contained in the slice will fire, either antidromically or orthodromically, as shown in Figure 4.6. As a consequence, ventral root stimulation would inevitably induce firing in different motor pools, including those that innervate synergist as well as antagonist muscle groups. It has always been accepted that Renshaw cell recurrent inhibition occurs mostly within synergistic motoneuron pools (Wilson et al. 1960, Eccles et al. 1961a), while Renshaw cells related to antagonist muscles tend to inhibit each other (Ryall et al. 1971). This is shown in scheme of Figure 5.2, where recurrent excitation between motoneurons is restricted to homologous motoneuron pools and the recurrent feedback loop is segregated between a flexor and extensor component, while antagonist related Renshaw cells inhibit each other. During our paired recordings, as well as during the recordings from single Renshaw cells, we do not have an indication of the motoneuron or Renshaw cell identities, namely, whether they are related to a flexor or an extensor circuit. We therefore cannot exclude that the number of release sites observed during ventral root stimulation could include projections from non-synergistic motoneuron pools. If the motoneuron to Renshaw cell synapse is not segregated between flexor and extensor muscle groups, and Renshaw cells receive excitatory inputs from motoneurons projecting to antagonistic muscle groups,

it is possible that our degree of convergence is an overestimate of the 'functional' connections. However, there are two reasons why this overestimate is unlikely to be an issue. Firstly, given the effectiveness of a single motoneuron to Renshaw cell synapse (see Figure 4.12), even if there was significantly less convergence, post-synaptic Renshaw cells are still likely to fire during motoneuron activity. Secondly, since Renshaw cell inhibition is segregated between antagonistic motor pools it is unlikely that Renshaw cell excitation is not also segregated. If Renshaw cell receive excitatory inputs from motoneuron that innervate antagonist muscles, it would mean that a motoneuron could induce recurrent inhibition of an antagonist muscle. This is not observed during recurrent inhibition and would be counterproductive during many muscle movements. Without being able to identify motoneurons by the muscle groups they innervate however it is not possible to determine conclusively the functional convergence and divergence of motoneuron and Renshaw cell connection in this circuit. Recently developed techniques that utilise the rabies virus to label motoneurons and their pre-synaptic cells (Stepien et al. 2010) has revealed the pattern of the premotor innervation and could be used to further investigate the connectivity of synergistic motoneurons and their respective Renshaw cells.

Given the well known recurrent nature of the motoneuron-Renshaw cell circuit (as described in Figure 5.2) it would be reasonable to assume a high level of reciprocal connections between the two cells types. However in our investigations we found that very few motoneuron to Renshaw cell pairs were reciprocally connected (only 3 out of 18 pairs tested). This suggests that, even in the hypothesis of a full segregation between flexor and extensor related recurrent circuits, recurrent inhibition operates more on the network level, than at the level of single cells.

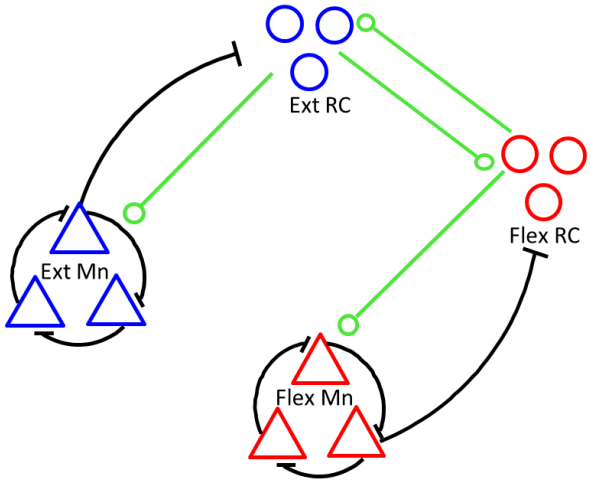

Figure 5.2: Schematic diagram of the recurrent inhibitory circuit. Recurent inhibition is segregated between flexor and extensor muscle groups. Extensor associated motoneurons and Renshaw cells are shown in blue and flexor associated cells are shown in red. Recurrent excitatory connections are shown between motoneurons within each homonymous group by black lines. Recurrent inhibition mediated by Renshaw cells is shown with motoneuron excitatory connections projecting from homonymous motorneurons to their associated Renshaw cells (the black lines) and the Renshaw cell inhibitory projections back onto the same motoneuron group are shown by the green lines. Mutual inhibition of Renshaw cells between flexor and extensor associated cells is shown by (green) inhibitory projections between the two groups.

5.5 The functional role of Renshaw cells and recurrent inhibition

As has been previously discussed, despite many decades of research there is still very little consensus on the role of recurrent inhibition of motoneurons. One of the more prominent theories is that Renshaw cell mediated inhibition acts as a variable gain regulator of motoneuron output (Hultborn and Pierrot-Deseilligny 1979). This suggestion is supported by evidence of a non-linear input-output relationship between motor activity and recurrent inhibition during muscles contraction in humans, suggesting that Renshaw cells are not simply providing a constant negative bias (Hultborn and Pierrot-Deseilligny 1979). It has also been suggested that the Renshaw cell mediated inhibition works in

conjunction with proprioceptive feedback from Ia interneurons (Windhorst 1989, Windhorst and Kokkoroyiannis 1991). The concept being that both proprioceptive feedback and recurrent inhibition are relaying information about motoneuron activity, with proprioceptive circuits bringing information from the muscles and Renshaw cells providing an efferent copy of motoneuron output, in this paradigm the recurrent inhibition allows the retrieval of feedback information from noise by mitigating the effect of continued firing thus allowing both feedback loops to co-determine - along with motoneuronal after-hyperpolarization - the firing rate adaptation of the motor unit (Windhorst and Kokkoroyiannis 1991).

A recent study of recurrent inhibition recorded *in vivo* from rats suggests that during rapid, forceful movements recurrent IPSPs actually support rather than impede motor pool activity (Obeidat et al. 2014). The Renshaw cells appear to achieve this by creating a bias in spike timing without effecting the average rate of firing, this was observed even at very high frequencies of recurrent inhibition (100 Hz, Obeidat et al. 2014). It is of course possible that the functional role of Renshaw cell activity changes with the intensity of motor activity and does not solely act by coordinating temporal motoneuron activity. In fact early hypothesis suggested that Renshaw cell inhibition mainly acted to coordinate motoneuron activity spatially by de-recruiting smaller motoneurons thus during repetitive firing stopping slower acting motoneurons from slowing down movement (see Windhorst 1996; for review). This theory was initially supported by studies of the cat hindlimb by Eccles et al. (1961b) that showed the amplitude of recurrent IPSPs were positively correlated with the duration of motoneuron after-hyperpolarization. However later studies have disputed this hypothesis and suggested that recurrent inhibition did not effect the rank order of motoneuron recruitment according to Henneman's size principle (Henneman et al. 1974, Clamann et al. 1974).

While the work presented in this thesis does not directly attempt to provide an answer to the question of the role and function of recurrent inhibition it does provide information about the circuit that could inform current and novel theories. In particular the primary findings of the studies in this thesis can summarised as i) showing the recurrent inhibitory circuit is made up of reliable

synapses that provide consistent synaptic transmission and effective inhibition and ii) providing evidence that in mature spinal circuits motor neuron inhibition is due to purely glycinergic transmission. The reliability of the circuit suggests that it is most likely to be constantly active during movement and therefore a necessary feedback step for the modulation of motor output. This is not to say that the role of recurrent inhibition is static and cannot change depending on the intensity of motor tasks (for an extensive review see Windhorst 1996). While frequency of motoneuron firing has little effect on the size of Renshaw cell EPSCs (Figure 4.13), the Renshaw to motoneuron synapse exhibits a high paired pulse ratio (~ 1.8 Bhumbra et al. 2014) suggesting there is scope for short term synaptic plasticity at the inhibitory synapse. The shift during maturation towards glycinergic inhibition is also suggestive of a circuit that relies on fast effective inhibition rather than a slower general decrease increase in excitability. This could be interpreted as supporting theories that view Renshaw inhibition as providing an efferent copy of motoneuron output as it would aid in producing a fast dynamic feedback during motoneuron firing (Loeb et al. 1989, Windhorst and Kokkoroyiannis 1991).

At the end of his review of recurrent inhibition Uwe Windhorst makes an "urgent call" for "a more concrete study of the relation of spinal (and other) networks with peripheral biomechanics" (Windhorst 1996). While this is still true today, it is also important to start using modern techniques such as viral tracing and optogenetics to dissect the various neuronal networks that influence motor output. Genetic studies have been very useful in defining the ontogeny of the various cell types that make up spinal cord networks (Lee and Pfaff 2001, Alvarez et al. 2005) but due to the complexity of the circuitry and the nervous systems ability to adapt we cannot rely on genetic knockin/knockout models to produce an understanding of motor control. Even though we have developed a much greater understanding of spinal cord systems in the decades since the pioneering work of Birdsey Renshaw and Sir John Eccles (Hultborn 2006) many of the confounding elements of the system such as the lack of easily identifiable interneuron populations still presents problems for experimenters today. Hopefully by utilising modern viral tracing, electrophysiological and optogenetic techniques we can overcome the majority of challenges the spinal

cord presents and no longer have to ask the question “Can sense be made of spinal interneuron circuits?”(McCrea 1992)

Bibliography

al Falahe NA, Nagaoka M, Vallbo AB (1990) Response profiles of human muscle afferents during active finger movements. *Brain* 113 (Pt 2):325–46.

Allain AE, BaÃŕri A, Meyrand P, Branchereau P (2004) Ontogenic changes of the GABAergic system in the embryonic mouse spinal cord. *Brain Res.* 1000:134–47.

Allain AE, BaÃŕri A, Meyrand P, Branchereau P (2006) Expression of the glycinergic system during the course of embryonic development in the mouse spinal cord and its co-localization with GABA immunoreactivity. *J. Comp. Neurol.* 496:832–46.

Altman J, Sudarshan K (1975) Postnatal development of locomotion in the laboratory rat. *Anim Behav* 23:896–920.

Alvarez FJ, Dewey DE, Harrington DA, Fyffe RE (1997) Cell-type specific organization of glycine receptor clusters in the mammalian spinal cord. *J. Comp. Neurol.* 379:150–70.

Alvarez FJ, Dewey DE, McMillin P, Fyffe RE (1999) Distribution of cholinergic contacts on Renshaw cells in the rat spinal cord: a light microscopic study. *J. Physiol. (Lond.)* 515 (Pt 3):787–97.

Alvarez F, Jonas P, Sapir T, Hartley R, Berrocal M, Geiman E, Todd A, Goulding M (2005) Postnatal phenotype and localization of spinal cord V1 derived interneurons. *J. Comp. Neurol.* 493:177–192.

Alvarez FJ, Fyffe REW (2007) The continuing case for the Renshaw cell. *J. Physiol. (Lond.)* 584:31–45.

Alvarez-Leefmans FJ, Gamiño SM, Giraldez F, Noguerón I (1988) Intracellular chloride regulation in amphibian dorsal root ganglion neurones studied with ion-selective microelectrodes. *J. Physiol. (Lond.)* 406:225–46.

Aprison MH, Werman R (1965) The distribution of glycine in cat spinal cord and roots. *Life Sci.* 4:2075–83.

Atwood HL, Bittner GD (1971) Matching of excitatory and inhibitory inputs to crustacean muscle fibers. *J. Neurophysiol.* 34:157–70.

Ballerini L, Galante M, Grandolfo M, Nistri A (1999) Generation of rhythmic patterns of activity by ventral interneurones in rat organotypic spinal slice culture. *J. Physiol. (Lond.)* 517 (Pt 2):459–75.

Bannatyne BA, Edgley SA, Hammar I, Jankowska E, Maxwell DJ (2003) Networks of inhibitory and excitatory commissural interneurons mediating crossed reticulospinal actions. *Eur. J. Neurosci.* 18:2273–84.

Barbour B, Isope P (2000) Combining loose cell-attached stimulation and recording. *J. Neurosci. Meth.* 103:199–208.

Barrett EF, Stevens CF (1972) The kinetics of transmitter release at the frog neuromuscular junction. *J. Physiol. (Lond.)* 227:691–708.

Beato M (2008) The time course of transmitter at glycinergic synapses onto motoneurons. *J. Neurosci.* 28:7412.

Bekkers JM, Richerson GB, Stevens CF (1990) Origin of variability in quantal size in cultured hippocampal neurons and hippocampal slices. *Proc. Natl. Acad. Sci. U.S.A.* 87:5359–62.

Bekoff A (1992) Neuroethological approaches to the study of motor development in chicks: achievements and challenges. *J. Neurobiol.* 23:1486–505.

Bellocchio EE, Reimer RJ, Fremeau RT, Edwards RH (2000) Uptake of glutamate into synaptic vesicles by an inorganic phosphate transporter. *Science* 289:957–60.

Ben-Ari Y (2001) Developing networks play a similar melody. *Trends Neurosci.* 24:353–60.

Ben-Ari Y, Cherubini E, Corradetti R, Gaiarsa JL (1989) Giant synaptic potentials in immature rat CA3 hippocampal neurones. *J. Physiol. (Lond.)* 416:303–25.

Bennett MR, Jones P, Lavidis NA (1986) The probability of quantal secretion along visualized terminal branches at amphibian (Bufo marinus) neuromuscular synapses. *J. Physiol. (Lond.)* 379:257–74.

Bennett MV, Zukin RS (2004) Electrical coupling and neuronal synchronization in the Mammalian brain. *Neuron* 41:495–511.

Bertrand S, Cazalets JR (2002) The respective contribution of lumbar segments to the generation of locomotion in the isolated spinal cord of newborn rat. *Eur. J. Neurosci.* 16:1741–50.

Bhumbra GS, Beato M (2013) Reliable evaluation of the quantal determinants of synaptic efficacy using Bayesian analysis. *J. Neurophysiol.* 109:603–20.

Bhumbra GS, Moore NJ, Moroni M, Beato M (2012) Co-release of GABA does not occur at glycinergic synapses onto lumbar motoneurons in juvenile mice. *Front Cell Neurosci* 6:8.

Bhumbra G, Bannatyne B, Todd A, Watanabe M, Maxwell D, Beato M (2014) The recurrent case for the Renshaw cell. *J. Neurosci.* 34:31–45.

Bhumbra G, Dyball R (2010) Reading between the spikes of the hypothalamic neural code. *J. Neuroendocrinol.* 22:1239–1250.

Bittner GD (1968) Differentiation of nerve terminals in the crayfish opener muscle and its functional significance. *J. Gen. Physiol.* 51:731–58.

Bohlhalter S, Mohler H, Fritschy J (1994) Inhibitory neurotransmission in rat spinal cord: co-localization of glycine-and $GABA_A$-receptors at GABAergic synaptic contacts demonstrated by triple immunofluorescence staining. *Brain Res.* 642:59–69.

Bonnot A, Morin D (1998) Hemisegmental localisation of rhythmic networks in the lumbosacral spinal cord of neonate mouse. *Brain Res.* 793:136–48.

Bonnot A, Whelan PJ, Mentis GZ, O'Donovan MJ (2002) Locomotor-like activity generated by the neonatal mouse spinal cord. *Brain Res. Brain Res. Rev.* 40:141–51.

Borst JG, Lodder JC, Kits KS (1994) Large amplitude variability of GABAergic IPSCs in melanotropes from Xenopus laevis: evidence that quantal size differs between synapses. *J. Neurophysiol.* 71:639–55.

Bracci E, Ballerini L, Nistri A (1996) Localization of rhythmogenic networks responsible for spontaneous bursts induced by strychnine and bicuculline in the rat isolated spinal cord. *J. Neurosci.* 16:7063–76.

Branco T, Staras K, Darcy KJ, Goda Y (2008) Local dendritic activity sets release probability at hippocampal synapses. *Neuron* 59:475–85.

Brooks VB, Wilson VJ (1958) Localization of stretch reflexes by recurrent inhibition. *Science* 127:472–3.

Buhl EH, Tamás G, Szilágyi T, Stricker C, Paulsen O, Somogyi P (1997) Effect, number and location of synapses made by single pyramidal cells onto aspiny interneurones of cat visual cortex. *J. Physiol. (Lond.)* 500 (Pt 3):689–713.

Burke RE, Fedina L, Lundberg A (1971) Spatial synaptic distribution of recurrent and group Ia inhibitory systems in cat spinal motoneurones. *J. Physiol. (Lond.)* 214:305–26.

Burzomato V, Groot-Kormelink P, Sivilotti L, Beato M (2003) Stoichiometry of recombinant heteromeric glycine receptors revealed by a pore-lining region point mutation. *Receptors and Channels* 9:353–361.

Burzomato V, Beato M, Groot-Kormelink PJ, Colquhoun D, Sivilotti LG (2004) Single-channel behavior of heteromeric $\alpha 1 \beta$ glycine receptors: an attempt to detect a conformational change before the channel opens. *J. Neurosci.* 24:10924–40.

Butt SJB, Kiehn O (2003) Functional identification of interneurons responsible for left-right coordination of hindlimbs in mammals. *Neuron* 38:953–63.

Butt SJB, Lebret JM, Kiehn O (2002a) Organization of left-right coordination in the mammalian locomotor network. *Brain Res. Brain Res. Rev.* 40:107–17.

Butt SJB, Lebret JM, Kiehn O (2002b) Organization of left-right coordination in the mammalian locomotor network. *Brain Res. Brain Res. Rev.* 40:107–17.

Carr PA, Alvarez FJ, Leman EA, Fyffe RE (1998) Calbindin D28k expression in immunohistochemically identified Renshaw cells. *Neuroreport* 9:2657–61.

Cazalets JR, Borde M, Clarac F (1995) Localization and organization of the central pattern generator for hindlimb locomotion in newborn rat. *J. Neurosci.* 15:4943–51.

Cheema SS, Rustioni A, Whitsel BL (1984) Light and electron microscopic evidence for a direct corticospinal projection to superficial laminae of the dorsal horn in cats and monkeys. *J. Comp. Neurol.* 225:276–90.

Chéry N, De Koninck Y (1999) Junctional versus extrajunctional glycine and $GABA_A$ receptor-mediated IPSCs in identified lamina I neurons of the adult rat spinal cord. *J. Neurosci.* 19:7342–7355.

Christakos CN, Windhorst U, Rissing R, Meyer-Lohmann J (1987) Frequency response of spinal Renshaw cells activated by stochastic motor axon stimulation. *Neuroscience* 23:613–23.

Christensen BN, Martin AR (1970) Estimates of probability of transmitter release at the mammalian neuromuscular junction. *J. Physiol. (Lond.)* 210:933–45.

Christie KJ, Whelan PJ (2005) Monoaminergic establishment of rostrocaudal gradients of rhythmicity in the neonatal mouse spinal cord. *J. Neurophysiol.* 94:1554–64.

Cina C, Hochman S (2000) Diffuse distribution of sulforhodamine-labeled neurons during serotonin-evoked locomotion in the neonatal rat thoracolumbar spinal cord. *J. Comp. Neurol.* 423:590–602.

Clamann HP, Gillies JD, Henneman E (1974) Effects of inhibitory inputs on critical firing level and rank order of motoneurons. *J. Neurophysiol.* 37:1350–60.

Clarac F, Pearlstein E, Pflieger JF, Vinay L (2004) The in vitro neonatal rat spinal cord preparation: a new insight into mammalian locomotor mechanisms. *J. Comp. Physiol. A Neuroethol. Sens. Neural. Behav. Physiol.* 190:343–57.

Cooper RL, Harrington CC, Marin L, Atwood HL (1996) Quantal release at visualized terminals of a crayfish motor axon: intraterminal and regional differences. *J. Comp. Neurol.* 375:583–600.

Cowley KC, Schmidt BJ (1997) Regional distribution of the locomotor pattern-generating network in the neonatal rat spinal cord. *J. Neurophysiol.* 77:247–59.

Cullheim S, Kellerth JO (1981) Two kinds of recurrent inhibition of cat spinal alpha-motoneurones as differentiated pharmacologically. *J. Physiol. (Lond.)* 312:209–24.

Cullheim S, Kellerth JO, Conradi S (1977) Evidence for direct synaptic interconnections between cat spinal α-motoneurons via the recurrent axon collaterals: a morphological study using intracellular injection of horseradish peroxidase. *Brain Res.* 132:1–10.

Curras MC, Dingledine R (1992) Selectivity of amino acid transmitters acting at N-methyl-D-aspartate and amino-3-hydroxy-5-methyl-4-isoxazolepropionate receptors. *Mol. Pharmacol.* 41:520–6.

Curtis DR, Duggan AW, Felix D, Johnston GA (1971b) Bicuculline, an antagonist of GABA and synaptic inhibition in the spinal cord of the cat. *Brain Res.* 32:69–96.

Curtis DR, Duggan AW, Johnston GA (1971a) The specificity of strychnine as a glycine antagonist in the mammalian spinal cord. *Exp Brain Res* 12:547–65.

Curtis DR, Hösli L, Johnston GA (1968) A pharmacological study of the depression of spinal neurones by glycine and related amino acids. *Exp Brain Res* 6:1–18.

Dai X, Noga BR, Douglas JR, Jordan LM (2005) Localization of spinal neurons activated during locomotion using the c-fos immunohistochemical method. *J. Neurophysiol.* 93:3442–52.

De Koninck Y, Mody I (1997) Endogenous GABA activates small-conductance K+ channels underlying slow IPSCs in rat hippocampal neurons. *J. Neurophysiol.* 77:2202.

De Robertis E, Bennett H (1955) Some features of the submicroscopic morphology of synapses in frog and earthworm. *JCB* 1:47–58.

Dehorter N, Vinay L, Hammond C, Ben-Ari Y (2012) Timing of developmental sequences in different brain structures: physiological and pathological implications. *Eur. J. Neurosci.* 35:1846–56.

Del Castillo J, Katz B (1954) Quantal components of the end-plate potential. *J. Physiol. (Lond.)* 124:560–73.

Delpy A, Allain AE, Meyrand P, Branchereau P (2008) NKCC1 cotransporter inactivation underlies embryonic development of chloride-mediated inhibition in mouse spinal motoneuron. *J. Physiol. (Lond.)* 586:1059–75.

Diamond JS, Jahr CE (1995) Asynchronous release of synaptic vesicles determines the time course of the AMPA receptor-mediated EPSC. *Neuron* 15:1097–107.

Diana M, Marty A (2003) Characterization of depolarization-induced suppression of inhibition using paired interneuron–Purkinje cell recordings. *J. Neurosci.* 23:5906–5918.

Dugué G, Dumoulin A, Triller A, Dieudonné S (2005) Target-dependent use of coreleased inhibitory transmitters at central synapses. *J. Neurosci.* 25:6490–6498.

Eccles JC, Eccles RM, Iggo A, Ito M (1961a) Distribution of recurrent inhibition among motoneurones. *J. Physiol. (Lond.)* 159:479–99.

Eccles JC, Eccles RM, Iggo A, Lundberg A (1961b) Electrophysiological investigations on Renshaw cells. *J. Physiol. (Lond.)* 159:461–78.

Eccles JC, Fatt P, Koketsu K (1954) Cholinergic and inhibitory synapses in a pathway from motor-axon collaterals to motoneurones. *J. Physiol. (Lond.)* 126:524–62.

Eccles JC, Jaeger JC (1958) The relationship between the mode of operation and the dimensions of the junctional regions at synapses and motor end-organs. *Proc. R. Soc. Lond., B, Biol. Sci.* 148:38–56.

Eide AL, Glover J, Kjaerulff O, Kiehn O (1999) Characterization of commissural interneurons in the lumbar region of the neonatal rat spinal cord. *J. Comp. Neurol.* 403:332–45.

Elliott TR (1905) The action of adrenalin. *J. Physiol. (Lond.)* 32:401–67.

Ernfors P, Lee KF, Kucera J, Jaenisch R (1994) Lack of neurotrophin-3 leads to deficiencies in the peripheral nervous system and loss of limb proprioceptive afferents. *Cell* 77:503–12.

Fatt P, Katz B (1951) An analysis of the end-plate potential recorded with an intracellular electrode. *J. Physiol. (Lond.)* 115:320–70.

Fatt P, Katz B (1952) Spontaneous subthreshold activity at motor nerve endings. *J. Physiol. (Lond.)* 117:109–28.

Fisher RA (1922) On the mathematical foundations of theoretical statistics. *Philosophical Transactions of the Royal Society of London, A* 222:309–368.

Forti L, Bossi M, Bergamaschi A, Villa A, Malgaroli A (1997) Loose-patch recordings of single quanta at individual hippocampal synapses. *Nature* 388:874–8.

Frank E (1973) Matching of facilitation at the neuromuscular junction of the lobster: a possible case for influence of muscle on nerve. *J. Physiol. (Lond.)* 233:635–58.

Fremeau RT, Burman J, Qureshi T, Tran CH, Proctor J, Johnson J, Zhang H, Sulzer D, Copenhagen DR, Storm-Mathisen J, Reimer RJ, Chaudhry FA, Edwards RH (2002) The identification of vesicular glutamate transporter 3 suggests novel modes of signaling by glutamate. *Proc. Natl. Acad. Sci. U.S.A.* 99:14488–93.

Fritschy JM, Paysan J, Enna A, Mohler H (1994) Switch in the expression of rat GABAA-receptor subtypes during postnatal development: an immunohistochemical study. *J. Neurosci.* 14:5302–24.

Fyffe RE (1991) Spatial distribution of recurrent inhibitory synapses on spinal motoneurons in the cat. *J. Neurophysiol.* 65:1134–49.

Gabbay H, Delvolvé I, Lev-Tov A (2002) Pattern generation in caudal-lumbar and sacrococcygeal segments of the neonatal rat spinal cord. *J. Neurophysiol.* 88:732–9.

Gallager DW (1978) Benzodiazepines: potentiation of a GABA inhibitory response in the dorsal raphe nucleus. *Eur. J. Pharmacol.* 49:133–43.

Gandhi SP, Stevens CF (2003) Three modes of synaptic vesicular recycling revealed by single-vesicle imaging. *Nature* 423:607–13.

Gao BX, Cheng G, Ziskind-Conhaim L (1998) Development of spontaneous synaptic transmission in the rat spinal cord. *J. Neurophysiol.* 79:2277–87.

Gao BX, Ziskind-Conhaim L (1995) Development of glycine- and GABA-gated currents in rat spinal motoneurons. *J. Neurophysiol.* 74:113–21.

Gao B, Stricker C, Ziskind-Conhaim L (2001) Transition from GABAergic to glycinergic synaptic transmission in newly formed spinal networks. *J. Neurophysiol.* 86:492.

Geiman EJ, Knox MC, Alvarez FJ (2000) Postnatal maturation of gephyrin/glycine receptor clusters on developing Renshaw cells. *J. Comp. Neurol.* 426:130–42.

Gidon A, Segev I (2012) Principles governing the operation of synaptic inhibition in dendrites. *Neuron* 75:330–41.

Gogan P, Gueritaud JP, Horcholle-Bossavit G, Tyc-Dumont S (1977) Direct excitatory interactions between spinal motoneurones of the cat. *J. Physiol. (Lond.)* 272:755–67.

González-Forero D, Alvarez FJ (2005) Differential postnatal maturation of GABAA, glycine receptor, and mixed synaptic currents in Renshaw cells and ventral spinal interneurons. *J. Neurosci.* 25:2010–23.

Gosgnach S, Lanuza G, Butt S, Saueressig H, Zhang Y, Velasquez T, Riethmacher D, Callaway E, Kiehn O, Goulding M (2006) V1 spinal neurons regulate the speed of vertebrate locomotor outputs. *Nature* 440:215–219.

Goulding M, Pfaff SL (2005) Development of circuits that generate simple rhythmic behaviors in vertebrates. *Curr. Opin. Neurobiol.* 15:14–20.

Granseth B, Odermatt B, Royle SJ, Lagnado L (2006) Clathrin-mediated endocytosis is the dominant mechanism of vesicle retrieval at hippocampal synapses. *Neuron* 51:773–86.

Grillner S, Zangger P (1979) On the central generation of locomotion in the low spinal cat. *Exp Brain Res* 34:241–61.

Grillner S (2003) The motor infrastructure: from ion channels to neuronal networks. *Nat. Rev. Neurosci.* 4:573–86.

Grillner S, Hellgren J, Ménard A, Saitoh K, Wikström MA (2005) Mechanisms for selection of basic motor programs–roles for the striatum and pallidum. *Trends Neurosci.* 28:364–70.

Gulyás AI, Miles R, Sík A, Tóth K, Tamamaki N, Freund TF (1993) Hippocampal pyramidal cells excite inhibitory neurons through a single release site. *Nature* 366:683–7.

Hadingham KL, Garrett EM, Wafford KA, Bain C, Heavens RP, Sirinathsinghji DJ, Whiting PJ (1996) Cloning of cDNAs encoding the human gamma-aminobutyric acid type A receptor alpha 6 subunit and characterization of the pharmacology of alpha 6-containing receptors. *Mol. Pharmacol.* 49:253–9.

Hanson MG, Landmesser LT (2003) Characterization of the circuits that generate spontaneous episodes of activity in the early embryonic mouse spinal cord. *J. Neurosci.* 23:587–600.

Heckman CJ, Lee RH, Brownstone RM (2003) Hyperexcitable dendrites in motoneurons and their neuromodulatory control during motor behavior. *Trends Neurosci.* 26:688–95.

Henneman E, Clamann HP, Gillies JD, Skinner RD (1974) Rank order of motoneurons within a pool: law of combination. *J. Neurophysiol.* 37:1338–49.

Herzog E, Bellenchi GC, Gras C, Bernard V, Ravassard P, Bedet C, Gasnier B, Giros B, Mestikawy SE (2001) The existence of a second vesicular glutamate transporter specifies subpopulations of glutamatergic neurons. *J. Neurosci.* 21:RC181.

Herzog E, Landry M, Buhler E, Bouali-Benazzouz R, Legay C, Henderson CE, Nagy F, Dreyfus P, Giros B, Mestikawy SE (2004) Expression of vesicular glutamate transporters, VGLUT1 and VGLUT2, in cholinergic spinal motoneurons. *Eur. J. Neurosci.* 20:1752–60.

Hessler NA, Shirke AM, Malinow R (1993) The probability of transmitter release at a mammalian central synapse. *Nature* 366:569–72.

Hoover JE, Durkovic RG (1992) Retrograde labeling of lumbosacral interneurons following injections of red and green fluorescent microspheres into hindlimb motor nuclei of the cat. *Somatosens Mot Res* 9:211–26.

Houston C, Bright D, Sivilotti L, Beato M, Smart T (2009) Intracellular chloride ions regulate the time course of GABA-mediated inhibitory synaptic transmission. *J. Neurosci.* 29:10416.

Hultborn H, Conway BA, Gossard JP, Brownstone R, Fedirchuk B, Schomburg ED, Enríquez-Denton M, Perreault MC (1998) How do we approach the locomotor network in the mammalian spinal cord? *Ann. N. Y. Acad. Sci.* 860:70–82.

Hultborn H, Jankowska E, Lindström S (1971a) Recurrent inhibition from motor axon collaterals of transmission in the Ia inhibitory pathway to motoneurones. *J. Physiol. (Lond.)* 215:591–612.

Hultborn H, Jankowska E, Lindström S (1971b) Recurrent inhibition of interneurones monosynaptically activated from group Ia afferents. *J. Physiol. (Lond.)* 215:613–36.

Hultborn H, Jankowska E, Lindström S (1971c) Relative contribution from different nerves to recurrent depression of Ia IPSPs in motoneurones. *J. Physiol. (Lond.)* 215:637–64.

Hultborn H, Katz R, Mackel R (1988) Distribution of recurrent inhibition within a motor nucleus. II. Amount of recurrent inhibition in motoneurones to fast and slow units. *Acta Physiol. Scand.* 134:363–74.

Hultborn H, Kiehn O (1992) Neuromodulation of vertebrate motor neuron membrane properties. *Curr. Opin. Neurobiol.* 2:770–5.

Hultborn H, Pierrot-Deseilligny E (1979) Changes in recurrent inhibition during voluntary soleus contractions in man studied by an H-reflex technique. *J. Physiol. (Lond.)* 297:229–51.

Hultborn H (2006) Spinal reflexes, mechanisms and concepts: from Eccles to Lundberg and beyond. *Prog. Neurobiol.* 78:215–32.

Husch A, Cramer N, Harris-Warrick RM (2011) Long-duration perforated patch recordings from spinal interneurons of adult mice. *J. Neurophysiol.* 106:2783–9.

Huzurbazar VS (1948) The likelihood equation, consistency and the maxima of the likelihood function. *Ann Eugen* 14 Pt:185–200.

Illert M, Kümmel H (1999) Reflex pathways from large muscle spindle afferents and recurrent axon collaterals to motoneurones of wrist and digit muscles: a comparison in cats, monkeys and humans. *Exp Brain Res* 128:13–9.

Isaacson JS, Walmsley B (1995) Counting quanta: direct measurements of transmitter release at a central synapse. *Neuron* 15:875–84.

Jack JJ, Redman SJ, Wong K (1981) The components of synaptic potentials evoked in cat spinal motoneurones by impulses in single group Ia afferents. *J. Physiol. (Lond.)* 321:65–96.

Jankowska E (1992) Interneuronal relay in spinal pathways from proprioceptors. *Prog. Neurobiol.* 38:335–78.

Jankowska E, Edgley SA (2010) Functional subdivision of feline spinal interneurons in reflex pathways from group Ib and II muscle afferents; an update. *Eur. J. Neurosci.* 32:881–93.

Jaynes ET (2003) *Probability theory: the logic of science* Cambridge university press.

Jean-Xavier C, Mentis GZ, O'Donovan MJ, Cattaert D, Vinay L (2007) Dual personality of GABA/glycine-mediated depolarizations in immature spinal cord. *Proc. Natl. Acad. Sci. U.S.A.* 104:11477–82.

Jean-Xavier C, Pflieger JF, Liabeuf S, Vinay L (2006) Inhibitory postsynaptic potentials in lumbar motoneurons remain depolarizing after neonatal spinal cord transection in the rat. *J. Neurophysiol.* 96:2274–81.

Jeffrey H (1998) *Theory of Probability* Oxford Univ. Press.

Jessell TM, Kandel ER (1993) Synaptic transmission: a bidirectional and self-modifiable form of cell-cell communication. *Cell* 72 Suppl:1–30.

Jonas P, Bischofberger J, Sandkühler J (1998) Corelease of two fast neurotransmitters at a central synapse. *Science* 281:419.

Katz R, Pierrot-Deseilligny E (1999) Recurrent inhibition in humans. *Prog. Neurobiol.* 57:325–55.

Keller A, Coull J, Chéry N, Poisbeau P, De Koninck Y (2001) Region-specific developmental specialization of GABA–glycine cosynapses in laminas I–II of the rat spinal dorsal horn. *J. Neurosci.* 21:7871–7880.

Kennedy PR (1990) Corticospinal, rubrospinal and rubro-olivary projections: a unifying hypothesis. *Trends Neurosci.* 13:474–9.

Kiehn O (2006) Locomotor circuits in the mammalian spinal cord. *Annu. Rev. Neurosci.* 29:279–306.

Kiehn O, Butt SJB (2003) Physiological, anatomical and genetic identification of CPG neurons in the developing mammalian spinal cord. *Prog. Neurobiol.* 70:347–61.

Kjaerulff O, Barajon I, Kiehn O (1994) Sulphorhodamine-labelled cells in the neonatal rat spinal cord following chemically induced locomotor activity in vitro. *J. Physiol. (Lond.)* 478 (Pt 2):265–73.

Kjaerulff O, Kiehn O (1996) Distribution of networks generating and coordinating locomotor activity in the neonatal rat spinal cord in vitro: a lesion study. *J. Neurosci.* 16:5777–94.

Knoflach F, Benke D, Wang Y, Scheurer L, Lüddens H, Hamilton BJ, Carter DB, Mohler H, Benson JA (1996) Pharmacological modulation of the diazepam-insensitive recombinant gamma-aminobutyric acidA receptors alpha 4 beta 2 gamma 2 and alpha 6 beta 2 gamma 2. *Mol. Pharmacol.* 50:1253–61.

Koester HJ, Johnston D (2005) Target cell-dependent normalization of transmitter release at neocortical synapses. *Science* 308:863–865.

Korn H, Mallet A, Triller A, Faber DS (1982) Transmission at a central inhibitory synapse. II. Quantal description of release, with a physical correlate for binomial n. *J. Neurophysiol.* 48:679–707.

Korn H, Triller A, Mallet A, Faber DS (1981) Fluctuating responses at a central synapse: n of binomial fit predicts number of stained presynaptic boutons. *Science* 213:898–901.

Kotak VC, Korada S, Schwartz IR, Sanes DH (1998) A developmental shift from GABAergic to glycinergic transmission in the central auditory system. *J. Neurosci.* 18:4646–55.

Kremer E, Lev-Tov A (1997) Localization of the spinal network associated with generation of hindlimb locomotion in the neonatal rat and organization of its transverse coupling system. *J. Neurophysiol.* 77:1155–70.

Küchler M, Fouad K, Weinmann O, Schwab ME, Raineteau O (2002) Red nucleus projections to distinct motor neuron pools in the rat spinal cord. *J. Comp. Neurol.* 448:349–59.

Kudo N, Yamada T (1987) N-methyl-D,L-aspartate-induced locomotor activity in a spinal cord-hindlimb muscles preparation of the newborn rat studied in vitro. *Neurosci. Lett.* 75:43–8.

Kullander K, Butt SJB, Lebret JM, Lundfald L, Restrepo CE, Rydström A, Klein R, Kiehn O (2003) Role of EphA4 and EphrinB3 in local neuronal circuits that control walking. *Science* 299:1889–92.

Kuno M (1964) Quantal components of excitatory synaptoc potentials in spinal motoneurones. *J. Physiol. (Lond.)* 175:81–99.

Lagerbäck PA, Ronnevi LO, Cullheim S, Kellerth JO (1981) An ultrastructural study of the synaptic contacts of alpha 1-motoneuron axon collaterals. II. Contacts in lamina VII. *Brain Res.* 222:29–41.

Lamotte d'Incamps B, Ascher P (2008) Four excitatory postsynaptic ionotropic receptors coactivated at the motoneuron-Renshaw cell synapse. *J Neurosci* 28:14121–14131.

Lamotte d'Incamps B, Krejci E, Ascher P (2012) Mechanisms shaping the slow nicotinic synaptic current at the motoneuron-renshaw cell synapse. *J. Neurosci.* 32:8413–23.

Lanuza GM, Gosgnach S, Pierani A, Jessell TM, Goulding M (2004) Genetic identification of spinal interneurons that coordinate left-right locomotor activity necessary for walking movements. *Neuron* 42:375–86.

Lawrence DG, Kuypers HG (1968) The functional organization of the motor system in the monkey. I. The effects of bilateral pyramidal lesions. *Brain* 91:1–14.

Lee S, Pfaff S (2001) Transcriptional networks regulating neuronal identity in the developing spinal cord. *nature neuroscience* 4:1183–1191.

Lemon RN (2008) Descending pathways in motor control. *Annu. Rev. Neurosci.* 31:195–218.

Lemon RN, Griffiths J (2005) Comparing the function of the corticospinal system in different species: organizational differences for motor specialization? *Muscle Nerve* 32:261–79.

Leyton A, Sherrington C (1917) Observations on the excitable cortex of the chimpanzee, orangutan, and gorilla. *Experimental Physiology* 11:135–222.

Lindsay AD, Binder MD (1991) Distribution of effective synaptic currents underlying recurrent inhibition in cat triceps surae motoneurons. *J. Neurophysiol.* 65:168–77.

Liu G, Choi S, Tsien RW (1999) Variability of neurotransmitter concentration and nonsaturation of postsynaptic AMPA receptors at synapses in hippocampal cultures and slices. *Neuron* 22:395–409.

Liu TT, Bannatyne BA, Jankowska E, Maxwell DJ (2009) Cholinergic terminals in the ventral horn of adult rat and cat: evidence that glutamate is a cotransmitter at putative interneuron synapses but not at central synapses of motoneurons. *Neuroscience* 161:111–22.

Liu T, Bannatyne B, Maxwell D (2010) Organization and neurochemical properties of intersegmental interneurons in the lumbar enlargement of the adult rat. *Neuroscience* 171:461–484.

Loeb GE, He J, Levine WS (1989) Spinal cord circuits: are they mirrors of musculoskeletal mechanics? *J Mot Behav* 21:473–91.

Loewi O (1957) On the background of the discovery of neurochemical transmission. *J Mt Sinai Hosp N Y* 24:1014–6.

Lu T, Rubio M, Trussell L (2008) Glycinergic transmission shaped by the corelease of GABA in a mammalian auditory synapse. *Neuron* 57:524–535.

Ma W, Behar T, Barker J (1992) Transient expression of GABA immunoreactivity in the developing rat spinal cord. *J. Comp. Neurol.* 325:271–290.

Ma W, Saunders P, Somogyi R, Poulter M, Barker J (1993) Ontogeny of $GABA_A$ receptor subunit mRNAs in rat spinal cord and dorsal root ganglia. *J. Comp. Neurol.* 338:337–359.

MacLachlan EM (1975) An analysis of the release of acetylcholine from preganglionic nerve terminals. *J. Physiol. (Lond.)* 245:447–66.

Magnuson DSK, Lovett R, Coffee C, Gray R, Han Y, Zhang YP, Burke DA (2005) Functional consequences of lumbar spinal cord contusion injuries in the adult rat. *J. Neurotrauma* 22:529–43.

Maier MA, Illert M, Kirkwood PA, Nielsen J, Lemon RN (1998) Does a C3-C4 propriospinal system transmit corticospinal excitation in the primate? An investigation in the macaque monkey. *J. Physiol. (Lond.)* 511 (Pt 1):191–212.

Malosio ML, Marquèze-Pouey B, Kuhse J, Betz H (1991) Widespread expression of glycine receptor subunit mRNAs in the adult and developing rat brain. *EMBO J.* 10:2401–9.

Maltenfort MG, McCurdy ML, Phillips CA, Turkin VV, Hamm TM (2004) Location and magnitude of conductance changes produced by Renshaw recurrent inhibition in spinal motoneurons. *J. Neurophysiol.* 92:1417–32.

Mathews G, Diamond J (2003) Neuronal glutamate uptake contributes to GABA synthesis and inhibitory synaptic strength. *J. Neurosci.* 23:2040.

Matsuyama K, Mori F, Kuze B, Mori S (1999) Morphology of single pontine reticulospinal axons in the lumbar enlargement of the cat: a study using the anterograde tracer PHA-L. *J. Comp. Neurol.* 410:413–30.

Matsuyama K, Takakusaki K, Nakajima K, Mori S (1997) Multi-segmental innervation of single pontine reticulospinal axons in the cervico-thoracic region of the cat: anterograde PHA-L tracing study. *J. Comp. Neurol.* 377:234–50.

Matsuyama K, Nakajima K, Mori F, Aoki M, Mori S (2004) Lumbar commissural interneurons with reticulospinal inputs in the cat: morphology and discharge patterns during fictive locomotion. *J. Comp. Neurol.* 474:546–61.

Mattson MP, Kater SB (1987) Calcium regulation of neurite elongation and growth cone motility. *J. Neurosci.* 7:4034–43.

Mattson MP, Taylor-Hunter A, Kater SB (1988) Neurite outgrowth in individual neurons of a neuronal population is differentially regulated by calcium and cyclic AMP. *J. Neurosci.* 8:1704–11.

McCrea DA (1992) Can sense be made of spinal interneuron circuits? *Behavioural and Brain Sciences* 15:633–643.

McCrea DA (1998) Neuronal basis of afferent-evoked enhancement of locomotor activity. *Ann. N. Y. Acad. Sci.* 860:216–25.

McCrea DA, Pratt CA, Jordan LM (1980) Renshaw cell activity and recurrent effects on motoneurons during fictive locomotion. *J. Neurophysiol.* 44:475–88.

McLean DL, Merrywest SD, Sillar KT (2000) The development of neuromodulatory systems and the maturation of motor patterns in amphibian tadpoles. *Brain Res. Bull.* 53:595–603.

Mentis GZ, Alvarez FJ, Bonnot A, Richards DS, Gonzalez-Forero D, Zerda R, O'Donovan MJ (2005) Noncholinergic excitatory actions of motoneurons in the neonatal mammalian spinal cord. *Proc. Natl. Acad. Sci. U.S.A.* 102:7344–9.

Mentis GZ, Siembab VC, Zerda R, O'Donovan MJ, Alvarez FJ (2006) Primary afferent synapses on developing and adult Renshaw cells. *J. Neurosci.* 26:13297–310.

Milner LD, Landmesser LT (1999) Cholinergic and GABAergic inputs drive patterned spontaneous motoneuron activity before target contact. *J. Neurosci.* 19:3007–22.

Mitra P, Brownstone RM (2012) An in vitro spinal cord slice preparation for recording from lumbar motoneurons of the adult mouse. *J. Neurophysiol.* 107:728–41.

Miyamoto MD (1975) Binomial analysis of quantal transmitter release at glycerol treated frog neuromuscular junctions. *J. Physiol. (Lond.)* 250:121–42.

Moody WJ (1998) Control of spontaneous activity during development. *J. Neurobiol.* 37:97–109.

Moody WJ, Bosma MM (2005) Ion channel development, spontaneous activity, and activity-dependent development in nerve and muscle cells. *Physiol. Rev.* 85:883–941.

Morland C, Nordengen K, Larsson M, Prolo LM, Farzampour Z, Reimer RJ, Gundersen V (2013) Vesicular uptake and exocytosis of L-aspartate is independent of sialin. *FASEB J.* 27:1264–74.

Moroni M, Biro I, Giugliano M, Vijayan R, Biggin P, Beato M, Sivilotti L (2011) Chloride ions in the pore of glycine and GABA channels shape the time course and voltage dependence of agonist currents. *J. Neurosci.* 31:14095–14106.

Muir GD, Whishaw IQ (2000) Red nucleus lesions impair overground locomotion in rats: a kinetic analysis. *Eur. J. Neurosci.* 12:1113–22.

Murthy VN, Sejnowski TJ, Stevens CF (1997) Heterogeneous release properties of visualized individual hippocampal synapses. *Neuron* 18:599–612.

Myers CP, Lewcock JW, Hanson MG, Gosgnach S, Aimone JB, Gage FH, Lee KF, Landmesser LT, Pfaff SL (2005) Cholinergic input is required during embryonic development to mediate proper assembly of spinal locomotor circuits. *Neuron* 46:37–49.

Nabekura J, Katsurabayashi S, Kakazu Y, Shibata S, Matsubara A, Jinno S, Mizoguchi Y, Sasaki A, Ishibashi H (2003) Developmental switch from GABA to glycine release in single central synaptic terminals. *Nat. Neurosci.* 7:17–23.

Nakayama K, Nishimaru H, Kudo N (2002) Basis of changes in left-right coordination of rhythmic motor activity during development in the rat spinal cord. *J. Neurosci.* 22:10388–98.

Nishimaru H, Iizuka M, Ozaki S, Kudo N (1996) Spontaneous motoneuronal activity mediated by glycine and GABA in the spinal cord of rat fetuses in vitro. *J. Physiol. (Lond.)* 497 (Pt 1):131–43.

Nishimaru H, Restrepo CE, Kiehn O (2006) Activity of Renshaw cells during locomotor-like rhythmic activity in the isolated spinal cord of neonatal mice. *J. Neurosci.* 26:5320–8.

Nishimaru H, Restrepo CE, Ryge J, Yanagawa Y, Kiehn O (2005) Mammalian motor neurons corelease glutamate and acetylcholine at central synapses. *Proc. Natl. Acad. Sci. U.S.A.* 102:5245–9.

Nissen UV, Mochida H, Glover JC (2005) Development of projection-specific interneurons and projection neurons in the embryonic mouse and rat spinal cord. *J. Comp. Neurol.* 483:30–47.

Noga BR, Shefchyk SJ, Jamal J, Jordan LM (1987) The role of Renshaw cells in locomotion: antagonism of their excitation from motor axon collaterals with intravenous mecamylamine. *Exp Brain Res* 66:99–105.

Obeidat A, Nardelli P, Powers R, Cope T (2014) Modulation of motoneuron firing by recurrent inhibition in the adult rat in vivo. *J. Neurophysiol.* EPub ahead of print.

O'Brien JA, Berger AJ (1999) Cotransmission of GABA and glycine to brain stem motoneurons. *J. Neurophysiol.* 82:1638–41.

Obrietan K, van den Pol AN (1995) GABA neurotransmission in the hypothalamus: developmental reversal from Ca^{2+} elevating to depressing. *J. Neurosci.* 15:5065–77.

O'Donovan MJ (1999) The origin of spontaneous activity in developing networks of the vertebrate nervous system. *Curr. Opin. Neurobiol.* 9:94–104.

Örnung G, Shupliakov O, Lindå H, Ottersen O, Storm-Mathisen J, Ulfhake B, Cullheim S (1996) Qualitative and quantitative analysis of glycine-and GABA-immunoreactive nerve terminals on motoneuron cell bodies in the cat spinal cord: A postembedding electron microscopic study. *J. Comp. Neurol.* 365:413–426.

Owens D, Kriegstein A (2002) Is there more to GABA than synaptic inhibition? *Nat. Rev. Neurosci.* 3:715–727.

Palay S, Palade G (1955) The fine structure of neurons. *JCB* 1:69–88.

Parnas I (1972) Differential block at high frequency of branches of a single axon innervating two muscles. *J. Neurophysiol.* 35:903–14.

Penfield W, Boldrey E (1937) Somatic motor and sensory representation in the cerebral cortex of man as studied by electrical stimulation. *Brain* 60:389–443.

Penn AA, Shatz CJ (1999) Brain waves and brain wiring: the role of endogenous and sensory-driven neural activity in development. *Pediatr. Res.* 45:447–58.

Pierrot-Deseilligny E, Burke D (2005) *The Circuitry of the Human Spinal Cord: Its Role in Motor Control and Movement Disorders.* Cambridge University Press.

Pitt S, Sivilotti L, Beato M (2008) High intracellular chloride slows the decay of glycinergic currents. *J. Neurosci.* 28:11454–11467.

Porter R, Lemon R (1993) Corticospinal function and voluntary movement. . *In Physiological Society Monograph* p. 428.

Pratt CA, Jordan LM (1987) Ia inhibitory interneurons and Renshaw cells as contributors to the spinal mechanisms of fictive locomotion. *J. Neurophysiol.* 57:56–71.

Prochazka A, Gorassini M (1998) Ensemble firing of muscle afferents recorded during normal locomotion in cats. *J. Physiol. (Lond.)* 507 (Pt 1):293–304.

Redman S (1990) Quantal analysis of synaptic potentials in neurons of the central nervous system. *Physiol. Rev.* 70:165–98.

Reichling DB, Kyrozis A, Wang J, MacDermott AB (1994) Mechanisms of GABA and glycine depolarization-induced calcium transients in rat dorsal horn neurons. *J. Physiol. (Lond.)* 476:411–21.

Ren J, Greer JJ (2003) Ontogeny of rhythmic motor patterns generated in the embryonic rat spinal cord. *J. Neurophysiol.* 89:1187–95.

Renshaw B (1941) Influence of the discharge of motoneurons upon exciation of neighboring motoneurons. . *J Neurophysiol* 4:167–183.

Renshaw B (1946) Central effects of centripetal impulses in axons of spinal ventral roots. *J. Neurophysiol.* 9:191–204.

Richards DS, Griffith RW, Romer SH, Alvarez FJ (2014) Motor axon synapses on renshaw cells contain higher levels of aspartate than glutamate. *PLoS ONE* 9:e97240.

Roberts A, Soffe SR, Wolf ES, Yoshida M, Zhao FY (1998) Central circuits controlling locomotion in young frog tadpoles. *Ann. N. Y. Acad. Sci.* 860:19–34.

Robinson J (1976a) Estimation of parameters for a model of transmitter release at synapses. *Biometrics* 32:61–8.

Robinson J (1976b) Estimation of parameters for a model of transmitter release at synapses. *Biometrics* 32:61–8.

Robitaille R, Tremblay JP (1987) Non-uniform release at the frog neuromuscular junction: evidence of morphological and physiological plasticity. *Brain Res.* 434:95–116.

Robitaille R, Tremblay JP (1991) Non-uniform responses to Ca^{2+} along the frog neuromuscular junction: effects on the probability of spontaneous and evoked transmitter release. *Neuroscience* 40:571–85.

Rohrbough J, Spitzer NC (1996) Regulation of intracellular Cl^- levels by Na^+-dependent Cl^- cotransport distinguishes depolarizing from hyperpolarizing $GABA_A$ receptor-mediated responses in spinal neurons. *J. Neurosci.* 16:82–91.

Rosenmund C, Clements JD, Westbrook GL (1993) Nonuniform probability of glutamate release at a hippocampal synapse. *Science* 262:754–7.

Ross HG, Cleveland S, Haase J (1975) Contribution of single motoneurons to renshaw cell activity. *Neurosci. Lett.* 1:105–8.

Ross HG, Cleveland S, Haase J (1976) Quantitative relation between discharge frequencies of a Renshaw cell and an intracellularly depolarized motoneuron. *Neurosci. Lett.* 3:129–32.

Russell JM (2000) Sodium-potassium-chloride cotransport. *Physiol. Rev.* 80:211–76.

Ryall RW, Piercey MF (1971) Excitation and inhibition of Renshaw cells by impulses in peripheral afferent nerve fibers. *J. Neurophysiol.* 34:242–51.

Ryall RW, Piercey MF, Polosa C (1971) Intersegmental and intrasegmental distribution of mutual inhibition of Renshaw cells. *J. Neurophysiol.* 34:700–7.

Schneider SP, Fyffe RE (1992) Involvement of GABA and glycine in recurrent inhibition of spinal motoneurons. *J. Neurophysiol.* 68:397–406.

Schomburg ED (1990) Spinal sensorimotor systems and their supraspinal control. *Neurosci. Res.* 7:265–340.

Sernagor E, Young C, Eglen S (2003) Developmental modulation of retinal wave dynamics: shedding light on the GABA saga. *J. Neurosci.* 23:7621–7629.

Sherrington C (1906) *The integrative action of the nervous system* Yale University Press.

Shimamoto K, Lebrun B, Yasuda-Kamatani Y, Sakaitani M, Shigeri Y, Yumoto N, Nakajima T (1998) DL-threo-β-benzyloxyaspartate, a potent blocker of excitatory amino acid transporters. *Mol. Pharmacol.* 53:195.

Sibilla S, Ballerini L (2009) GABAergic and glycinergic interneuron expression during spinal cord development: dynamic interplay between inhibition and excitation in the control of ventral network outputs. *Progress in neurobiology* 89:46–60.

Silver RA, Cull-Candy SG, Takahashi T (1996) Non-NMDA glutamate receptor occupancy and open probability at a rat cerebellar synapse with single and multiple release sites. *J. Physiol. (Lond.)* 494 (Pt 1):231–50.

Silver RA, Momiyama A, Cull-Candy SG (1998) Locus of frequency-dependent depression identified with multiple-probability fluctuation analysis at rat climbing fibre-Purkinje cell synapses. *J. Physiol. (Lond.)* 510 (Pt 3):881–902.

Silver RA (2003) Estimation of nonuniform quantal parameters with multiple-probability fluctuation analysis: theory, application and limitations. *J. Neurosci. Methods* 130:127–41.

Singer J, Talley E, Bayliss D, Berger A (1998) Development of glycinergic synaptic transmission to rat brain stem motoneurons. *J. Neurophysiol.* 80:2608.

Spitzer NC (2006) Electrical activity in early neuronal development. *Nature* 444:707–12.

Stepien AE, Tripodi M, Arber S (2010) Monosynaptic rabies virus reveals premotor network organization and synaptic specificity of cholinergic partition cells. *Neuron* 68:456–72.

Stil A, Liabeuf S, Jean-Xavier C, Brocard C, Viemari JC, Vinay L (2009) Developmental up-regulation of the potassium-chloride cotransporter type 2 in the rat lumbar spinal cord. *Neuroscience* 164:809–21.

Stil A, Jean-Xavier C, Liabeuf S, Brocard C, Delpire E, Vinay L, Viemari JC (2011) Contribution of the potassium-chloride co-transporter KCC2 to the modulation of lumbar spinal networks in mice. *Eur. J. Neurosci.* 33:1212–22.

Stokke MF, Nissen UV, Glover JC, Kiehn O (2002) Projection patterns of commissural interneurons in the lumbar spinal cord of the neonatal rat. *J. Comp. Neurol.* 446:349–59.

Stricker C, Field AC, Redman SJ (1996) Statistical analysis of amplitude fluctuations in EPSCs evoked in rat CA1 pyramidal neurones in vitro. *J. Physiol. (Lond.)* 490 (Pt 2):419–41.

Sugiuchi Y, Kakei S, Izawa Y, Shinoda Y (2004) Functional synergies among neck muscles revealed by branching patterns of single long descending motor-tract axons. *Prog. Brain Res.* 143:411–21.

Szatkowski M, Barbour B, Attwell D (1990) Non-vesicular release of glutamate from glial cells by reversed electrogenic glutamate uptake. *Nature* 348:443–6.

Taal W, Holstege J et al. (1994) GABA and glycine frequently colocalize in terminals on cat spinal motoneurons. *Neuroreport* 5:2225.

Takahashi T (1984) Inhibitory miniature synaptic potentials in rat motoneurons. *Proc. R. Soc. Lond., B, Biol. Sci.* 221:103–9.

Takahashi T, Momiyama A, Hirai K, Hishinuma F, Akagi H (1992) Functional correlation of fetal and adult forms of glycine receptors with developmental changes in inhibitory synaptic receptor channels. *Neuron* 9:1155–61.

Talpalar A, Endo T, Löw P, Borgius L, Hägglund M, Dougherty K, Ryge J, Hnasko T, Kiehn O (2011) Identification of minimal neuronal networks involved in flexor-extensor alternation in the mammalian spinal cord. *Neuron* 71:1071–1084.

Thomas RC, Wilson VJ (1965) Precise localization of Renshaw cells with a new marking technique. *Nature* 206:211–3.

Todd A, Watt C, Spike R, Sieghart W (1996) Colocalization of GABA, glycine, and their receptors at synapses in the rat spinal cord. *J. Neurosci.* 16:974.

Tran T, Alijani A, Phelps P (2003) Unique developmental patterns of GABAergic neurons in rat spinal cord. *J. Comp. Neurol.* 456:112–126.

Tresch MC, Kiehn O (1999) Coding of locomotor phase in populations of neurons in rostral and caudal segments of the neonatal rat lumbar spinal cord. *J. Neurophysiol.* 82:3563–74.

Valenstein E (2006) *The War of the Soups and the Sparks: The Discovery of Neurotransmitters and the Dispute Over How Nerves Communicate* Columbia University Press.

Varoqui H, Zhu H, Yao D, Ming H, Erickson J (2000) Cloning and functional identification of a neuronal glutamine transporter. *J. Biol. Chem.* 275:4049.

Varoqui H, Schäfer MKH, Zhu H, Weihe E, Erickson JD (2002) Identification of the differentiation-associated Na+/PI transporter as a novel vesicular glutamate transporter expressed in a distinct set of glutamatergic synapses. *J. Neurosci.* 22:142–55.

Wall PD (1967) The laminar organization of dorsal horn and effects of descending impulses. *J. Physiol. (Lond.)* 188:403–23.

Wall PD, Lidierth M (1997) Five sources of a dorsal root potential: their interactions and origins in the superficial dorsal horn. *J. Neurophysiol.* 78:860–71.

Walmsley B, Edwards FR, Tracey DJ (1988) Nonuniform release probabilities underlie quantal synaptic transmission at a mammalian excitatory central synapse. *J. Neurophysiol.* 60:889–908.

Walmsley B, Tracey DJ (1981) An intracellular study of Renshaw cells. *Brain Res.* 223:170–5.

Walro JM, Kucera J (1999) Why adult mammalian intrafusal and extrafusal fibers contain different myosin heavy-chain isoforms. *Trends Neurosci.* 22:180–4.

Werman R, Davidoff RA, Aprison MH (1967) Inhibition of motoneurones by iontophoresis of glycine. *Nature* 214:681–3.

Willis WD (1971) The case for the Renshaw cell. *Brain Behav. Evol.* 4:5–52.

Wilson VJ, Talbot WH, Diecke FP (1960) Distribution of recurrent facilitation and inhibition in cat spinal cord. *J. Neurophysiol.* 23:144–53.

Windhorst U (1989) Do Renshaw cells tell spinal neurones how to interpret muscle spindle signals? *Prog. Brain Res.* 80:283–94; discussion 269–71.

Windhorst U (1996) On the role of recurrent inhibitory feedback in motor control. *Prog. Neurobiol.* 49:517–87.

Windhorst U (2007) Muscle proprioceptive feedback and spinal networks. *Brain Res. Bull.* 73:155–202.

Windhorst U, Adam D, Inbar GF (1978) The effects of recurrent inhibitory feedback in shaping discharge patterns of motoneurones excited by phasic muscle stretches. *Biol Cybern* 29:221–7.

Windhorst U, Kokkoroyiannis T (1991) Interaction of recurrent inhibitory and muscle spindle afferent feedback during muscle fatigue. *Neuroscience* 43:249–59.

Wisden W, Herb A, Wieland H, Keinänen K, Lüddens H, Seeburg PH (1991) Cloning, pharmacological characteristics and expression pattern of the rat GABAA receptor alpha 4 subunit. *FEBS Lett.* 289:227–30.

Wojcik S, Katsurabayashi S, Guillemin I, Friauf E, Rosenmund C, Brose N, Rhee J (2006) A shared vesicular carrier allows synaptic corelease of GABA and glycine. *Neuron* 50:575–587.

Woolsey CN, Settlage PH, Meyer DR, Sencer W, Hamuy TP, Travis AM (1952) Patterns of localization in precentral and "supplementary" motor areas and their relation to the concept of a premotor area. *Res Publ Assoc Res Nerv Ment Dis* 30:238–64.

Wu WL, Ziskind-Conhaim L, Sweet MA (1992) Early development of glycine- and GABA-mediated synapses in rat spinal cord. *J. Neurosci.* 12:3935–45.

Xie H, Ziskind-Conhaim L (1995) Blocking Ca^{2+}-dependent synaptic release delays motoneuron differentiation in the rat spinal cord. *J. Neurosci.* 15:5900–11.

Zakharenko SS, Zablow L, Siegelbaum SA (2001) Visualization of changes in presynaptic function during long-term synaptic plasticity. *Nat. Neurosci.* 4:711–7.

Zeilhofer H, Studler B, Arabadzisz D, Schweizer C, Ahmadi S, Layh B, Bösl M, Fritschy J (2005) Glycinergic neurons expressing enhanced green fluorescent protein in bacterial artificial chromosome transgenic mice. *J. Comp. Neurol.* 482:123–141.

Zhang JH, Morita Y, Hironaka T, Emson PC, Tohyama M (1990) Ontological study of calbindin-D28k-like and parvalbumin-like immunoreactivities in rat spinal cord and dorsal root ganglia. *J. Comp. Neurol.* 302:715–28.